AD-A063 554 ARMY MISSILE RESEARCH AND DEVELOPMENT COMMAND REDSTO--ETC F/G 17/7
SPECTRAL DENSITY ANALYSIS OF GYRO VIBRATIONS.(U)
JUN 78 L J LITTLE

UNCLASSIFIED DRDMI-T-78-59 NL

1 OF 2
AD A063554

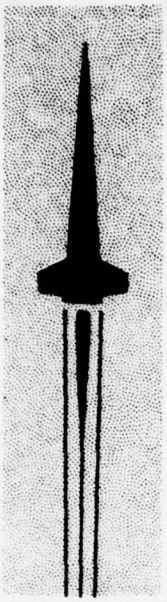

U.S. ARMY MISSILE RESEARCH AND DEVELOPMENT COMMAND

Redstone Arsenal, Alabama 35809

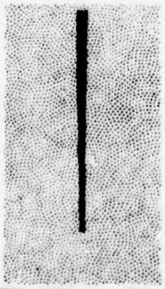

DMI FORM 1000, 1 APR 77

LEVEL II

12

(9) TECHNICAL REPORT T-78-59

(6) SPECTRAL DENSITY ANALYSIS OF GYRO VIBRATIONS,

(14) DRDMI-T-78-59

(10) L. J. Little
Guidance and Control Directorate
Technology Laboratory

(12) 92 p.

(11) 19 June 1978

Approved for Public Release; Distribution Unlimited.

DISPOSITION INSTRUCTIONS

DESTROY THIS REPORT WHEN IT IS NO LONGER NEEDED. DO NOT RETURN IT TO THE ORIGINATOR.

DISCLAIMER

THE FINDINGS IN THIS REPORT ARE NOT TO BE CONSTRUED AS AN OFFICIAL DEPARTMENT OF THE ARMY POSITION UNLESS SO DESIGNATED BY OTHER AUTHORIZED DOCUMENTS.

TRADE NAMES

USE OF TRADE NAMES OR MANUFACTURERS IN THIS REPORT DOES NOT CONSTITUTE AN OFFICIAL INDORSEMENT OR APPROVAL OF THE USE OF SUCH COMMERCIAL HARDWARE OR SOFTWARE.

UNCLASSIFIED

SECURITY CLASSIFICATION OF THIS PAGE *(When Data Entered)*

REPORT DOCUMENTATION PAGE

READ INSTRUCTIONS BEFORE COMPLETING FORM

1. REPORT NUMBER: T-78-59	2. GOVT ACCESSION NO.
3. RECIPIENT'S CATALOG NUMBER	
4. TITLE *(and Subtitle)*: SPECTRAL DENSITY ANALYSIS OF GYRO VIBRATIONS	5. TYPE OF REPORT & PERIOD COVERED: Technical Report
6. PERFORMING ORG. REPORT NUMBER: T-78-59	
7. AUTHOR(s): L. J. Little	8. CONTRACT OR GRANT NUMBER(s)
9. PERFORMING ORGANIZATION NAME AND ADDRESS: Commander, US Army Missile Research and Development Command, ATTN: DRDMI-TGL, Redstone Arsenal, Alabama 35809	10. PROGRAM ELEMENT, PROJECT, TASK AREA & WORK UNIT NUMBERS
11. CONTROLLING OFFICE NAME AND ADDRESS: Commander, US Army, ATTN: DRDMI-TI, Redstone Arsenal, Alabama 35809	12. REPORT DATE: 19 June 1978
	13. NUMBER OF PAGES
14. MONITORING AGENCY NAME & ADDRESS *(if different from Controlling Office)*	15. SECURITY CLASS. *(of this report)*: UNCLASSIFIED
	15a. DECLASSIFICATION/DOWNGRADING SCHEDULE

16. DISTRIBUTION STATEMENT *(of this Report)*

Approved for public release. Distribution unlimited.

17. DISTRIBUTION STATEMENT *(of the abstract entered in Block 20, if different from Report)*

18. SUPPLEMENTARY NOTES

19. KEY WORDS *(Continue on reverse side if necessary and identify by block number)*

Shaker Research Test
Lear Seigler Gyro Wheel

20. ABSTRACT *(Continue on reverse side if necessary and identify by block number)*

In Newtonian gyros, the bearings have been identified as a first order source of error. Over the years, a significant amount of research has been devoted to improving the quality of different type contact bearnings. In conjunction with task of improving the bearings, a similar effort has involved identifying the bearing effects on gyro performance.

The thrust in this report involves two similar types of measurements of gyro vibrations to enable detecting faulty bearings or establish a signature of

DD FORM 1 JAN 73 1473 EDITION OF 1 NOV 65 IS OBSOLETE

UNCLASSIFIED

SECURITY CLASSIFICATION OF THIS PAGE *(When Data Entered)*

20. ABSTRACT (Continued)

gyro performance. A gyro wheel from a precise instrument application was selected for this study because of the very high quality performance required in the parent system.

CONTENTS

TABLES

ILLUSTRATIONS

ILLUSTRATIONS

ILLUSTRATIONS

ILLUSTRATIONS

ILLUSTRATIONS

ILLUSTRATIONS (CONCLUDED)

1. INTRODUCTION

In Newtonian gyros, the bearings have been identified as a first order source of error. Over the years, a significant amount of research has been devoted to improving the quality of different type contact bearings. In conjunction with task of improving the bearings, a similar effort has involved identifying the bearing effects on gyro performance.

The thrust in this report involves two similar types of measurements of gyro vibrations to enable detecting faulty bearings or establish a signature of gyro performance. A gyro wheel from a precise instrument application was selected for this study because of the very high quality performance required in the parent system.

2. DESCRIPTION

A. Test Specimen

Two gyro wheels that are used as the inertial element in a precision gyro compass were test specimens for this task. *Figures 1 and 2* illustrate the general mechanical configuration of the devise. *Table 1* list the bearing parameters associated with each wheel. Thus, the primary factors of the test specimen are described.

The vibration data of the gyro wheels are detected with instrument grade accelerometers. These accelerometers were mounted nominally over each bearing trunnion in order to gain the best transmissibility and signature from each bearing.

B. MIRADCOM Test

Test were conducted at MIRADCOM and at Shaker Research Corporation. At MIRADCOM, the vibration data was subjected to a power spectral density analysis on the Hewlett Packard Fourier Analyzer. The ABSCISSA data is a function of the accelerometer output voltage squared. However, this is related to the g level through the particular accelerometer scale factor. Also, the voltage output is plotted as a function of frequency. Thus, the curves readily illustrate the most predominant vibration at a given frequency.

C. Shaker Research Test

The second test, conducted at Shaker Research, employed their vibration envelope detector. This instrument employed the same instrument type accelerometer sensors for signals. However, once a broad band of frequencies were scanned, similar to

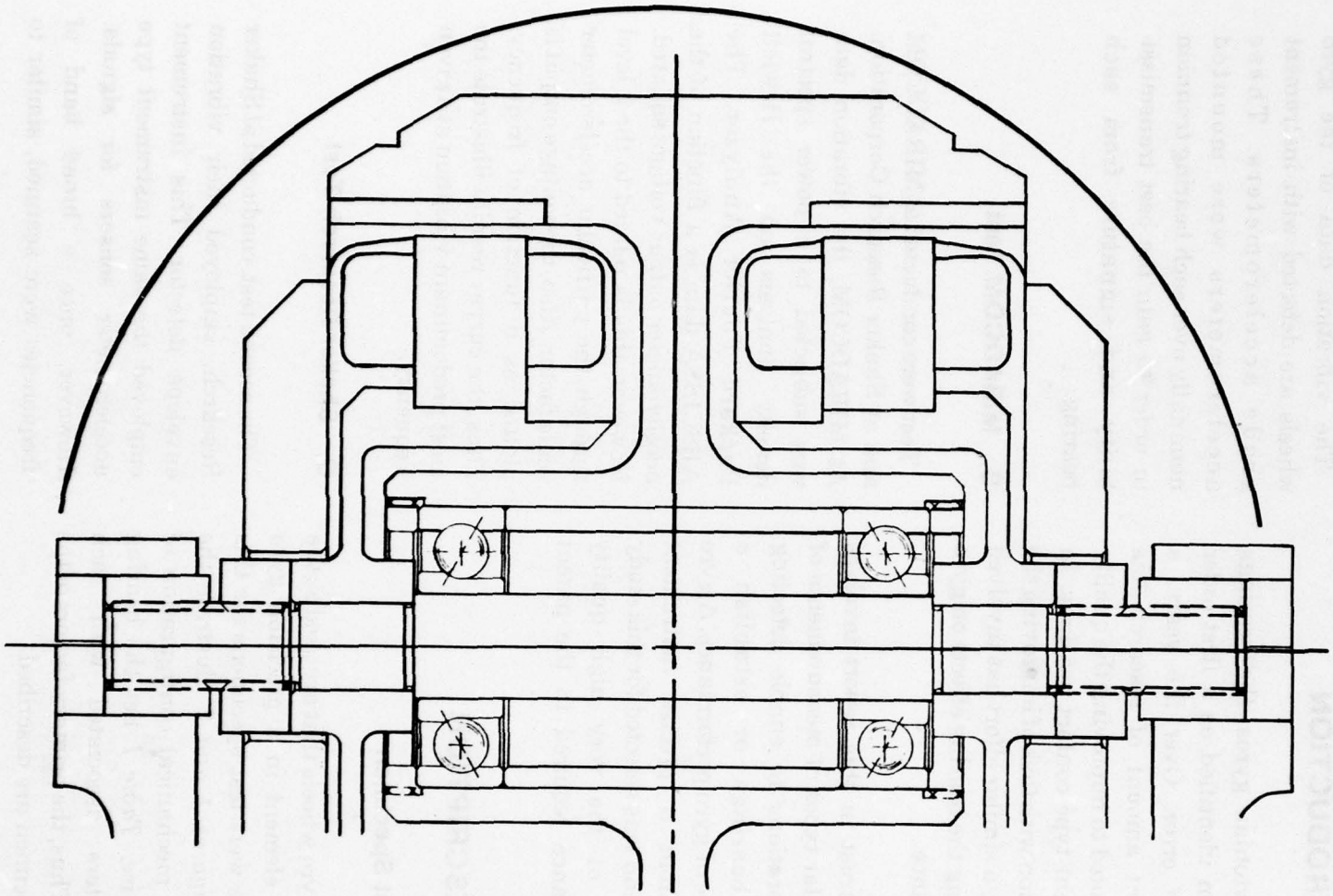

ANGULAR CONTACT BALL BEARING CONFIGURATION

Figure 1. Gyro Wheel AG8, half section serial no. 325

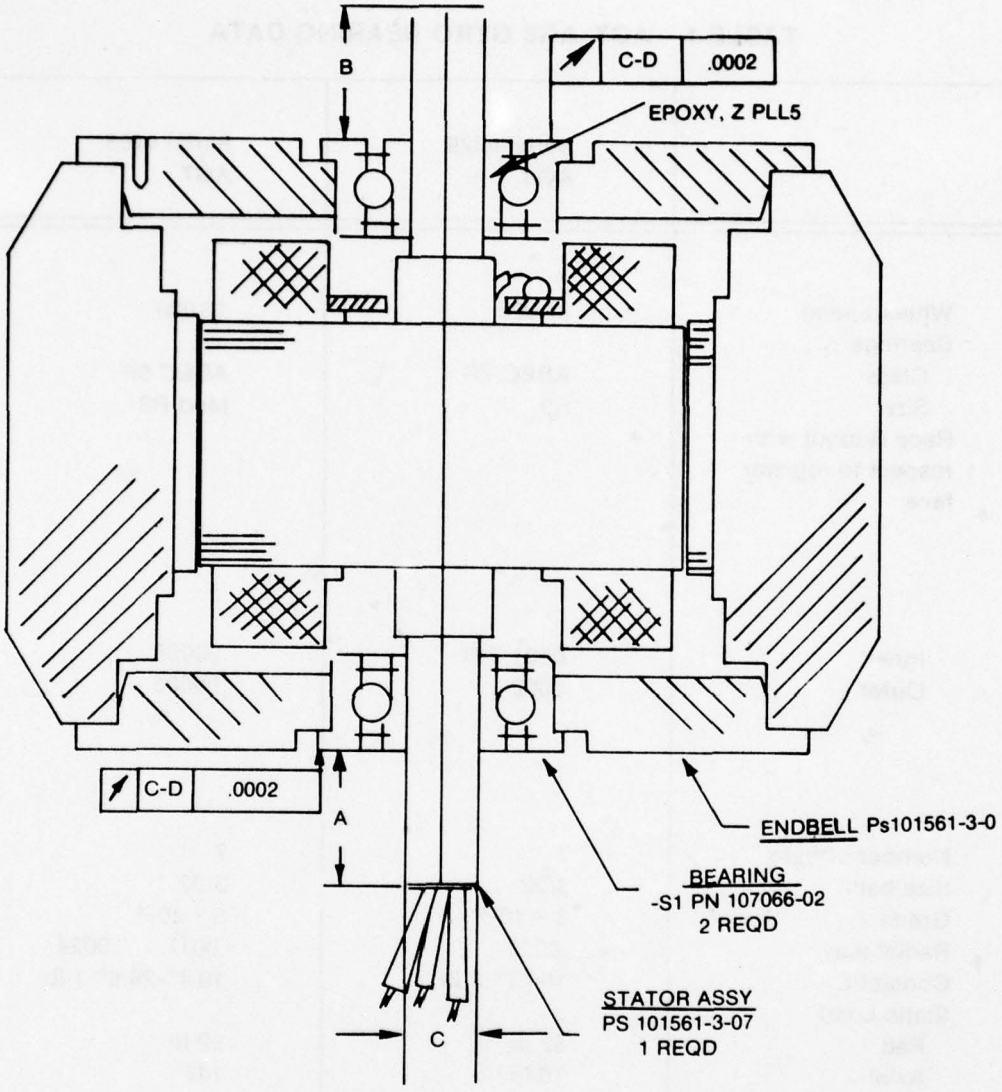

H = 3.5 10^6 DYN CM SEL

FIRST ID DESIGN ADAPTION TO TIMEX GYRO WHEEL. EPOXY AT INNER BEARING DIAMETER WOULD NOT HOLD RELIABLY. SECOND ADAPTION INCLUDED A NUT TO REINFORCE THE EPOXY BOND.

NOTES:

1. DIM A & B SHALL BE EQUAL WITHIN .010
2. ASSEMBLE AND BALANCE AW APPLICABLE NOTES OF MC 159554.

Figure 2. Gyro Wheel AG7, half section serial no. 405

TABLE 1. AG7, AG8 GYRO BEARING DATA

	Serial #325 AG8	Serial #405 AG7
Wheel Speed	24,000	12,000
Bearings		
Class	ABEC 7P	ABEC 9P
Size	R3	Mod R3
Race Runout with respect to register face		
Inner	.0001 TIR	.00005
Outer	.0002	.00005
Number of balls	7	7
Size ball	3/32	3/32
Grade	3×10^{-6}	5×10^{-6}
Radial play	.0009	.0017 .0024
Contact L	15-17° 2 lb	19.4°-26.8° 1 lb
Static Load		
Rad	52 lb	52 lb
Axial	79 lb	147
Material	52100-60C	same
Shield	Stainless	Same
Retainers	Phenolic	Same
Load	DB matched pair @ spacer	load at assy dead wt.

MIRADCOM power spectral density analysis, a peak at a given frequency could selected by a variable notch filter. This narrow band of vibration signals passed by the notch filter were then detected such that the low frequency content of the high frequency burst could be observed.

3. RESULTS

A. General

Data was collected from four different gyro wheels. Preliminary data was collected on various configurations of two different gyro wheels from the Lear Seigler gyro compass. *Figures 3 through 6* illustrate the data collected on a U.S. time gyro wheel, serial number 519, as noted, the 100 mv/g instrument accelerometer was mounted on the mounting surface of the gyro wheel and adjacent to a trunnion for the wheel bearing. *Figure 3* shows that there are noise present out to approximately 50 KH_Z with the most prevelent discretes below 25 KH_Z. *Figure 4* and *5* illustrate that the predominant factor is the 2X excitation frequency and harmonics of that turn should be discrete.

Lear gyro wheel, serial number 513, was the next wheel considered in the preliminary data. Unit 513 was operated without, *Figures 7-9*, and with the gyro compass pendulum, *Figures 10-17*.

Figure 7 shows the vibration data over a 2500 H_Z spectrum. In this spectrum, a 70 mg peak is present at 1500 H_Z. However, when the pass band is dropped to 1000 H_Z, the 2X excitation frequency peak shows up. In *Figures 8* and *9*, there seems to be a discrete at 100 H_Z intervals beginning at 400 H_Z.

Figure 10 was recorded with the ballast in place and the 100 mv/g accelerometer mounted on the bottom of the ballast. The 2X excitation frequency is very obvious the only significant discrete in this data. Over the 1000 H_Z spectrums in *Figure 11*, the 800 H_Z discrete is still predominant. However, when the spectrum is reduced below 800 H_Z, see *Figure 12*, other discretes appear with no particular pattern.

Figure 13 illustrates the vibration data on the pendulum mast out to 100 KH_Z. Distinct bands of noise can be seen. One such band occurs from the low end out to 25 KH_Z, and a similar band centered at 51 KH_Z.

Figure 14 distinctly reflect the 2X excitation frequency discrete. However, as expected, when the spectrum deletes the 800 H_Z discrete,

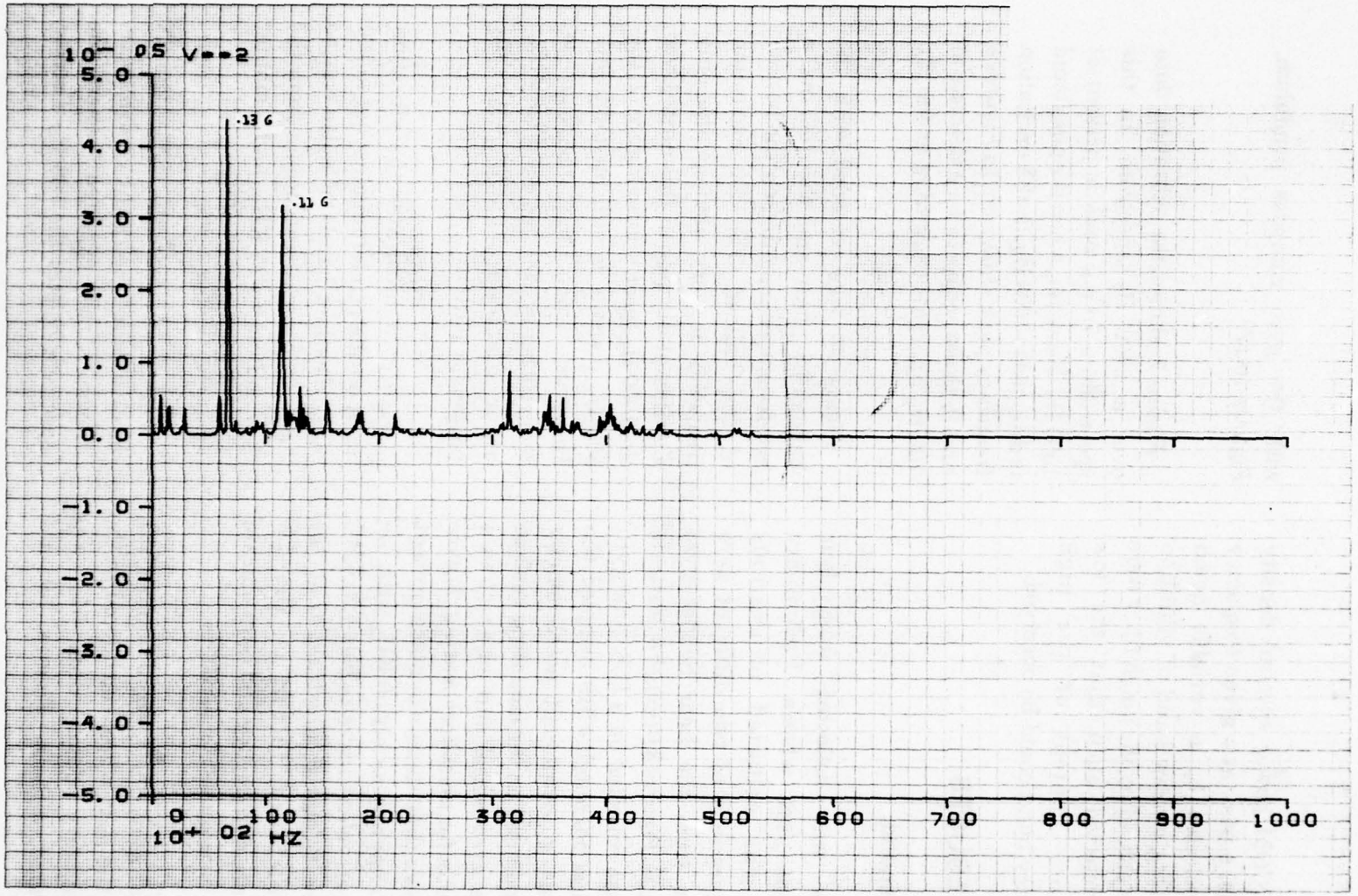

Figure 3. U.S. Time Gyro (Ser. No. 519) 100 mv/g Accelerometer Monitor mounted on Gyro Flange
Filter: 2 pole low pass at frequency limit

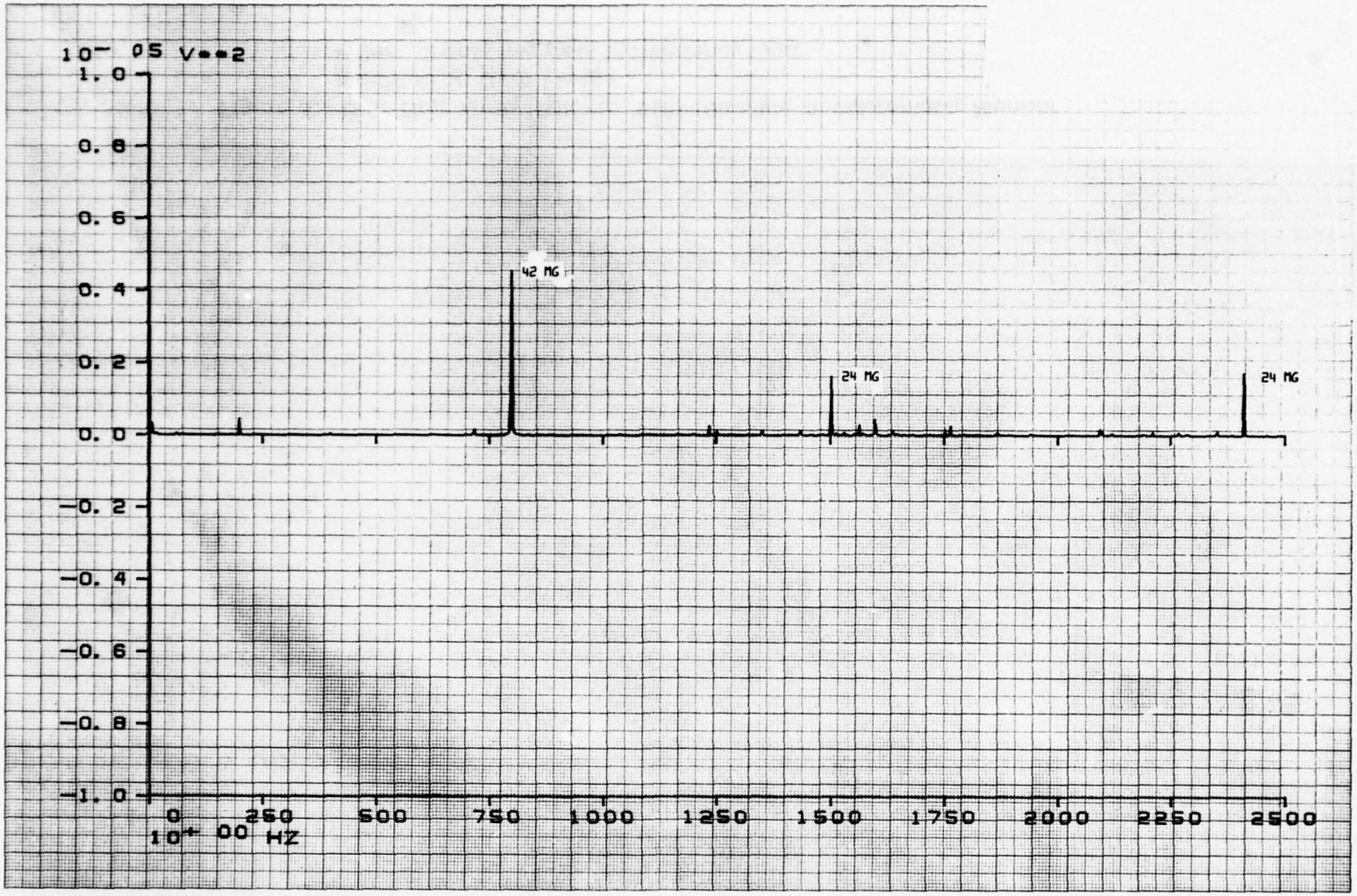

Figure 4. U.S. Time Gyro (Ser. No. 519) 100 mv/g Accelerometer Monitor mounted on Gyro Flange
Filter: 2 pole low pass at frequency limit

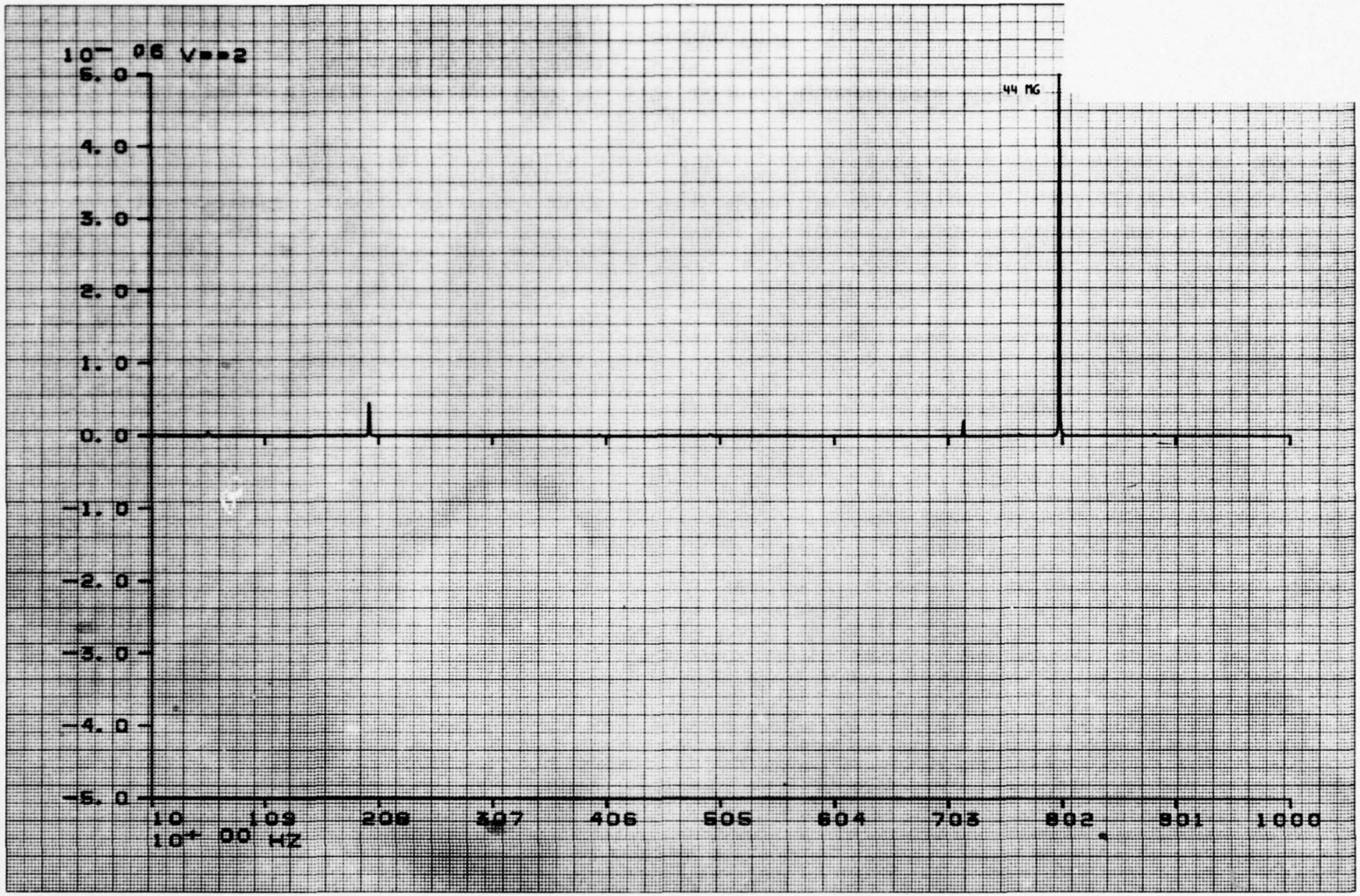

Figure 5. U.S. Time Gyro (Ser. No. 519) 100 mv/g Accelerometer Monitor mounted on Gyro Flange
Filter: 2 pole low pass at frequency limit

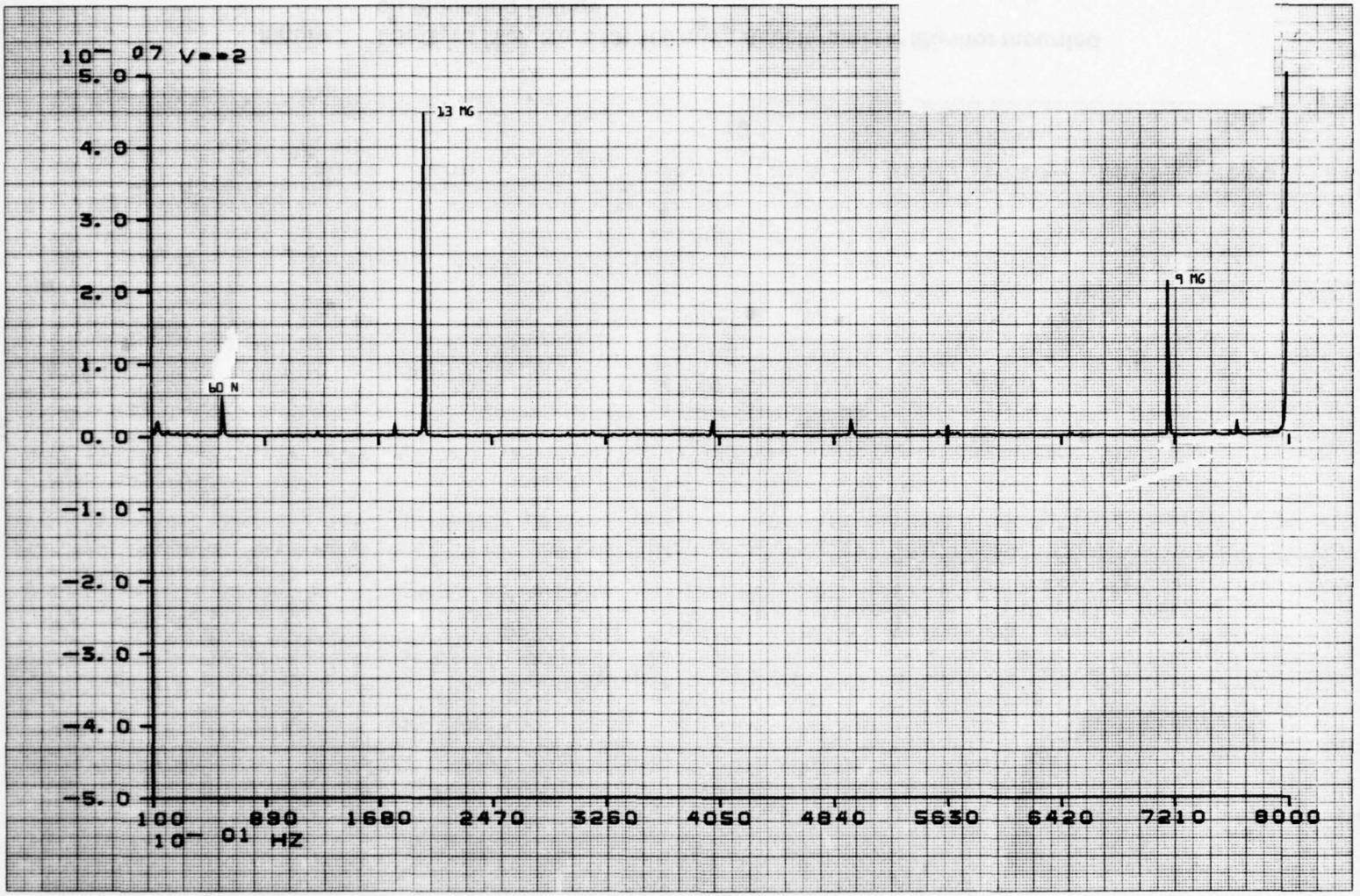

Figure 6. U.S. Time Gyro (Ser. No. 519) 100 mv/g Accelerometer Monitor mounted on Gyro Flange
Filter: 2 pole low pass at frequency limit

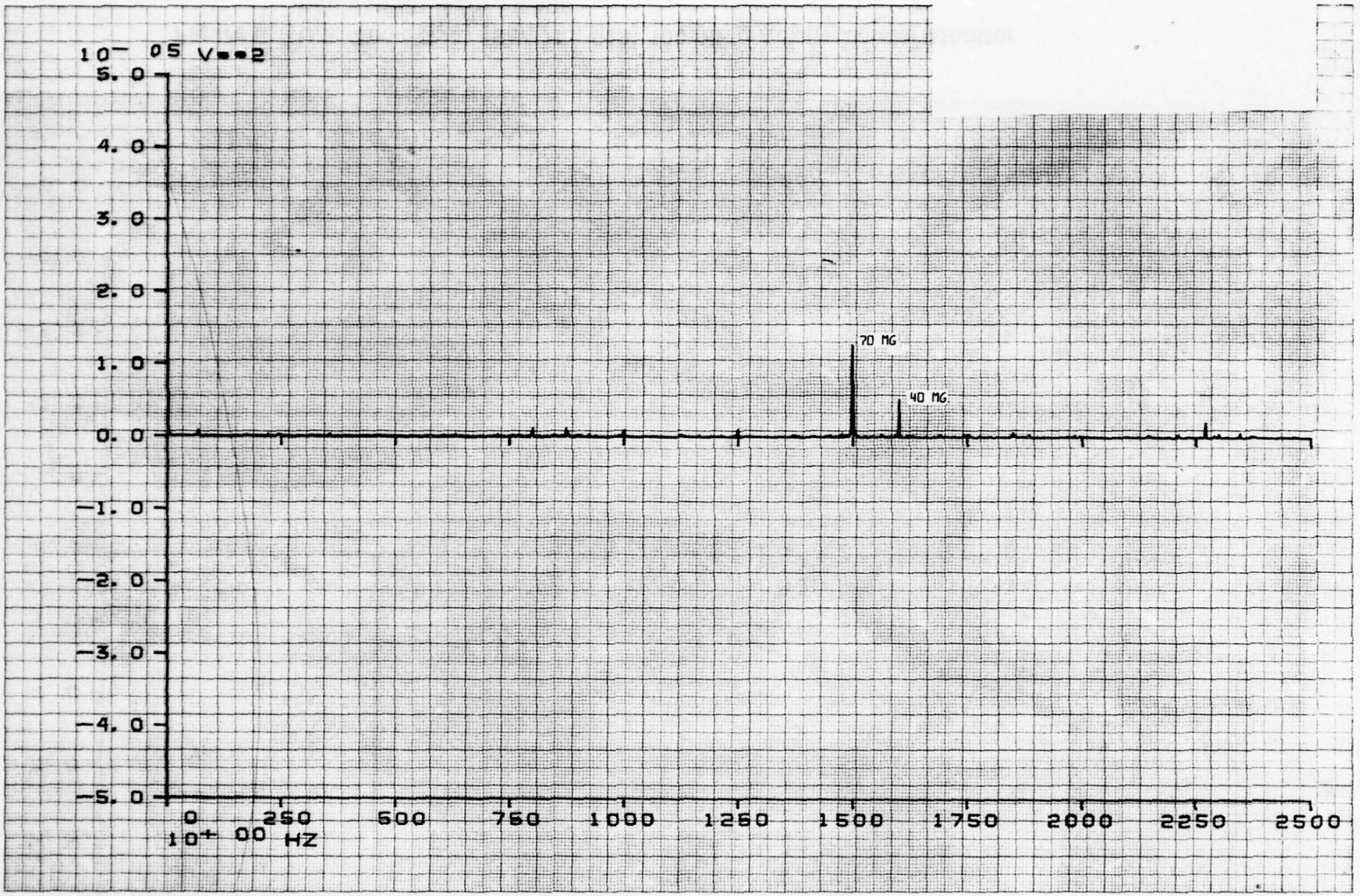

Figure 7. LSI Gyro (Ser. No. 513) 100 mv/g Accelerometer Monitor mounted on Mounting Flange
Filter: 2 pole low pass at frequency limit

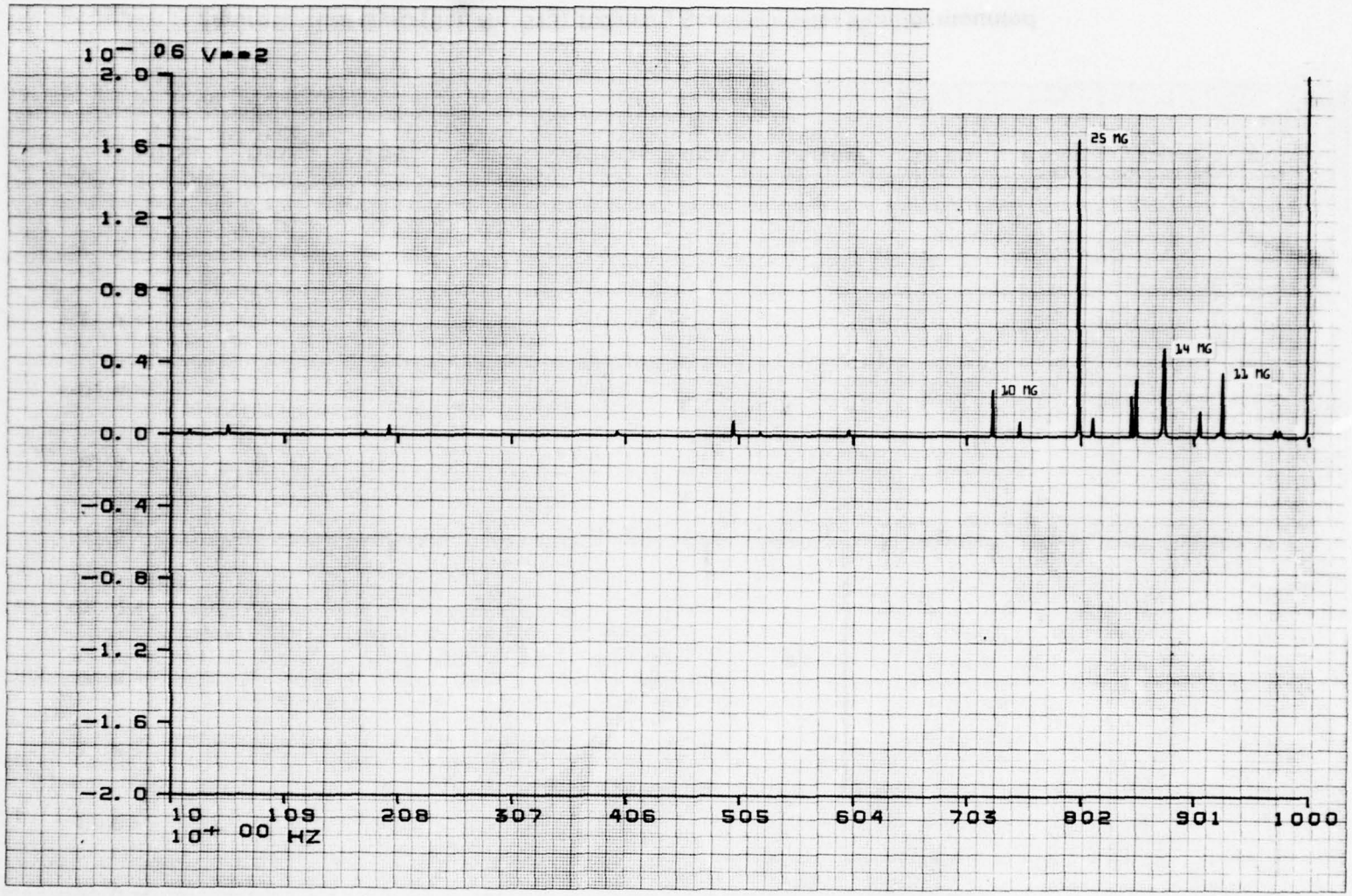

Figure 8. LSI Gyro (Ser. No. 513) 100 mv/g Accelerometer Monitor mounted on Mounting Flange
Filter: 2 pole low pass at frequency limit

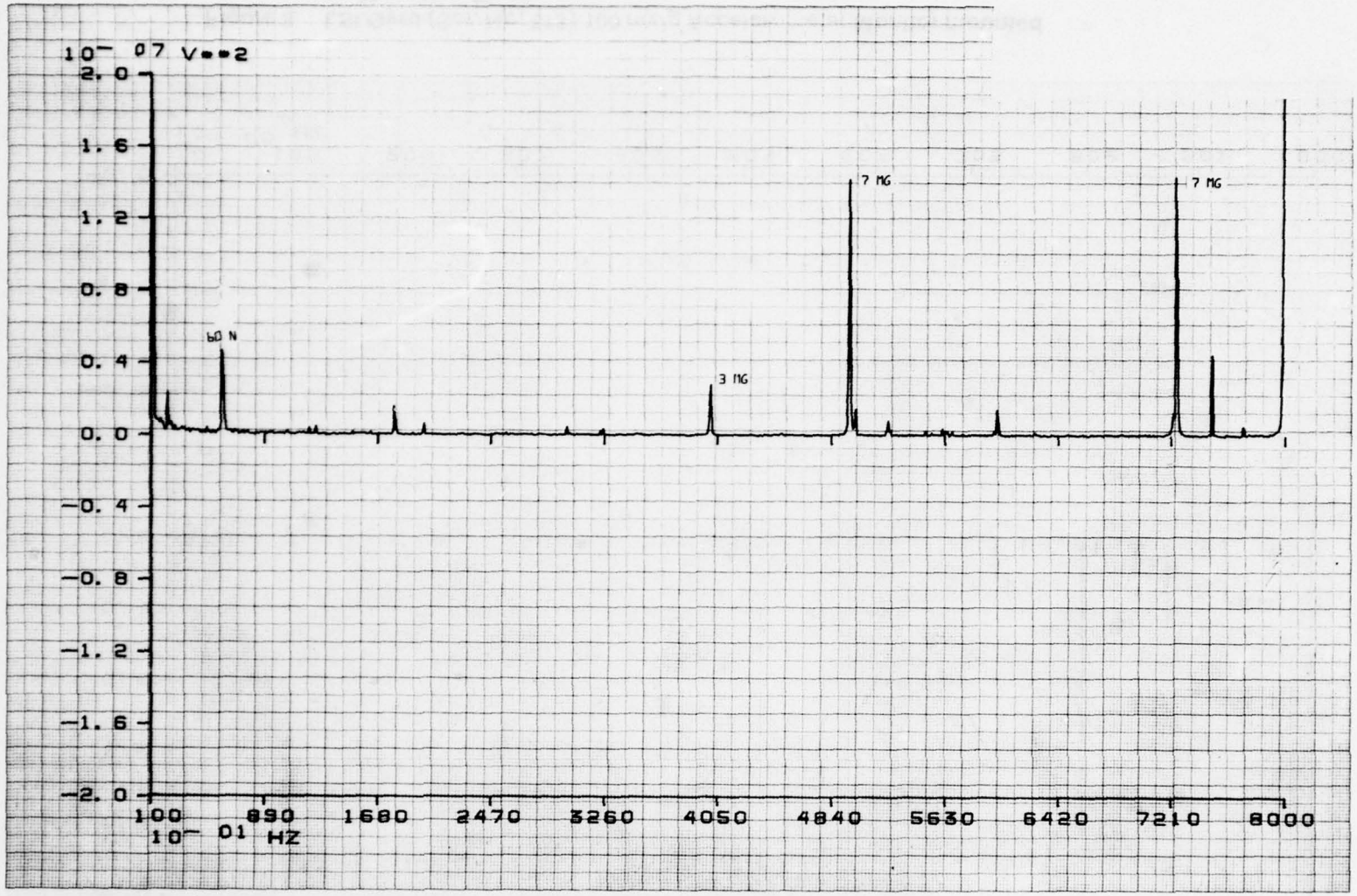

Figure 9. LSI Gyro (Ser. No. 513) 100 mv/g Accelerometer Monitor mounted on Mounting Flange
Filter: 2 pole low pass at frequency limit

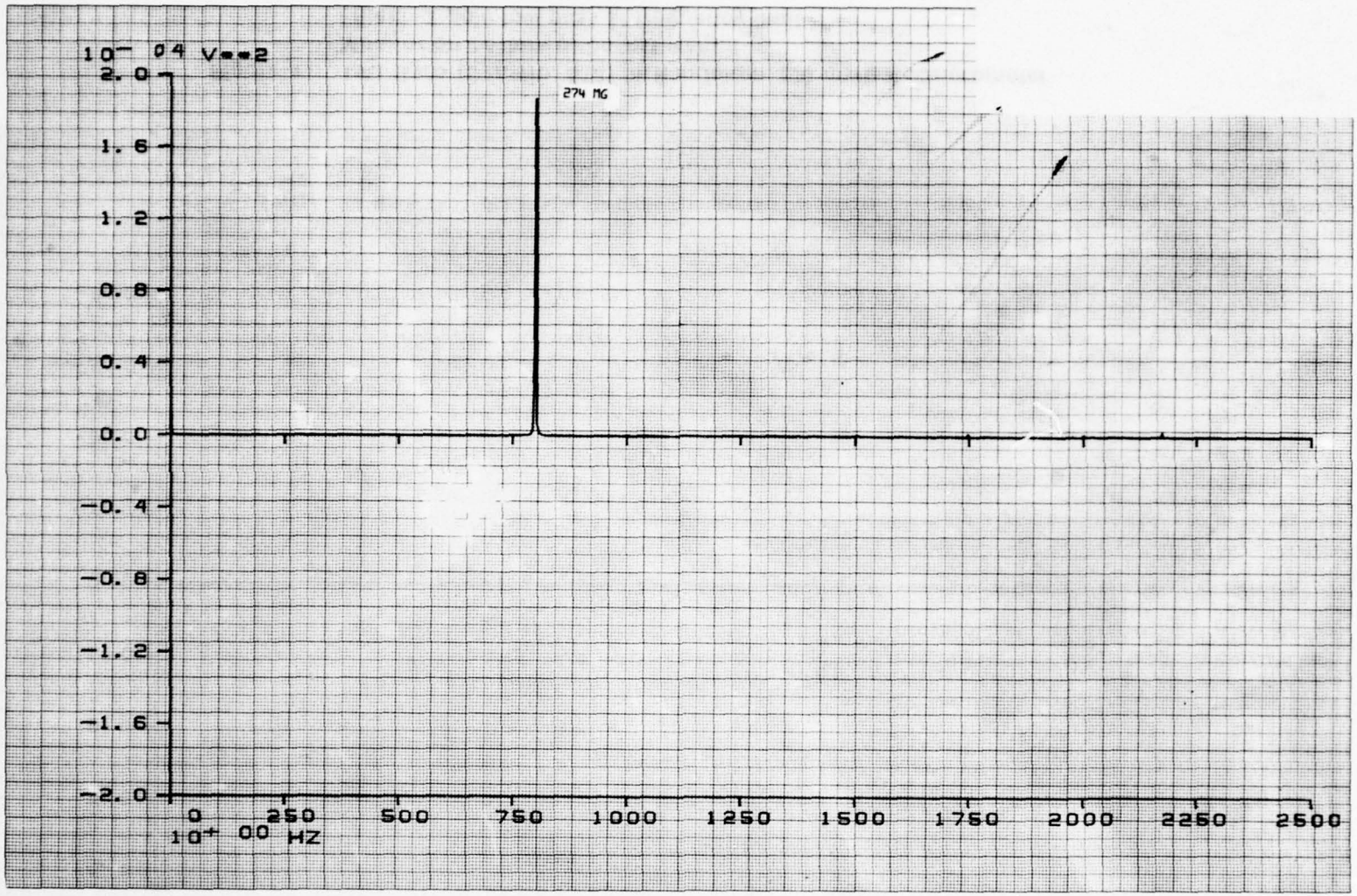

Figure 10. LSI Gyro (Ser. No. 513) in Pendulum 100 mv/g Accelerometer
Monitor on bottom of ballast weight
Filter: 2 pole low pass at frequency limit

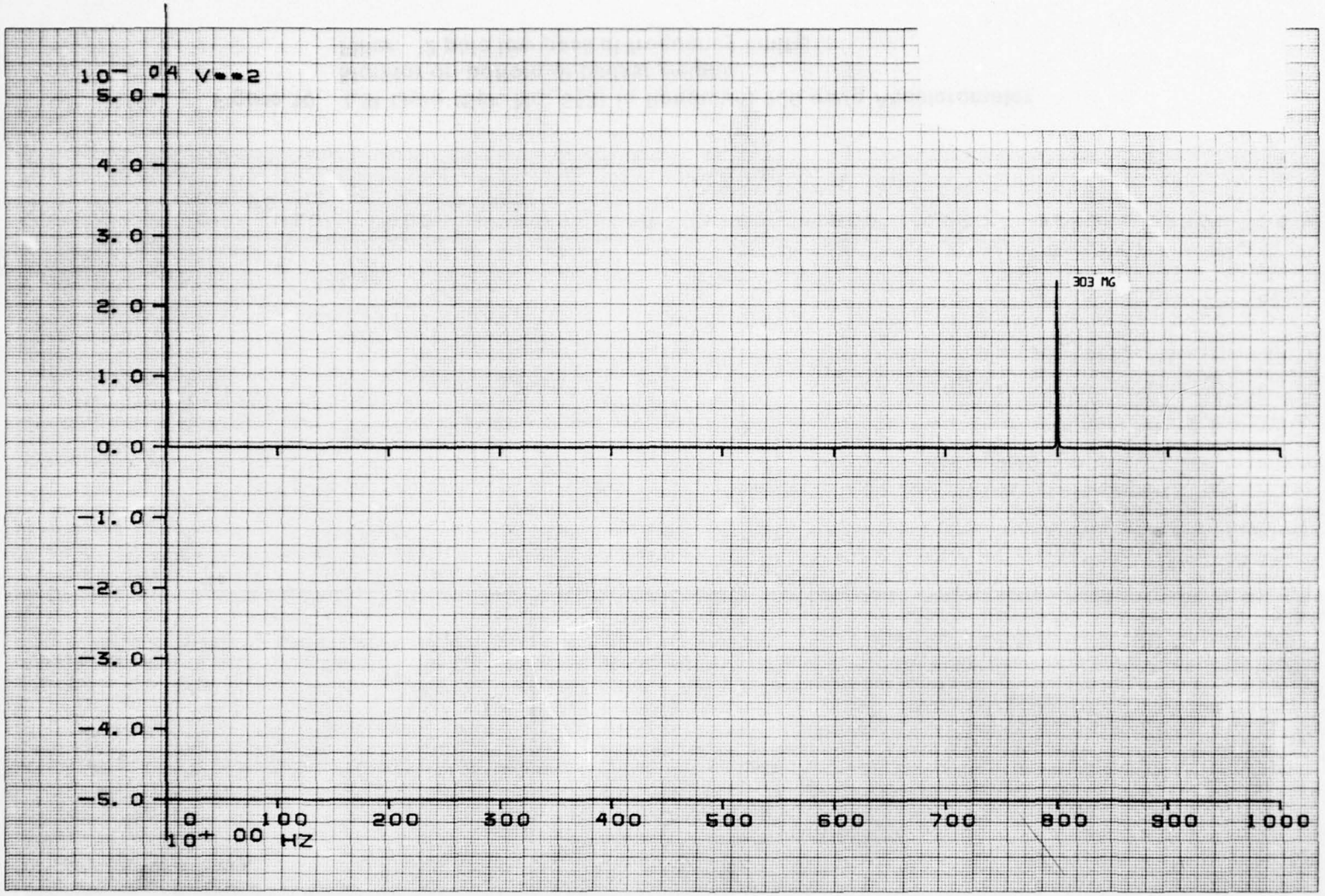

Figure 11. LAI Gyro (Ser. No. 513) in Pendulum 100 mv/g Accelerometer
Monitor on bottom of ballast weight
Filter: 2 pole low pass at frequency limit

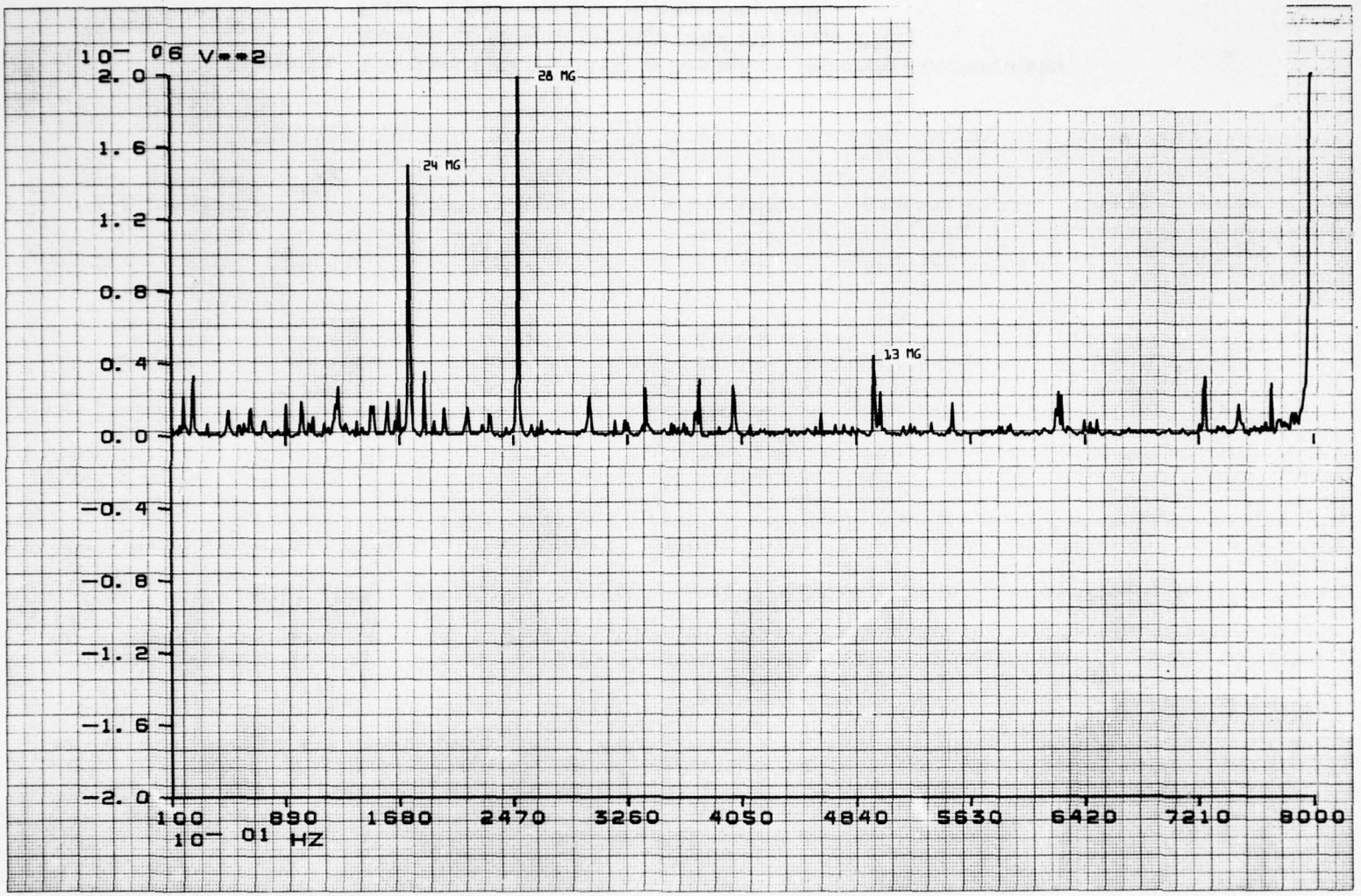

Figure 12. LSI Gyro (Ser. No. 513) in Pendulum 100 mv/g Accelerometer
Monitor on bottom of ballast weight
Filter: 2 pole low pass at frequency limit

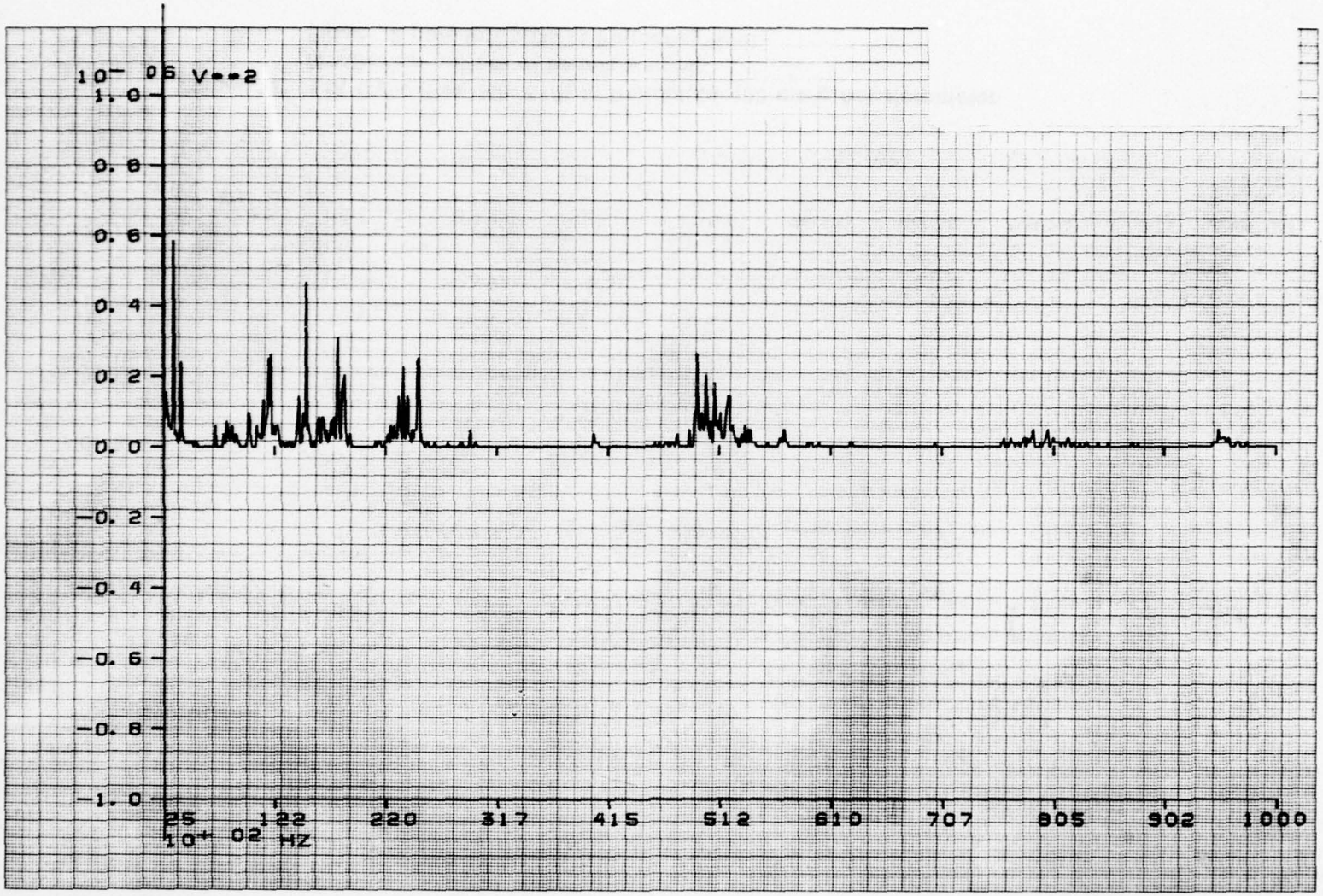

Figure 13. LSI Gyro (Ser. No. 513) in Pendulum. 100 mv/g Accelerometer Monitor on Mast of top disk (disk thickness .070")
Filter: 2 pole low pass at frequency limit

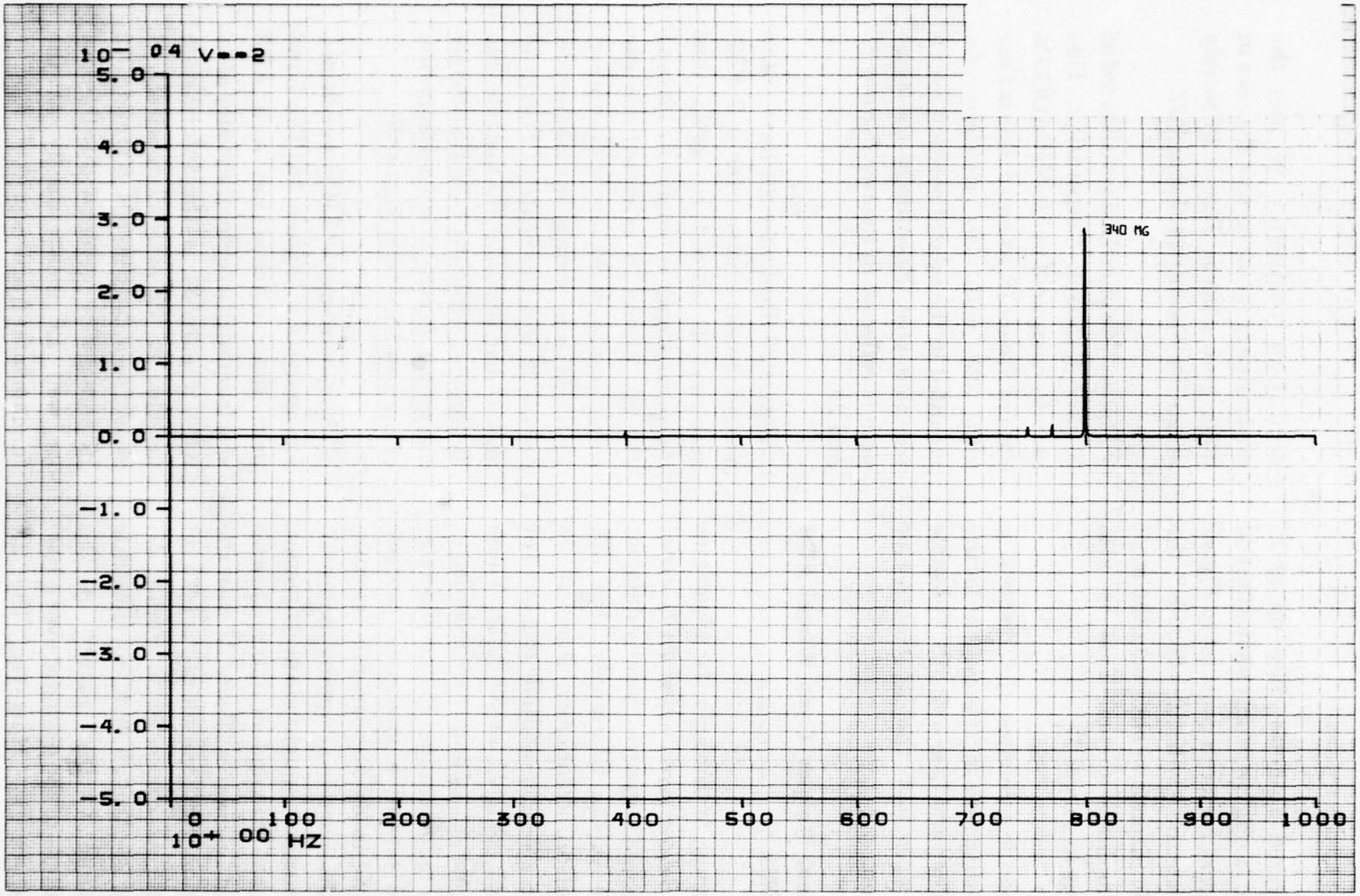

Figure 14. LSI Gyro (Ser. No. 513) in Pendulum 100 mv/g Accelerometer Monitor on Mast of top disk (disk thickness .070")
Filter: 2 pole low pass at frequency limit

suppressed discretes show up as in *Figure 15*. *Figure 16* only shows the 800 H3 discrete. But in contrast to *Figure 13* where the low limit is 2500 H3, the 800 H3 discrete is obviously the most predominated factor. This is also obvious in *Figure 17*.

Table 2 tabulates the discrete g levels that were most prevalent for the U.S. Time and Lear unit 513. The table also specifies the accelerometer location.

B. Lear Seigler Gyro Wheel AG8 Data

Figures 18 through 21 illustrates Lear Seigler gyro wheel AG8, serial number 325, spectral density data out to 50 KH3. Obviously, the 2X excitation frequency discrete is comparable in magnitude to a band of discrete centered at 23 KH3. These duplicate sets of data were recorded in order to determine if the discretes tended toward a stochastic process. This did in deed occur. For example, note the discrete at approximately 10 KH3 varies in amplitude as a function of time. This random nature is more evident in *Figures 22 and 23* with the variation in magnitude of the 1425 H3 discrete as compared to *Figure 21*. *Figure 24 through 27* again illustrate the time varing nature of the magnitude of the discretes over a 1000 H3 spectrum. However, the 2X excitation frequency is not the predominant factor as was the case in other gyro wheels. *Figure 28* merely magnifies *Figures 24 through 27*.

Figure 29 begins the data collected at Shaker Research Corporation. This may be compared to the MIRADCOM data of *Figure 18*, as noted, this is Lear unit 325 with the accelerometer mounted in the second position over a trunnion post. Essentially the same data is reflected in the two *Figures 18* and *29*.

Figure 30 illustrates the data of the second accelerometer over a 2 KH3 spectrum. It should be noted that discrete spacing is nominally 170 and 240 H3. *Figure 31* is essentially the same as *Figure 30*, but a discrete at 1360 H3 has grown in magnitude. *Figure 32* is a duplicate of *Figure 30 and 31* but the 1360 H3 discrete has diminished while the 1478 H3 discrete has grown. *Figure 33* is a continuation of the sequence from *Figure 30*.

The spectrum at 22 KH3 was selected for analysis in *Figure 34*. The band pass filter notched out a 2 KH3 spectrum with a center frequency at 22 KH3. *Figure 34* is the information detected in the selected spectrum. It should be noted that 504, 800 and 1372 H3 signal were present within the data as well as independently at the fundamental frequency.

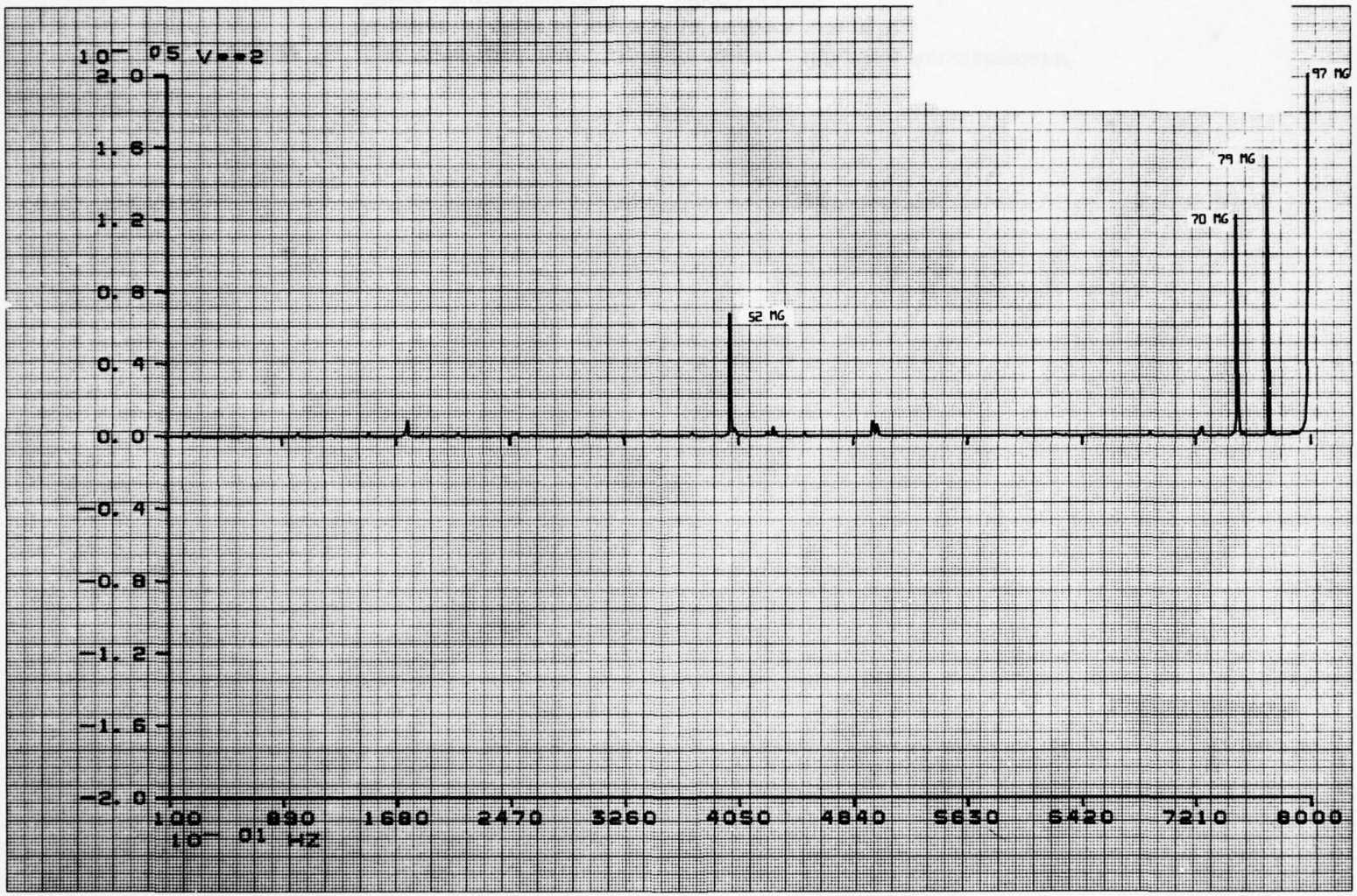

Figure 15. LSI Gyro (Ser. No. 513) in Pendulum 100 mv/g Accelerometer Monitor on Mast of top disk (disk thickness .070")
Filter: 2 pole low pass at frequency limit

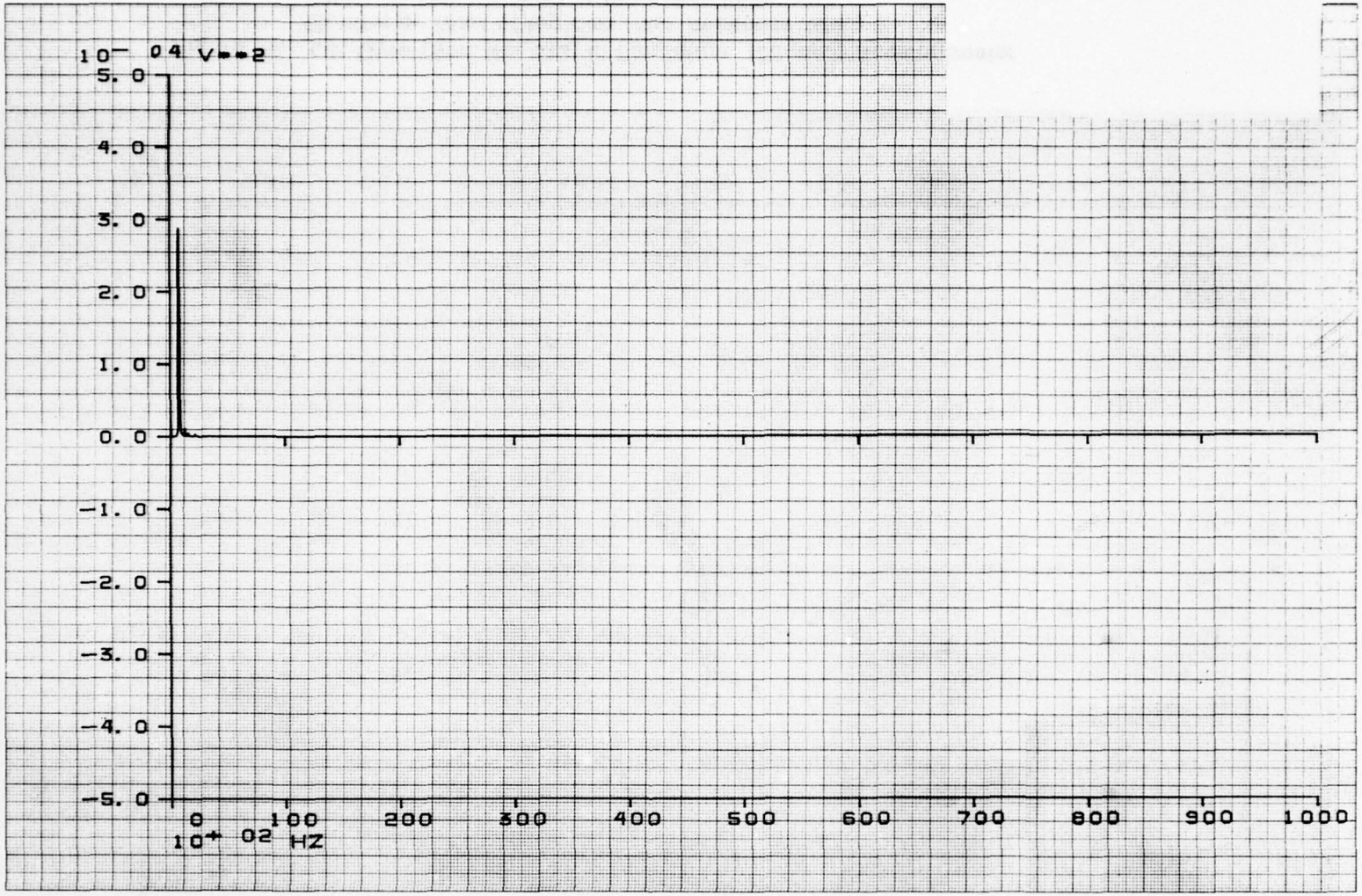

Figure 16. LSI Gyro (Ser. No. 513) in Pendulum 100 mv/g Accelerometer Monitor on Mast of top disk (disk thickness .070")
Filter: 2 pole low pass at frequency limit

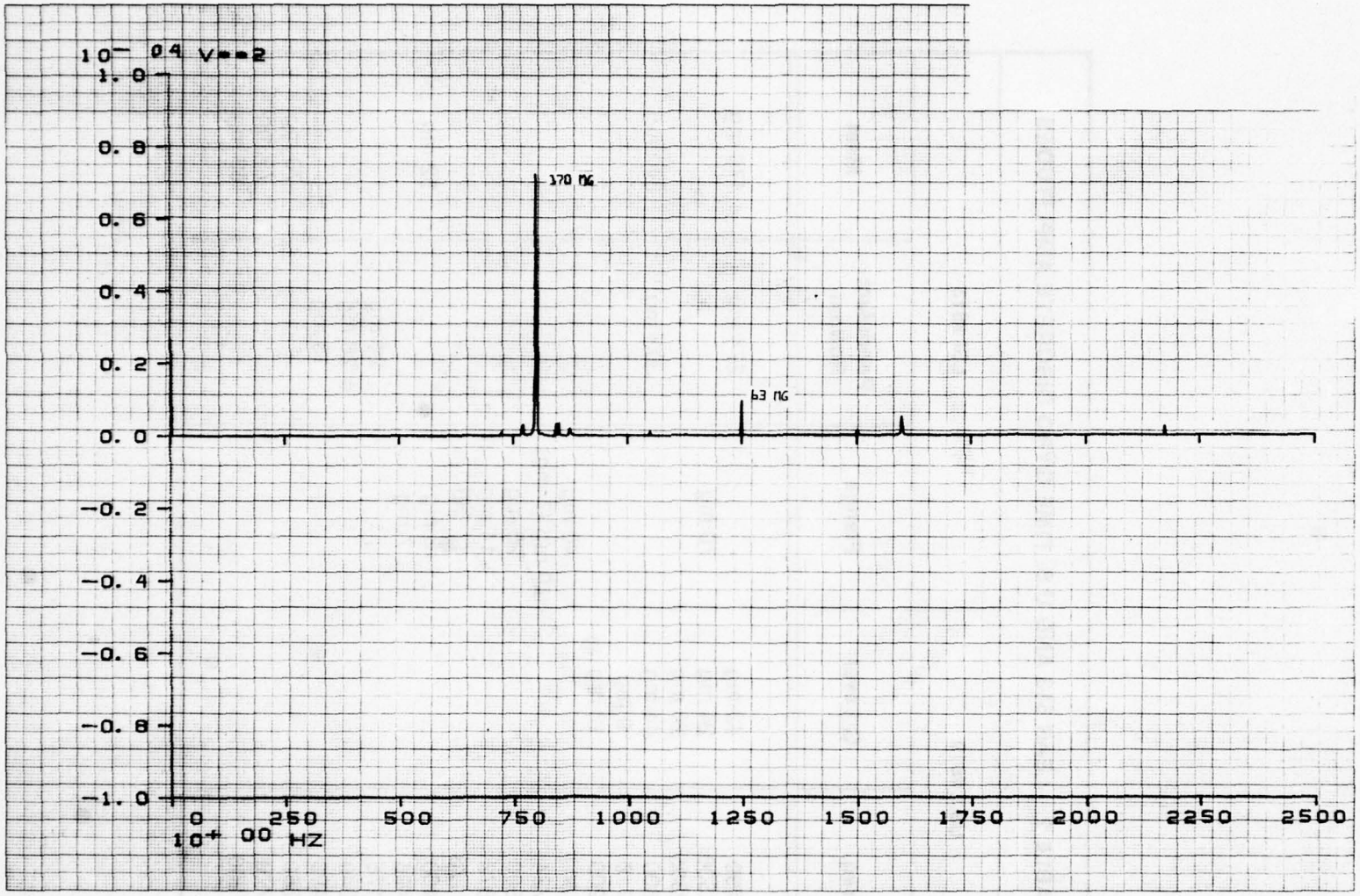

Figure 17. LSI Gyro (Ser. No. 513) in Pendulum 100 mv/g Accelerometer Monitor on Mast of top disk (disk thickness .070")
Filter: 2 pole low pass at frequency limit

TABLE 2. LEAR 513 AND U.S. TIME GYRO DISCRETE AMPLITUDES

UST #519		LSI #513		
Freq.	**G Level**	**Flange**	**Pendulum Bottom**	**Mast**
790	42 mg		274 mg	170 mg
1500	24 mg	70 mg		
2385	24 mg			
800	44 mg		303 mg	340 mg
716	9 mg			
200	13 mg			
1601		40 mg		
724		10 mg (7 mg)		
800		25 mg		
873		14 mg		
1173		11 mg		
400		3 mg		52 mg
496		7 mg		
175			24 mg	
249			28 mg	
496			13 mg	
750				70 mg
770				79 mg
1250				63 mg

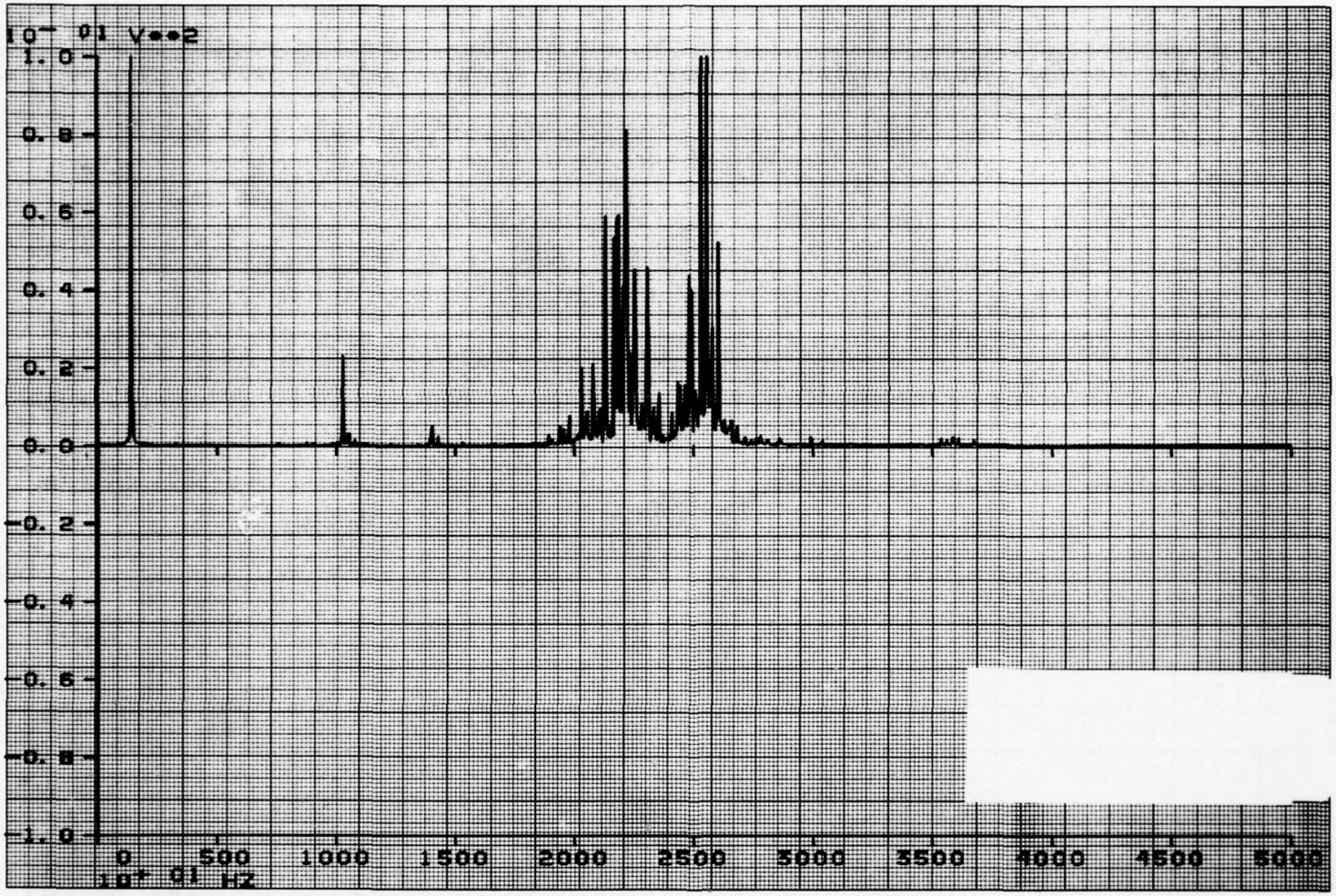

Figure 18. LSI Gyro Serial #325, 2 pole lo-pass filter @ 52 Kc, 26 volt, 1 phase, 400 Hz excitation, scale 16 mg/div

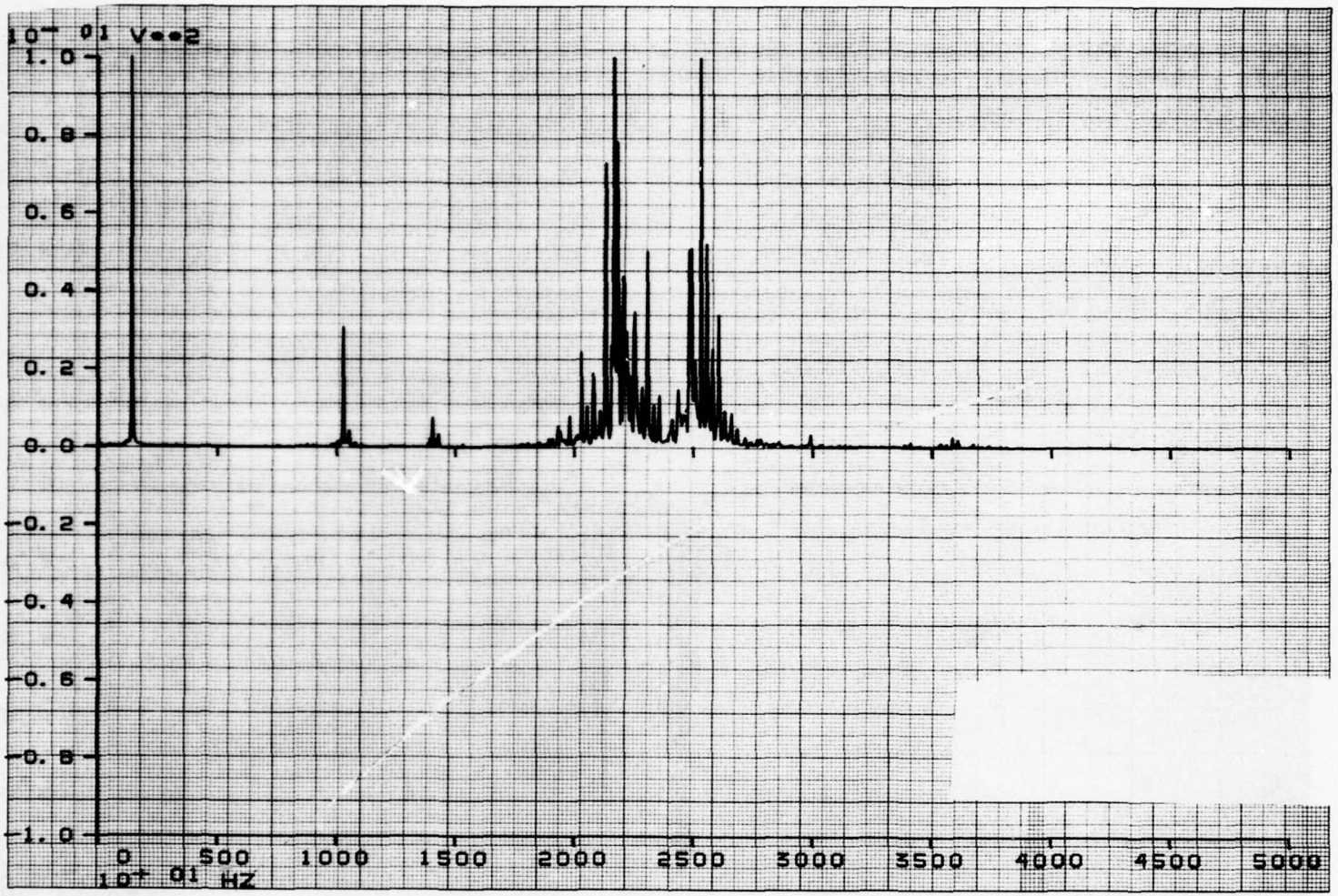

Figure 19. LSI Gyro Serial #325, 2 pole lo-pass filter @ 52 Kc, 26 volt, 1 phase, 400 Hz excitation, scale 16 mg/div

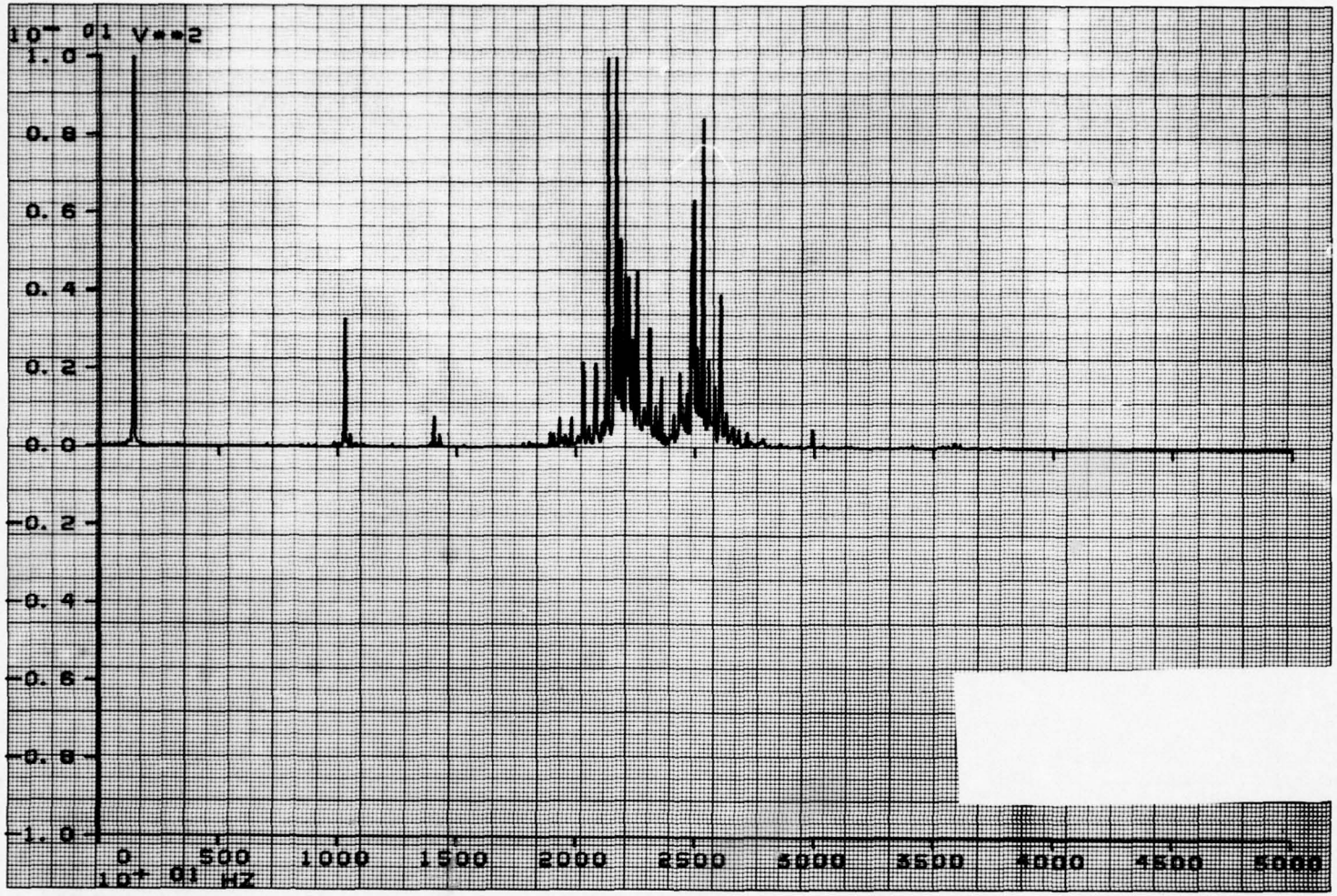

Figure 20. LSI Gyro Serial #325, 2 pole lo-pass filter @ 52 Kc, 26 volt, 1 phase, 400 Hz excitation, scale 16 mg/div

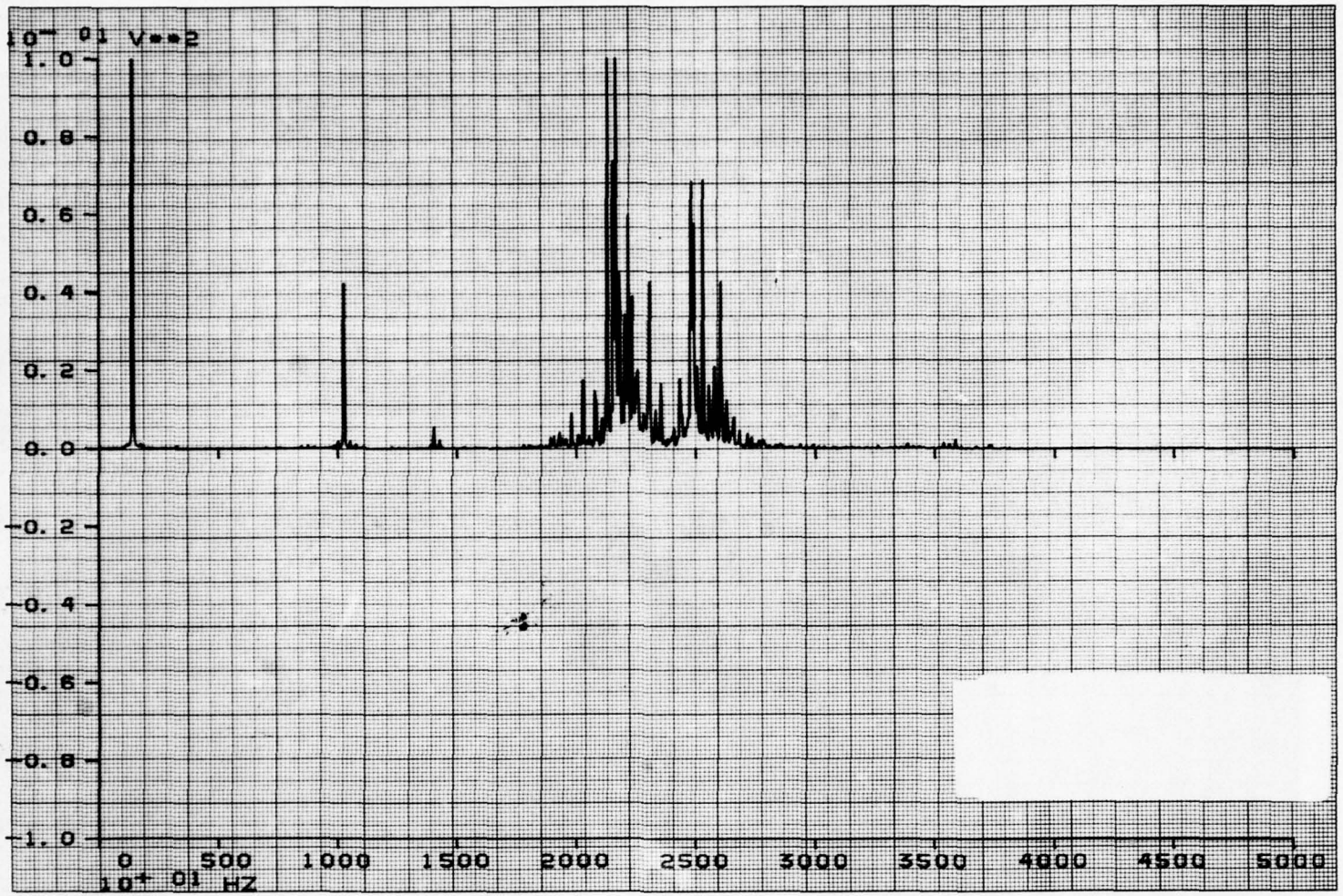

Figure 21. LSI Gyro Serial #325, 2 pole lo-pass filter @ 52 Kc, 26 volt, 1 phase, 400 Hz excitation, scale 16 mg/div

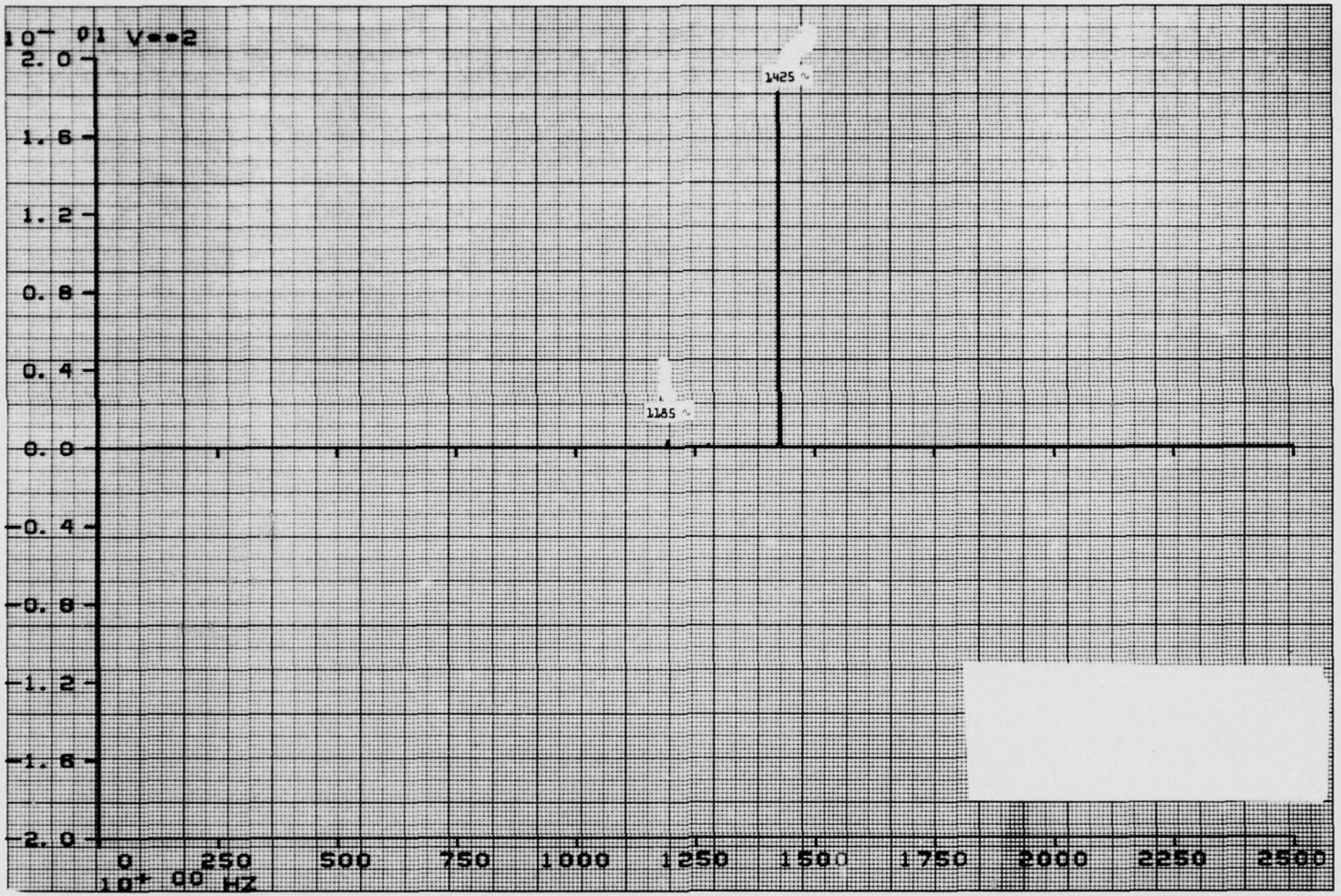

Figure 22. LSI Gyro Serial #325, 2 pole lo-pass filter @ 3 Kc, 26 volt, 1 phase, 400 Hz excitation, scale 23 mg/div

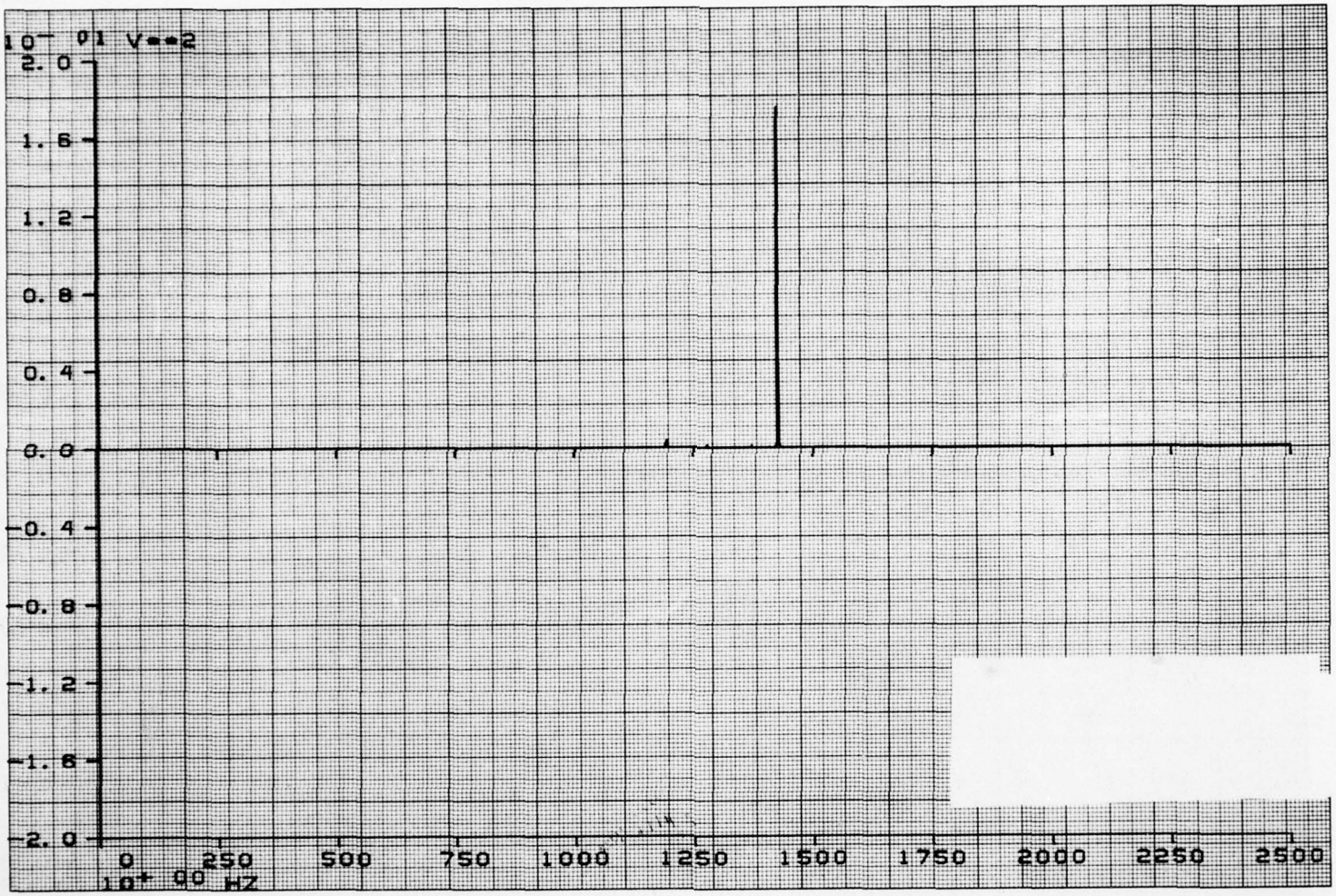

Figure 23. LSI Gyro Serial #325, 2 pole lo-pass filter @ 3 Kc, 26 volt, 1 phase, 400 Hz excitation, scale 23 mg/div

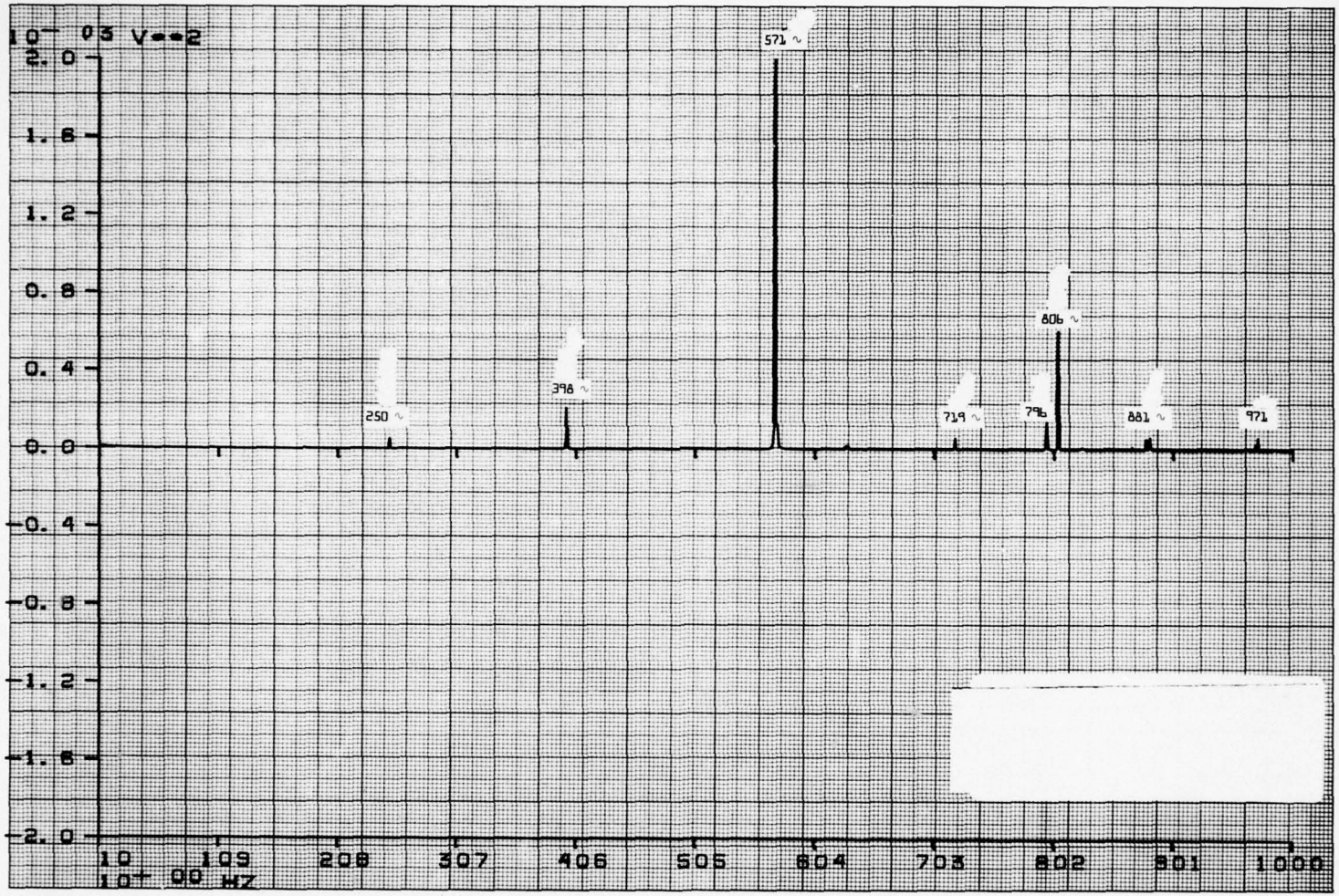

Figure 24. LSI Gyro Serial #325, 2 pole lo-pass filter ® 1 Kc, 26 volt, 1 phase, 400 Hz excitation, scale 2.3 mg/div.

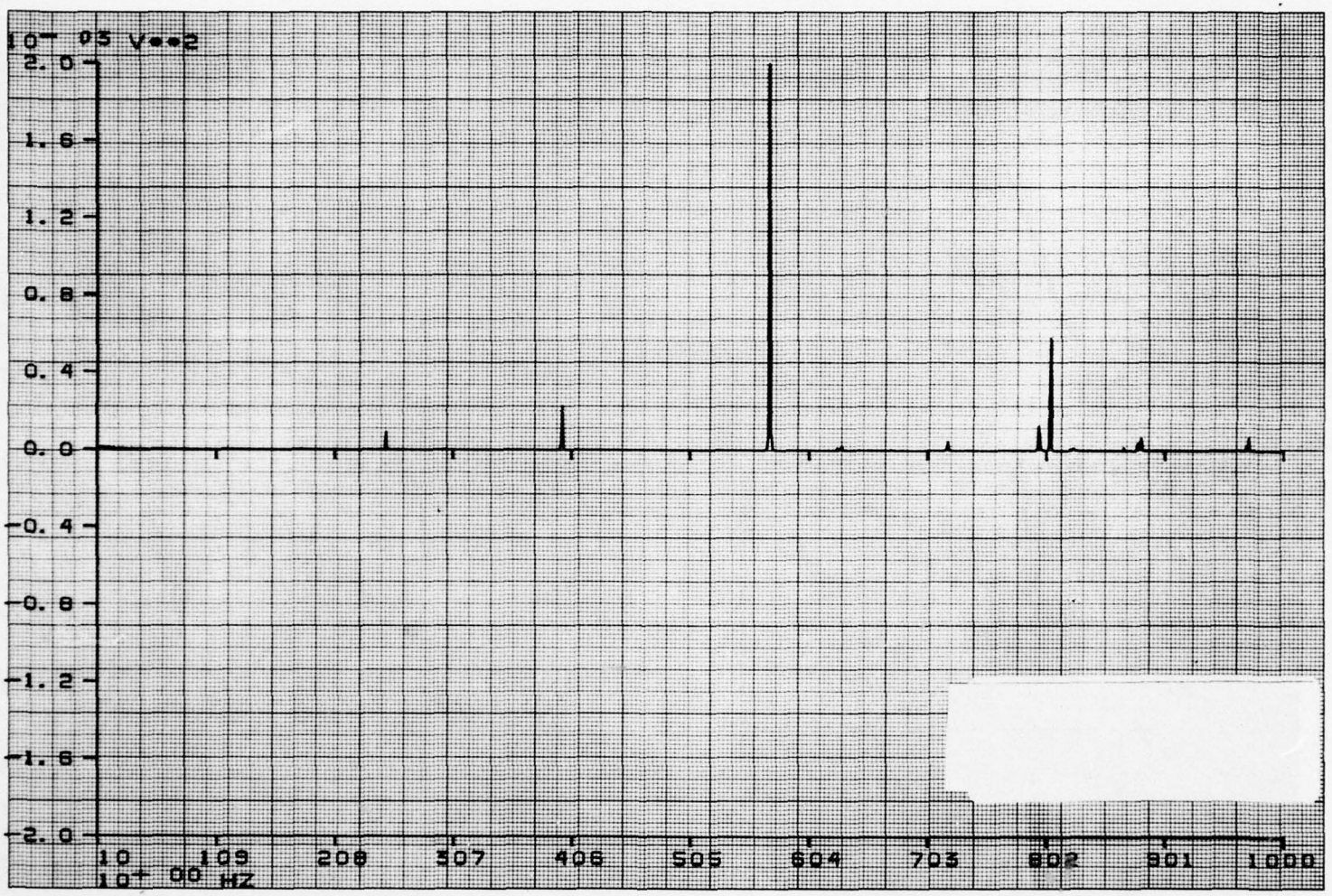

Figure 25. LSI Gyro Serial #325, 2 pole lo-pass filter @ 1 Kc, 26 volt, 1 phase, 400 Hz excitation, scale 2.3 mg/div

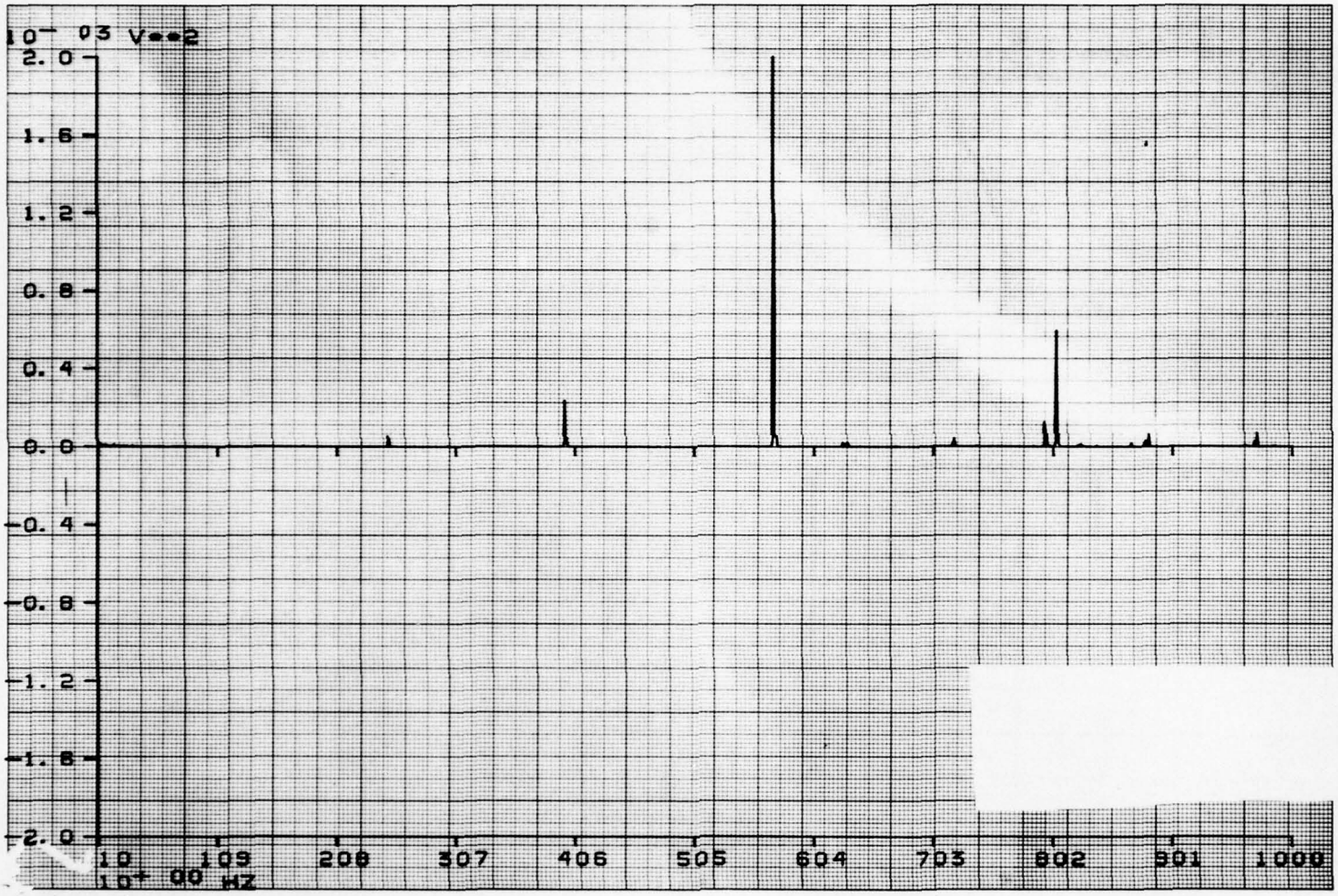

Figure 26. LSI Gyro Serial #325, 2 pole lo-pass filter @ 1 Kc, 26 volt, 1 phase, 400 Hz excitation, scale 2.3 mg/div

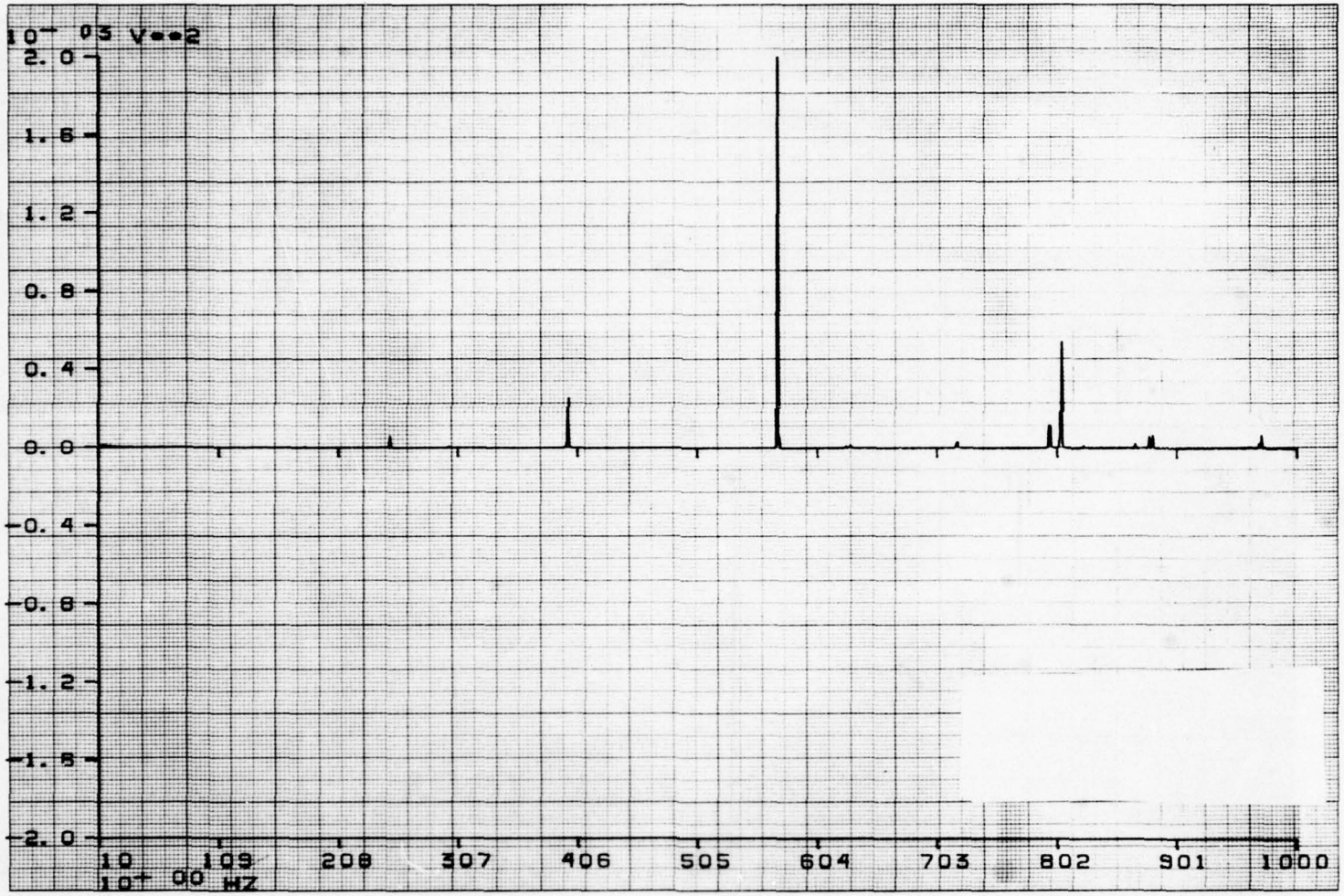

Figure 27. LSI Gyro Serial #325, 2 pole lo-pass filter @ 1 Kc, 26 volt, 1 phase, 400 Hz excitation, scale 2.3 mg/div

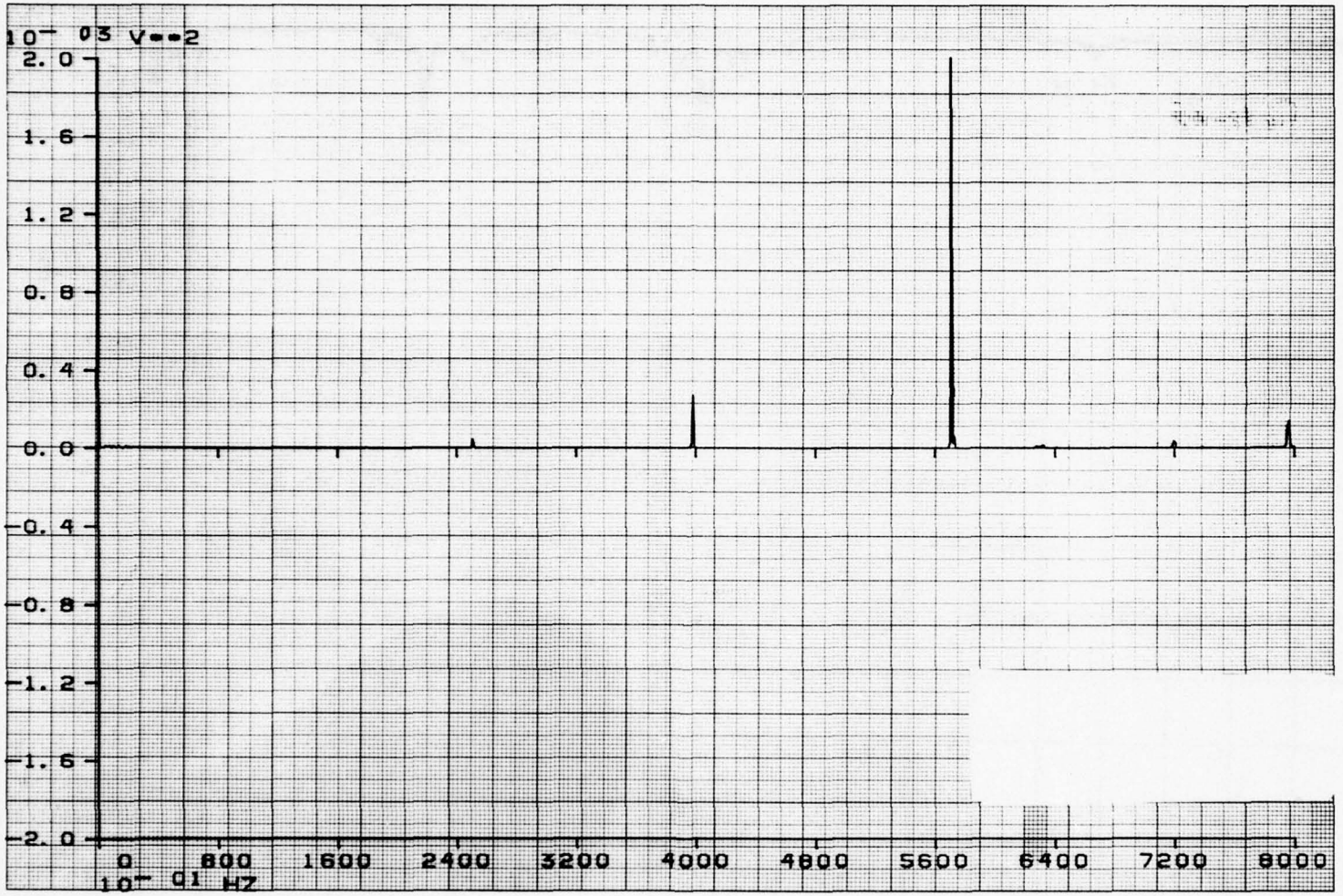

Figure 28. LSI Gyro Serial #325, 2 pole lo-pass filter @ 1 Kc, 26 volt, 1 phase, 400 Hz excitation, scale 2.3 mg/div

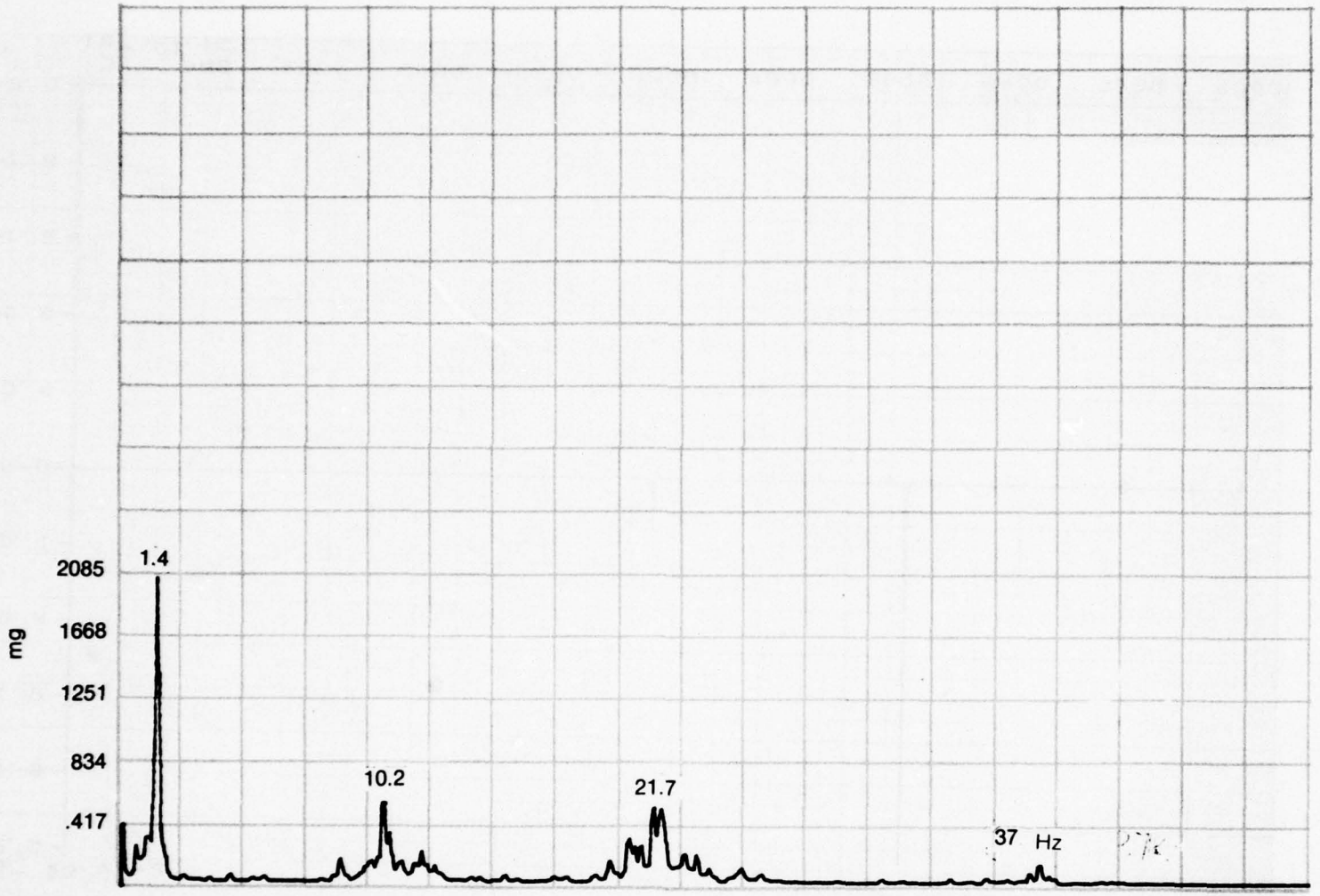

Figure 29. Shaker res. power spectral density 50 KHz.

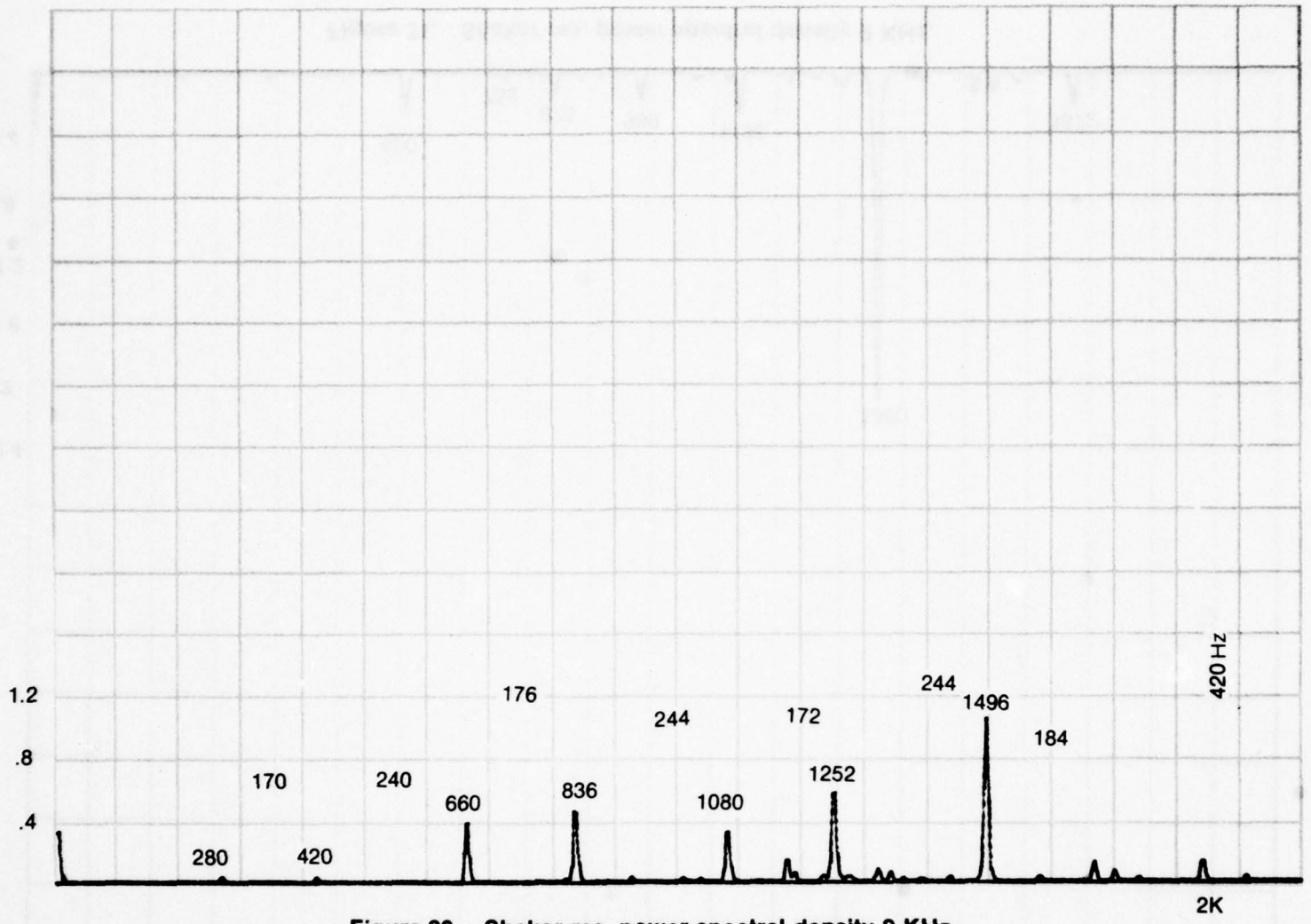

Figure 30. Shaker res. power spectral density 2 KHz.

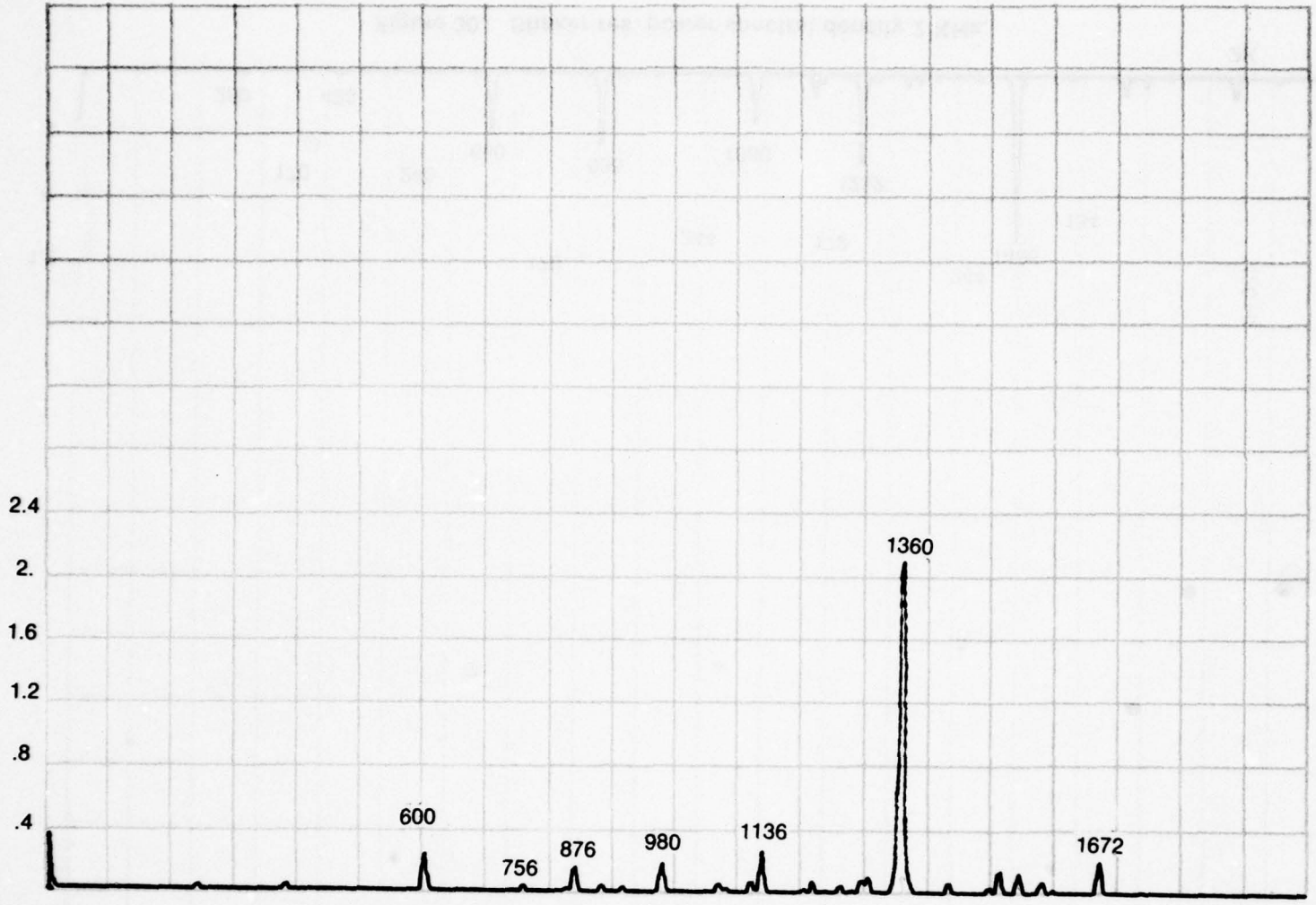

Figure 31. Shaker res. power spectral density 2 KHz.

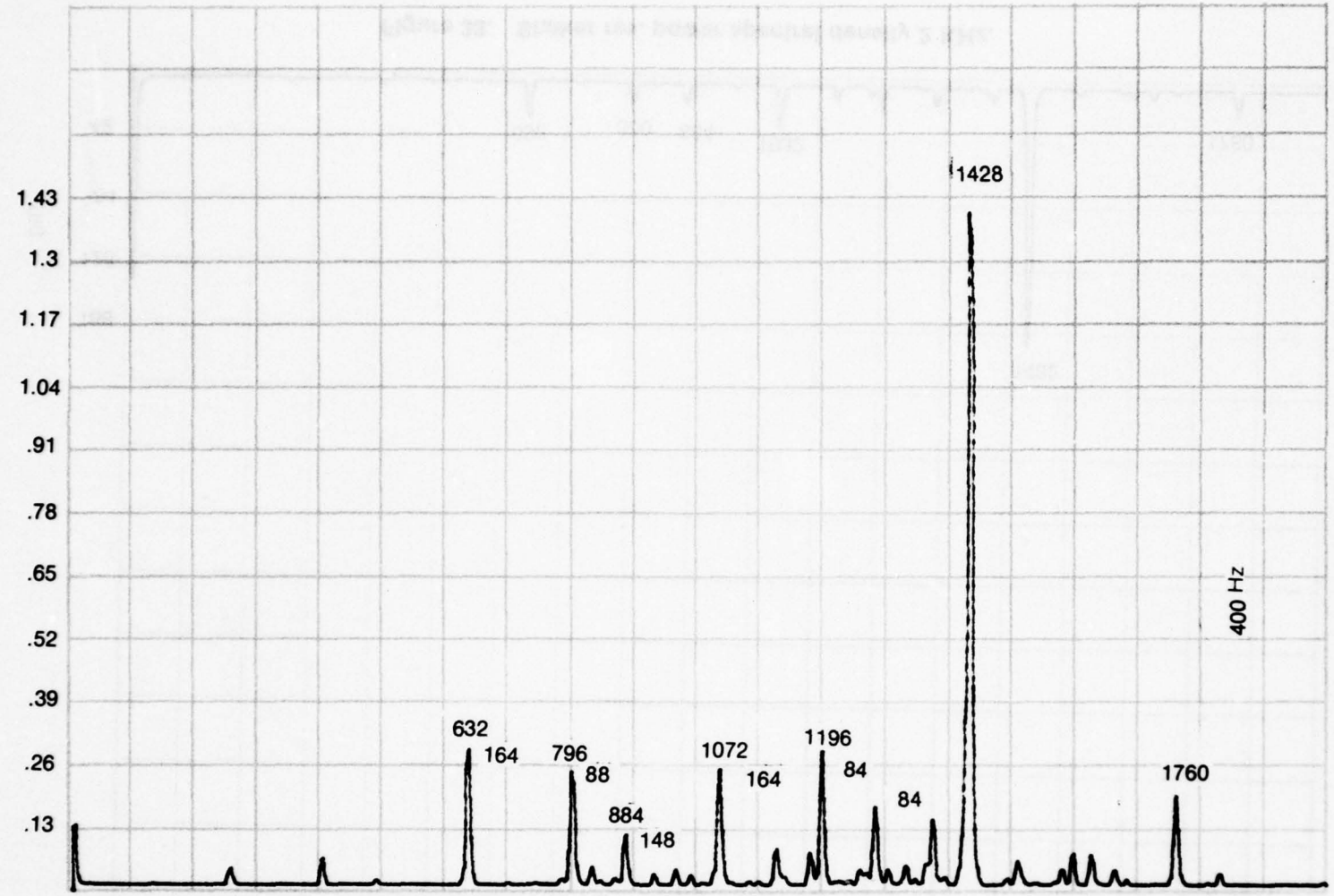

Figure 32. Shaker res. power spectral density 2 KHz.

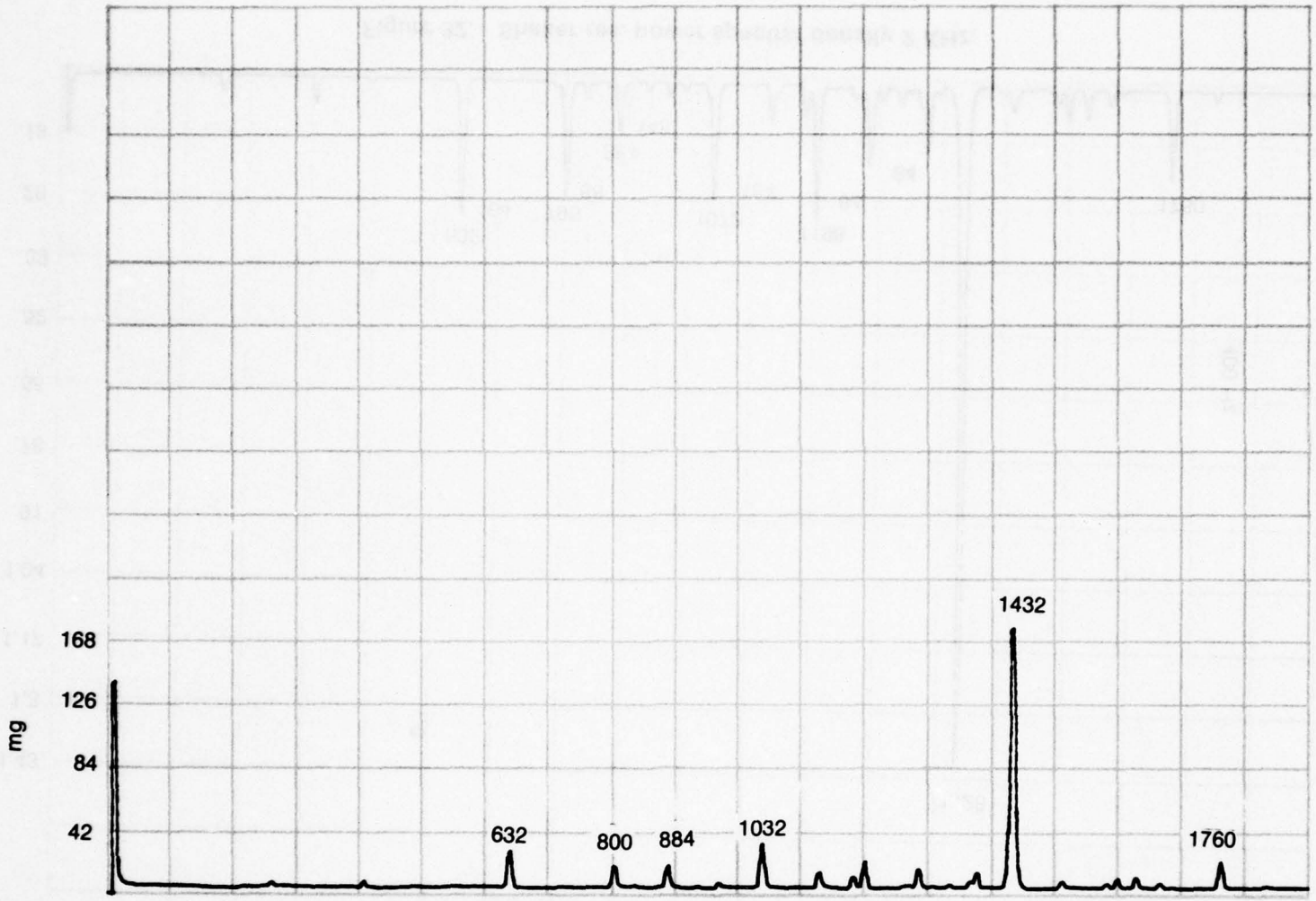

Figure 33. Shaker res. power spectral density 2 KHz.

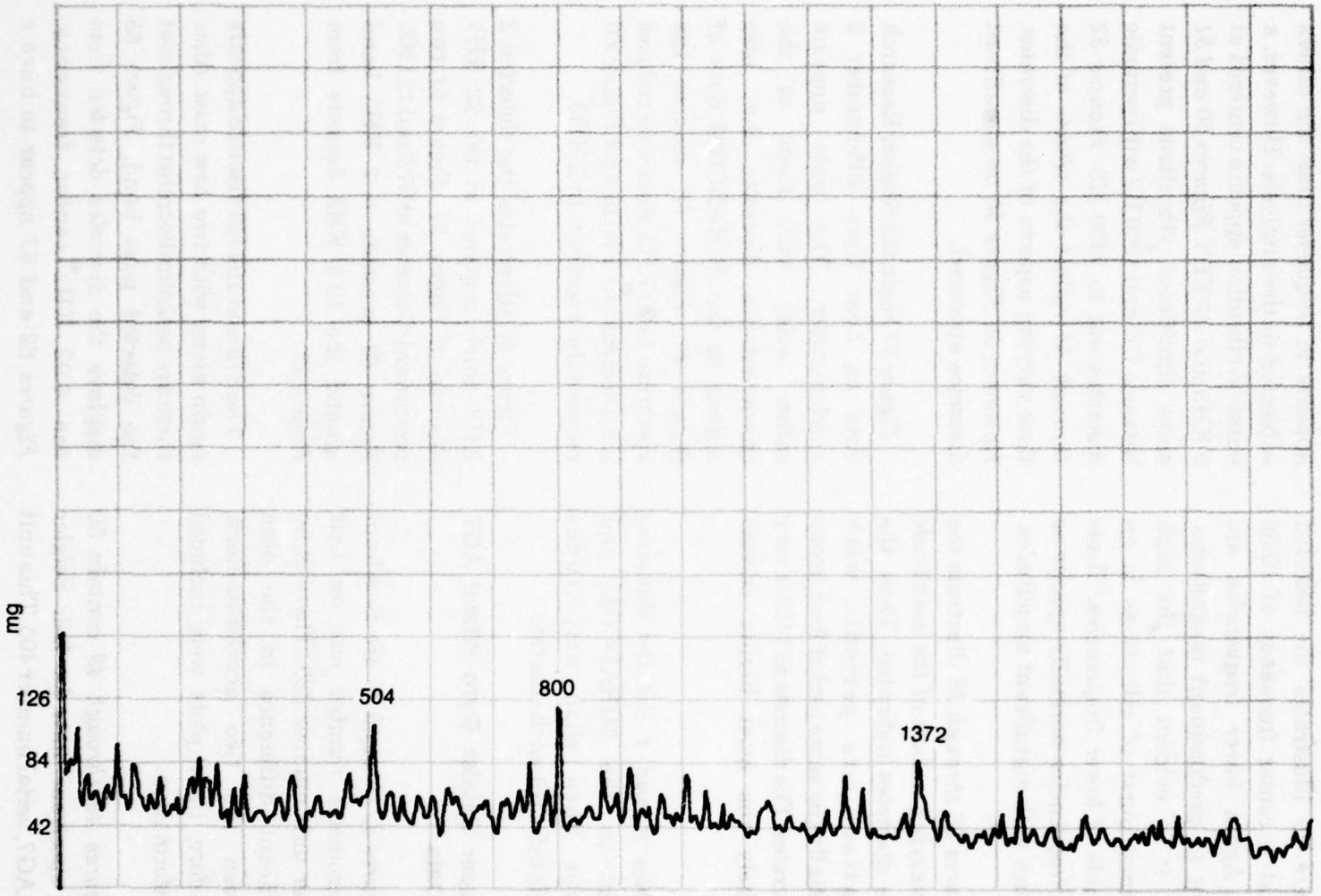

Figure 34. 22 KHz Detected spectrum.

Figure 35 illustrates the detected data at a center frequency of 10.56 KH3. Again lower frequencies are present in predominant magnitudes. Thus, it is evident that the high frequency burst of vibrations is an ensemble of lower frequencies. These lower frequencies normally appear as discretes with significant amplitudes.

Figures 36 through 38 illustrate the time varying nature of the amplitude of the discretes indicated. Thus, the variations are periodic with essentially the same period for a group of discretes. The discrete at 1428 is very definitely the most highly excited mode.

Tables 3 and 4 list the discretes present in the MIRADCOM and Shaker data with amplitudes associated with each discrete.

C. Lear Seigler Gyro Wheel AG7 Data

Figures 39 through 45 are data from accelerometer number one on Leir Seigler unit number 325. There is no significant difference in the data between the two accelerometers. Therefore, these plots were included for information.

Figures 46 through 49 contain 50 KH3 spectrum data for Leir Seigler gyro AG7, serial number 405. This unit appears to be quieter than the others subjected to the analysis. However, a burst of vibration appears centered at 9 KH3 and 24 KH3. *Figures 50 and 51* show significant vibrations present between 750 and 1000 H3 with periodic discretes out to 2400 H3. *Figures 52 through 55* reflect the effects of the time varying aspects of the discretes. However, in *Figure 56* no significant discretes appeared.

Figure 57 begin the Shaker Research data on Lear Gyro 405-number 2 accelerometer. The data appears rather noisy with some of the characteristics discretes that also appear in the MIRADCOM data of *Figure 46*. *Figure 58* reduces the spectrum to 20 KH3, *Figure 59* reduces the spectrum to 5 KH3 and *Figure 60* reduces the spectrum to 2 KH3.

Figure 61 illustrates the detected 2 KH3 notch centered at the 22 KH3 discrete of *Figure 57*. *Figure 61* two prominant discretes at 872 and 124 H3. *Figure 62* presents a 2 KH3 band around the 10.9 KH3 discrete from *Figure 57*.

The 872 and 124 H3 discrete appears again along with two new ones. Also, there are periodic discretes throughout the detected pass band. *Figure 63* displays the discretes detected from the 4.92 KHz center frequency. *Figures 62 and 63* appear to have a

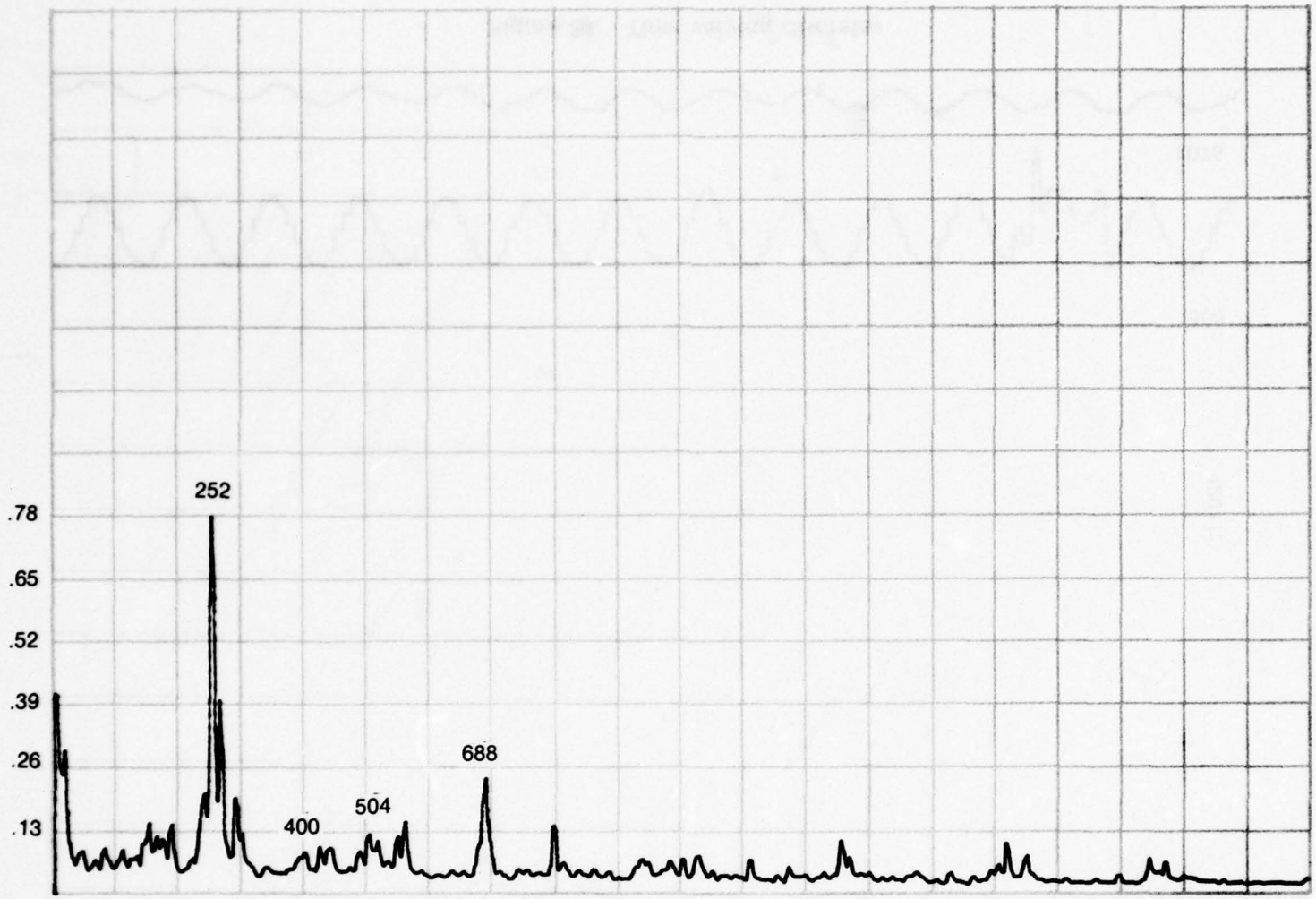

Figure 35. 10.56 KHz Detected spectrum.

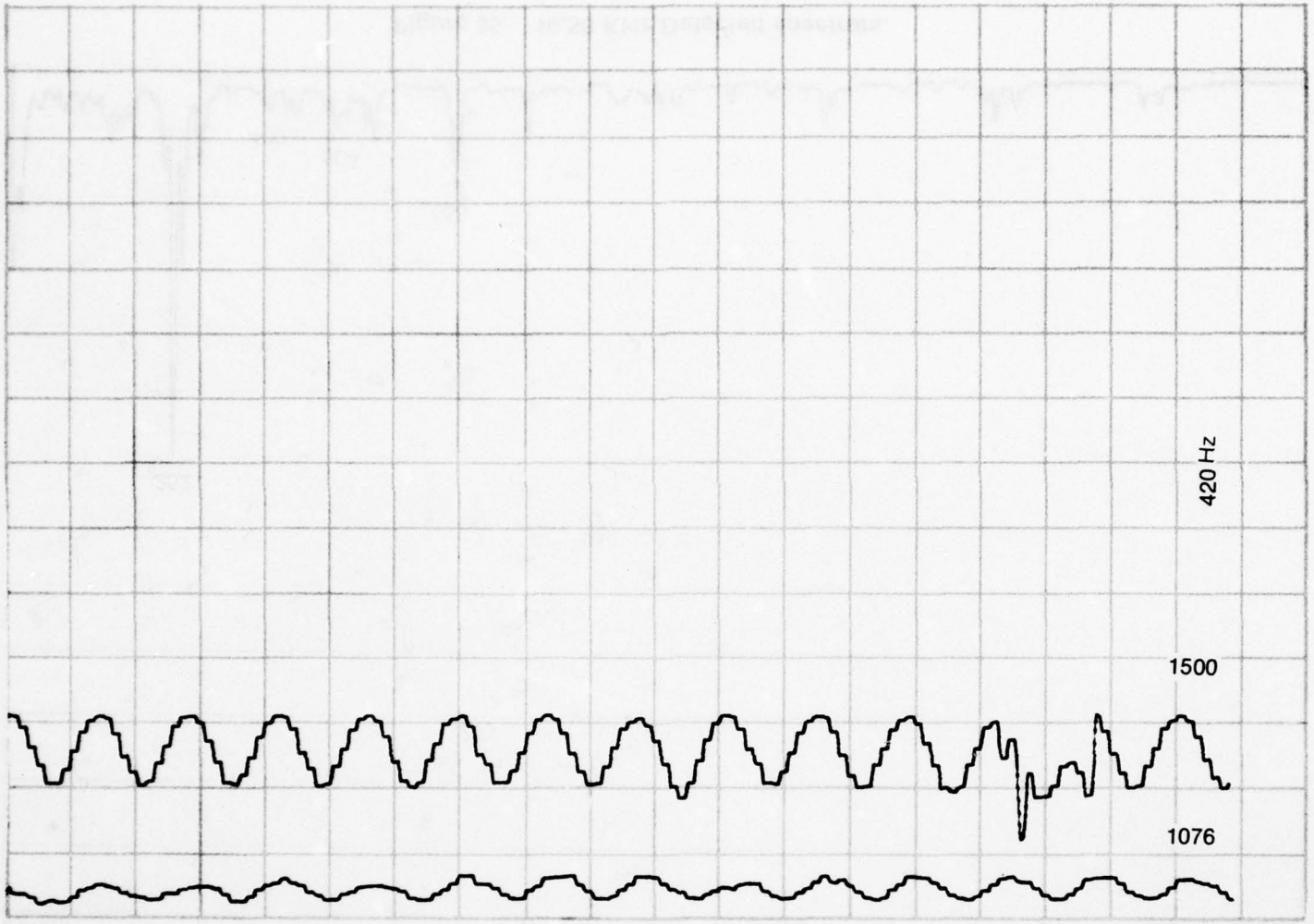

Figure 36. Time varying discretes

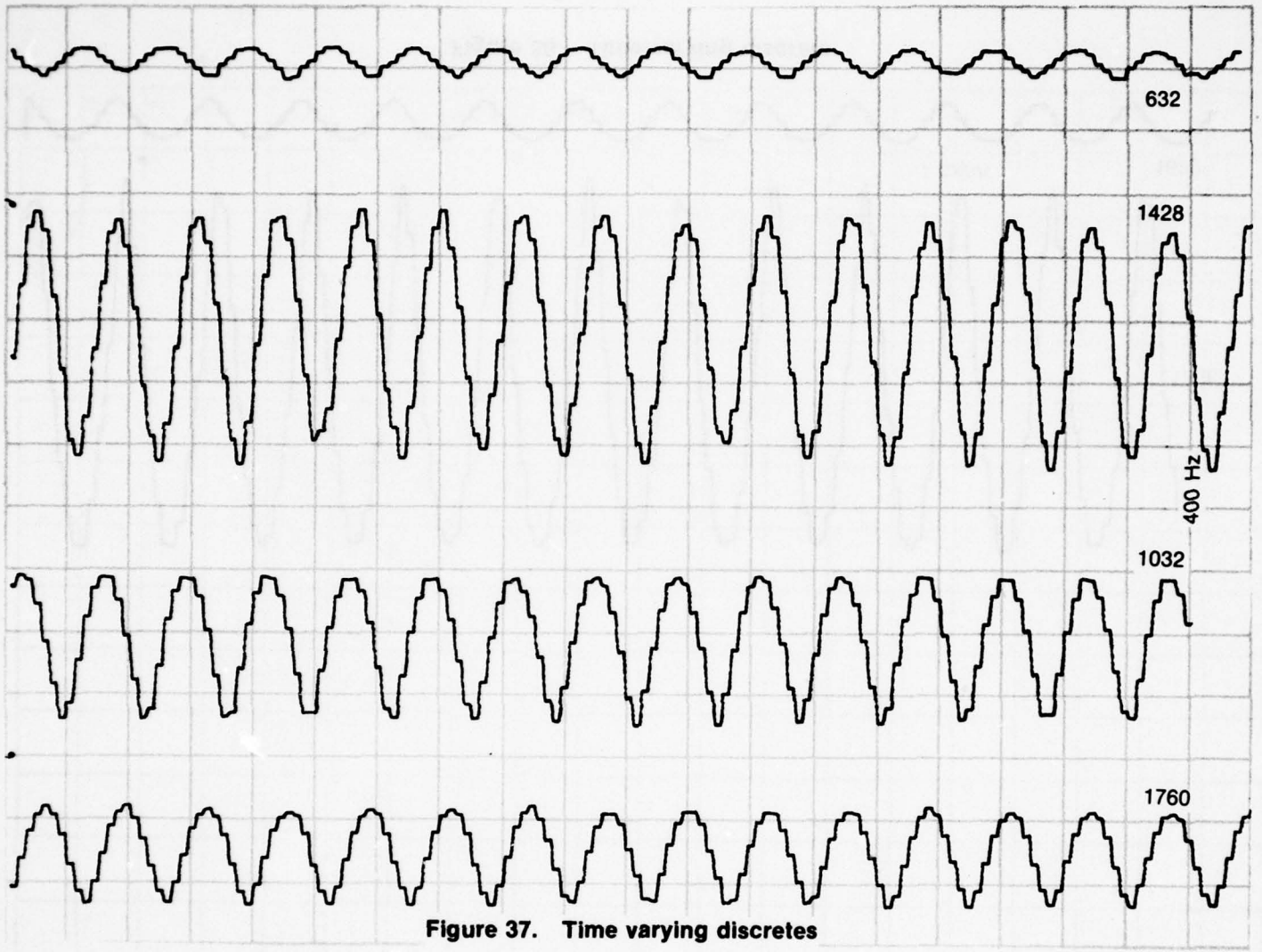

Figure 37. Time varying discretes

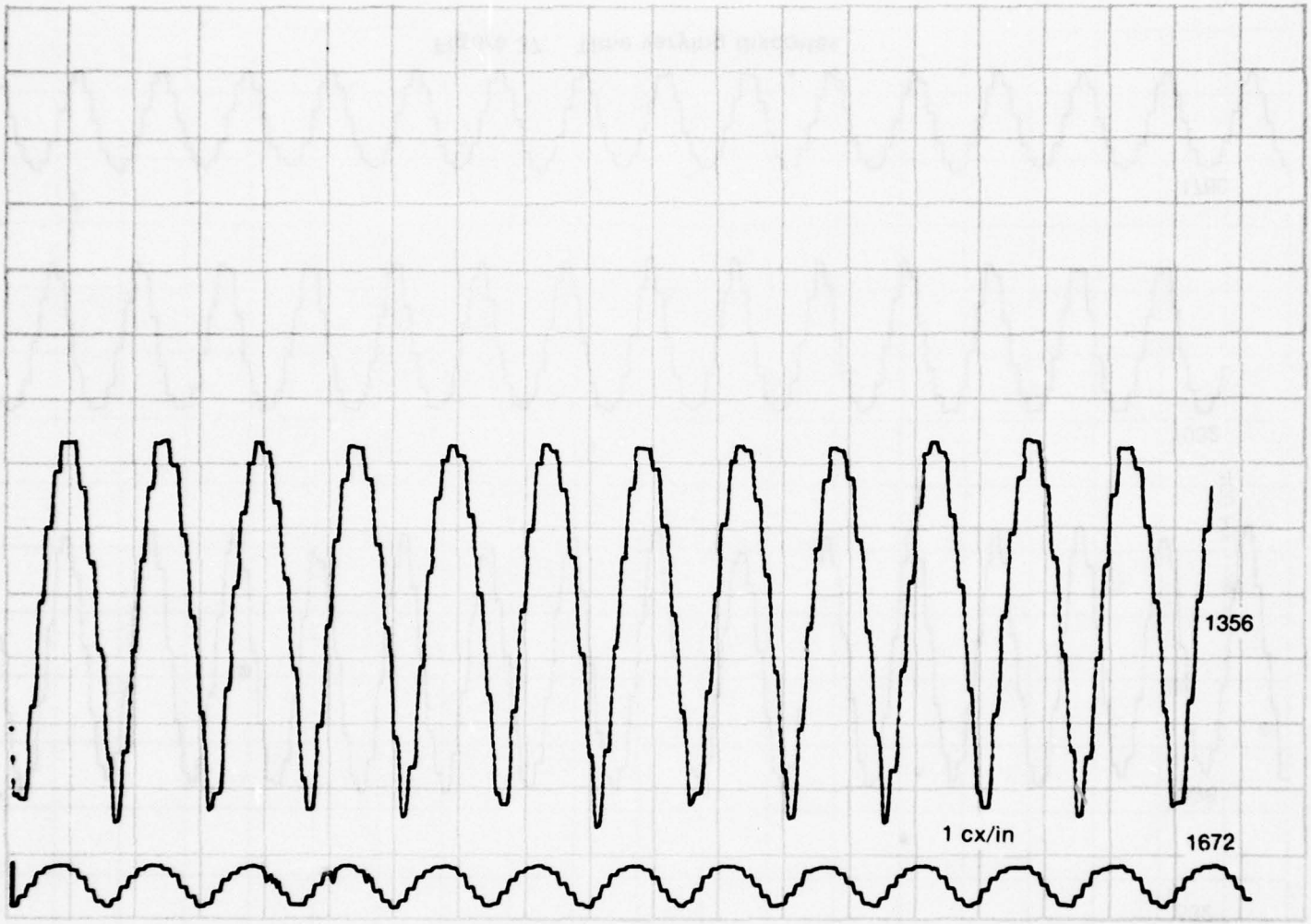

Figure 38. Time varying discrete

TABLE 3. LEAR GYRO AG8 DISCRETE AMPLITUDE	
Discrete HZ	**Amplitude mg**
1425	1840
1185	46 mg
971	4.6 mg
881	4.6 mg
806	60 mg
796	11.5 mg
791	4.6 mg
571	202 mg
398	21 mg
250	5 mg

TABLE 4. LEAR GYRO AG8; FIRST AND SECOND TRUNNION VIBRATION DATA			
Discrete HZ	**First Readout mg**	**Discrete HZ**	**Second Readout mg**
			199 mg
		1672	3125 mg
1596	266 mg		
1504	904 mg		
1432	1782 mg		
		1428	1423 mg
		1372	84 mg
		1360	33125 mg
1256	904 mg		
			279
		1136	4375
1084	266 mg		
		1032	239
		980	3125
		884	106.4
		876	2500 mg
836	133 mg		
			118 mg
		796	239 mg
		756	625 mg
		688	226
664	66.5 mg	632	306 mg
628	66.5 mg	600	3125 mg
		504	133 mg
		400	66.5 mg
		252	780 mg

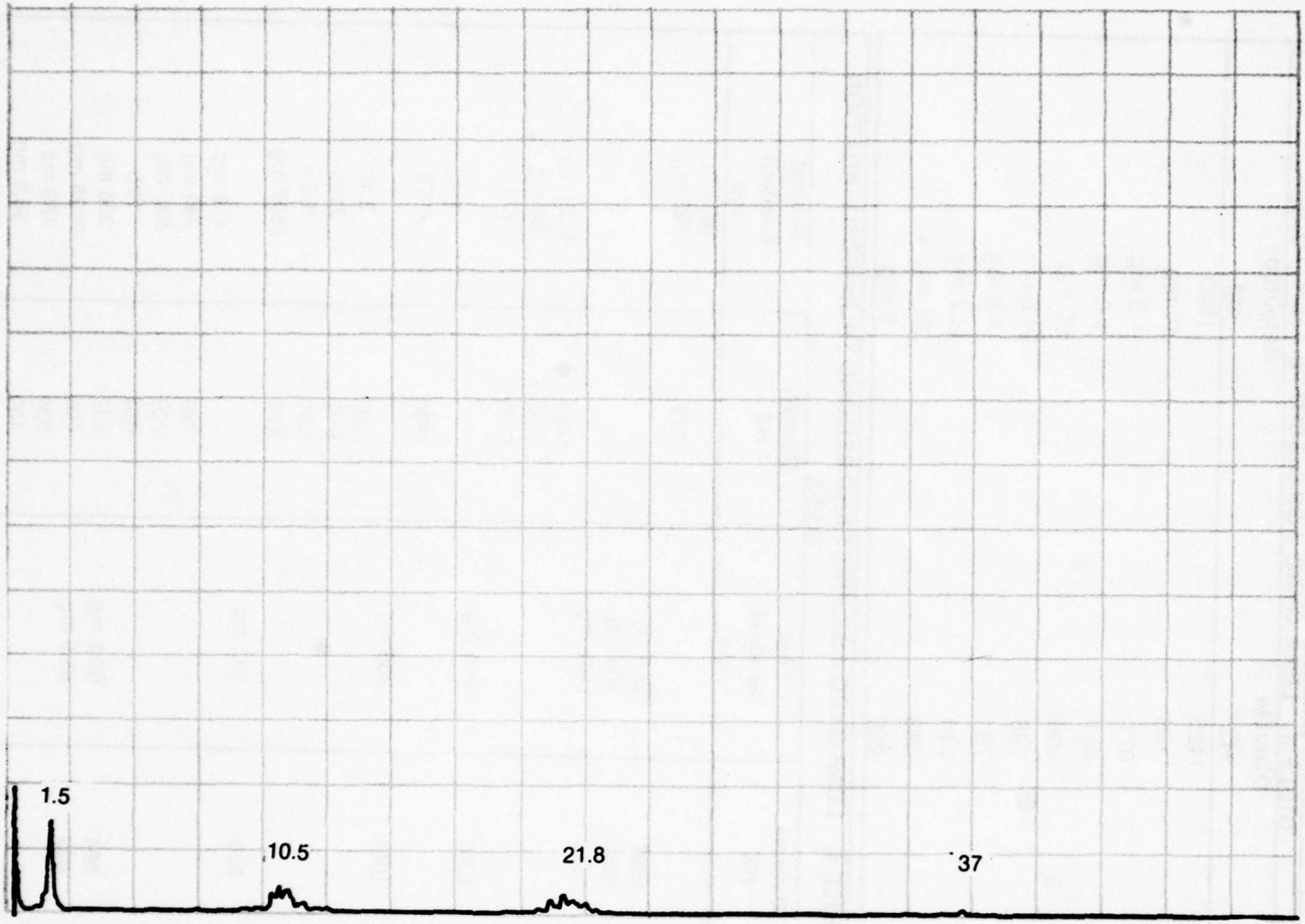

Figure 39. First sensor power spectral density 50 KHz.

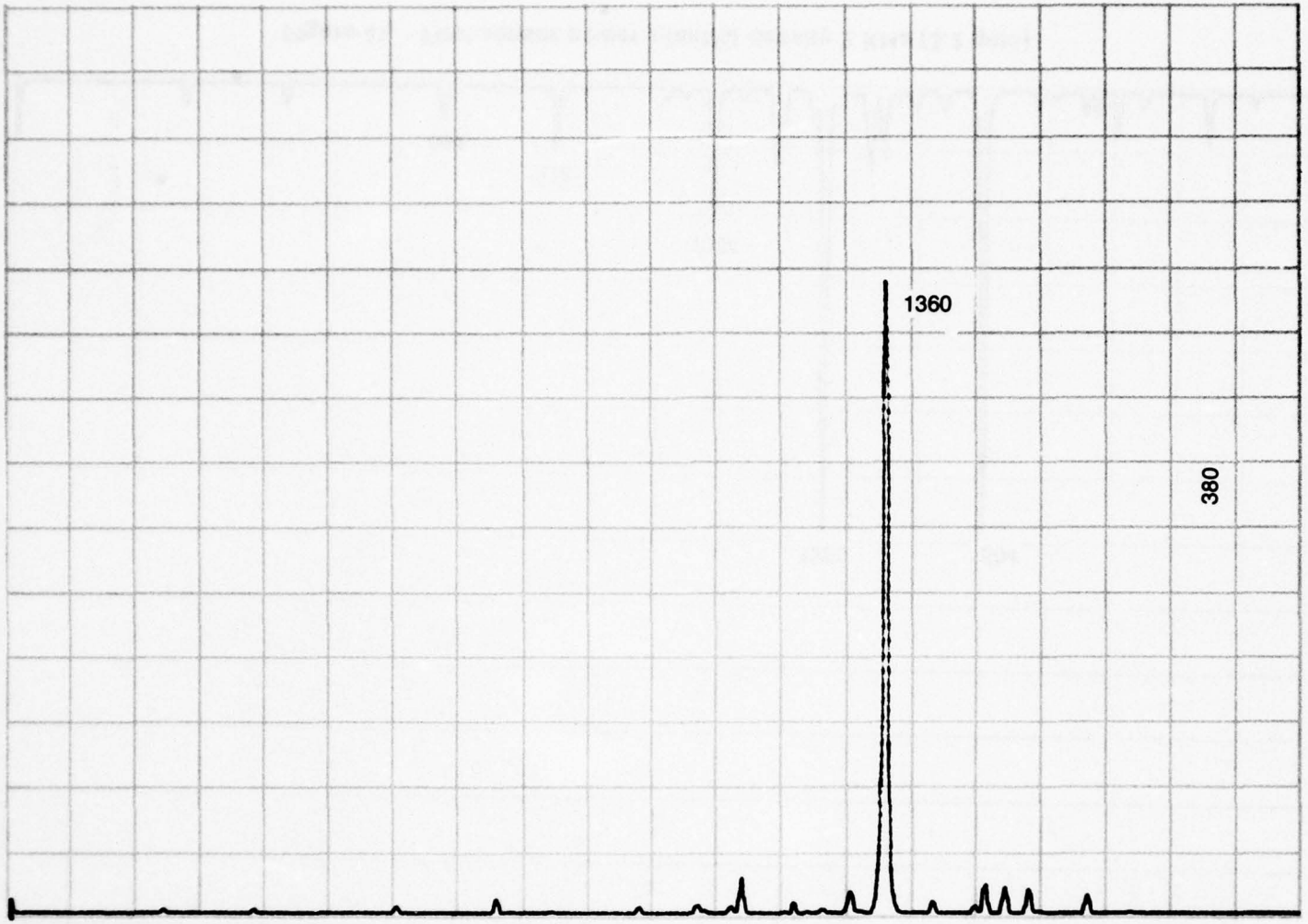

Figure 40. First sensor power spectral density 2 KHz (1 gain)

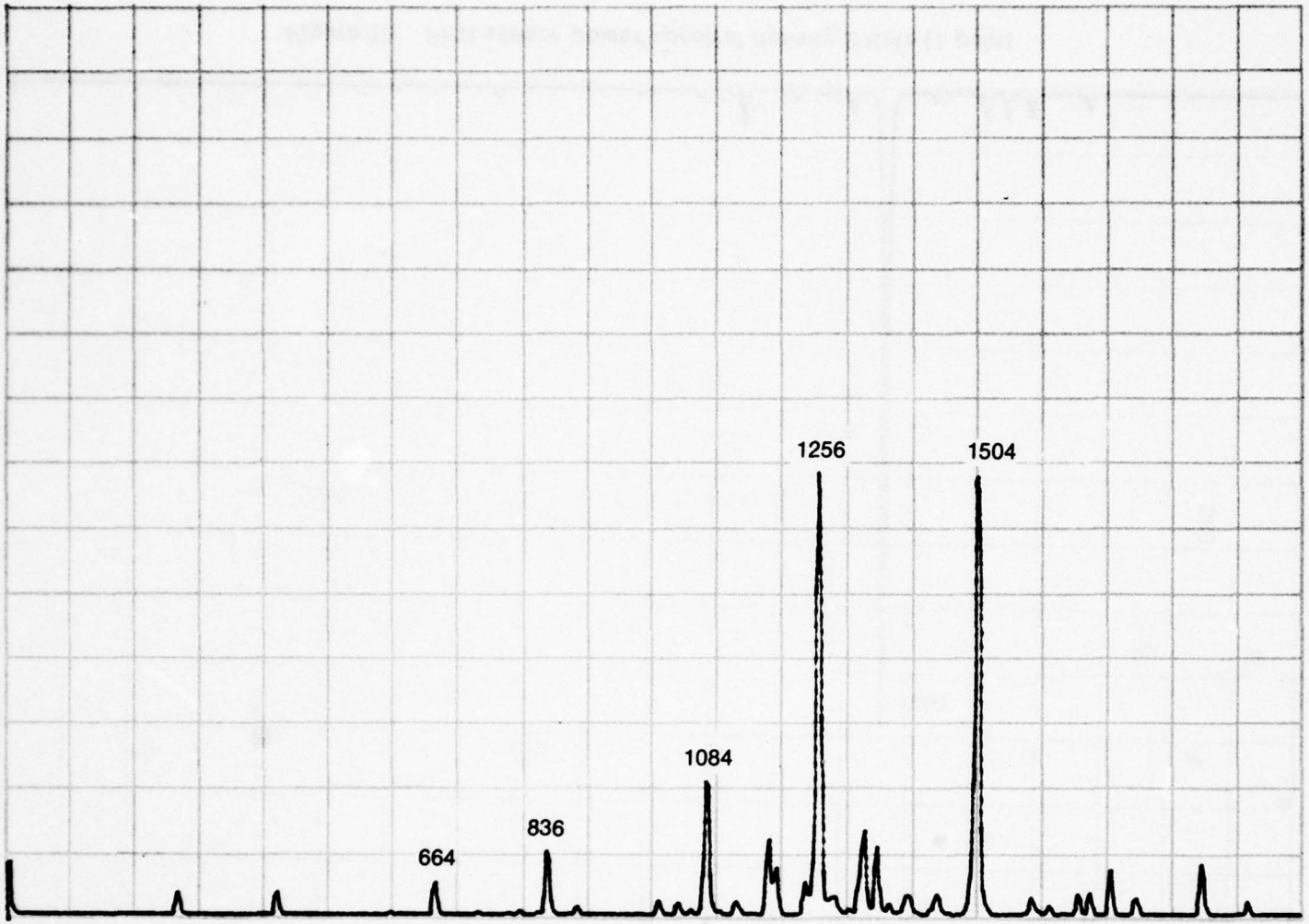

Figure 41. First sensor power spectral density 2 KHz (3.2 gain)

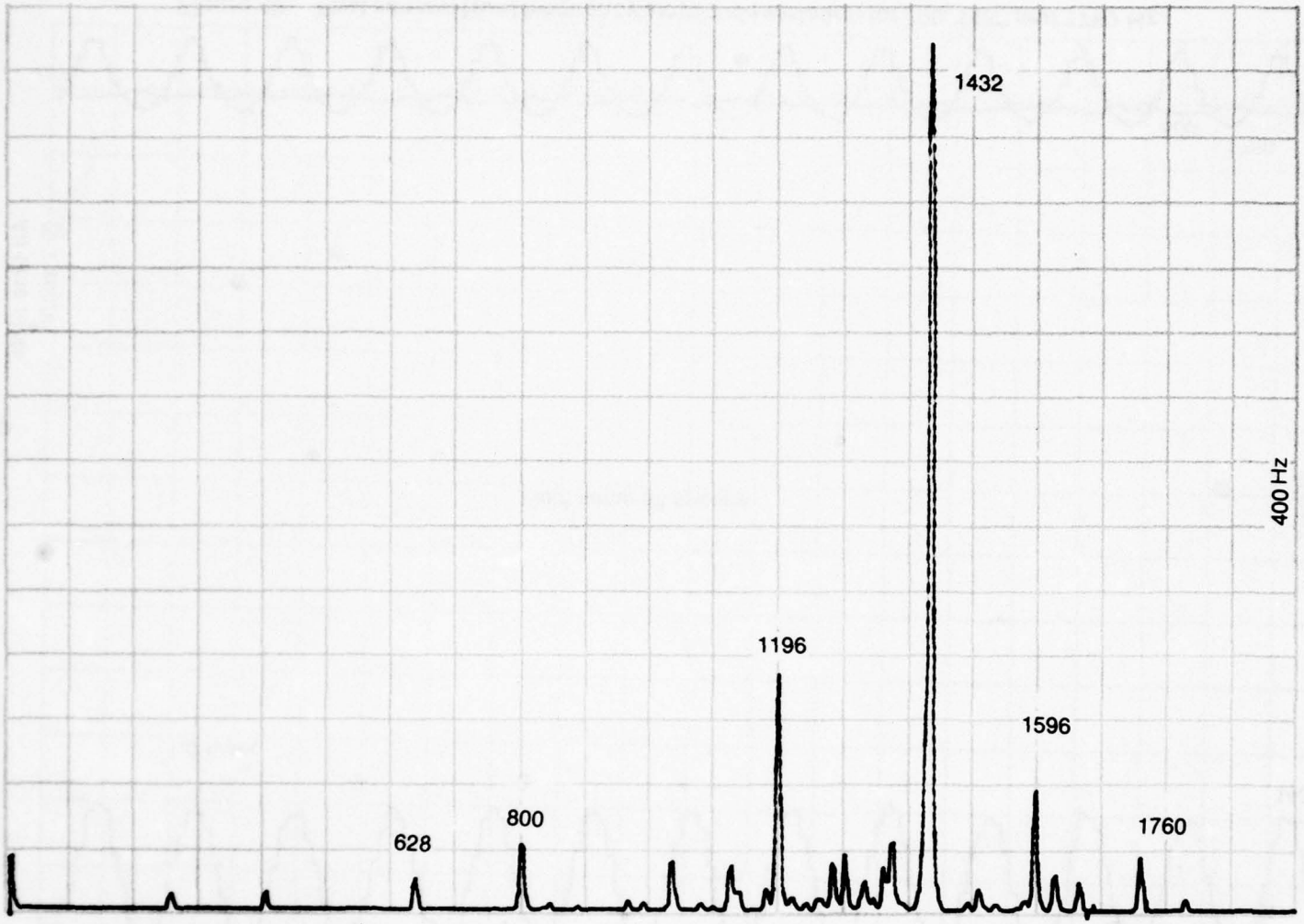

Figure 42. First sensor power spectral density 2 KHz (Demod 21 KHz center frequency).

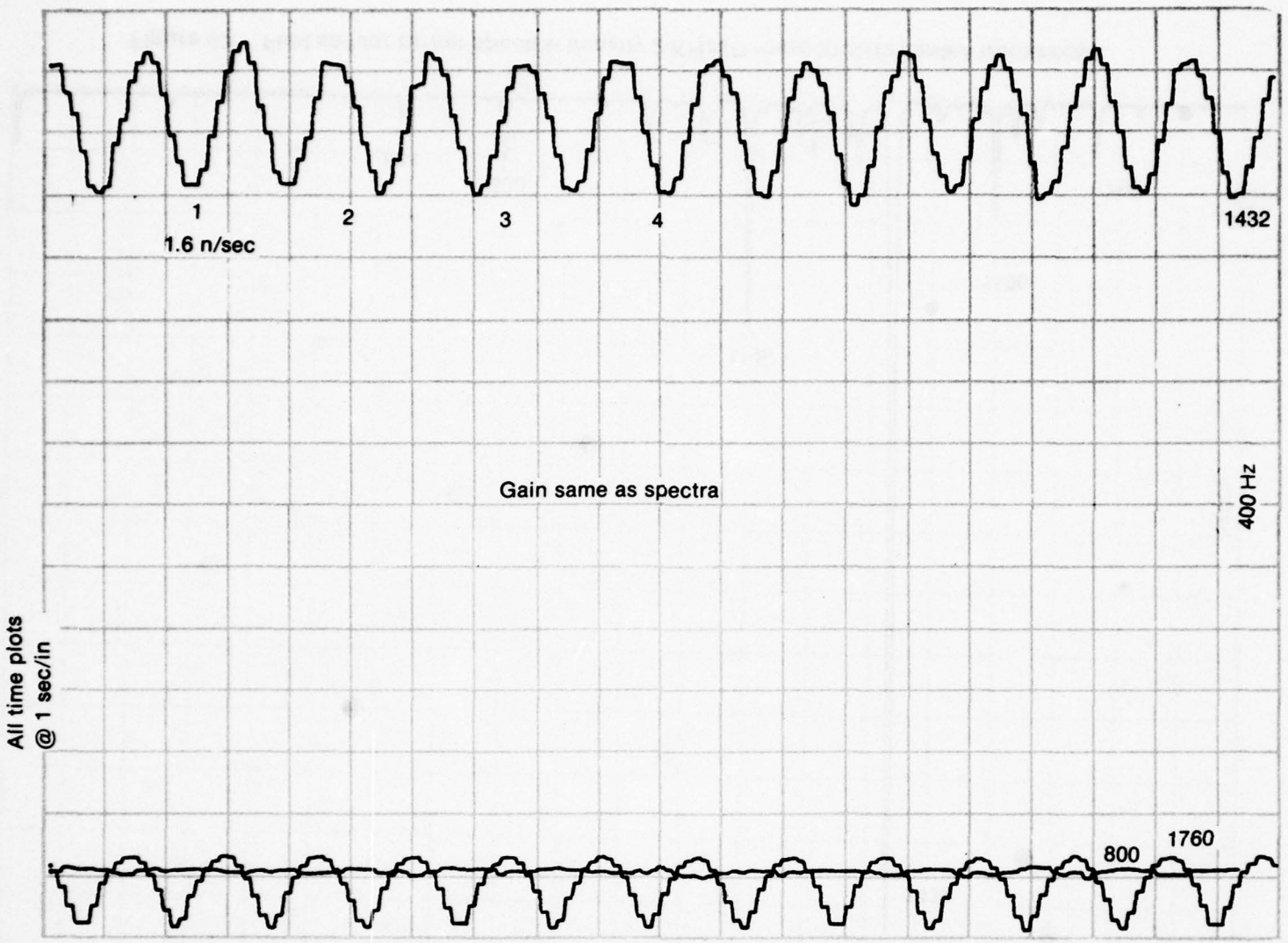

Figure 43. First sensor; Hunt frequency amplitude variation for 800, 1432 and 1760 Hz.

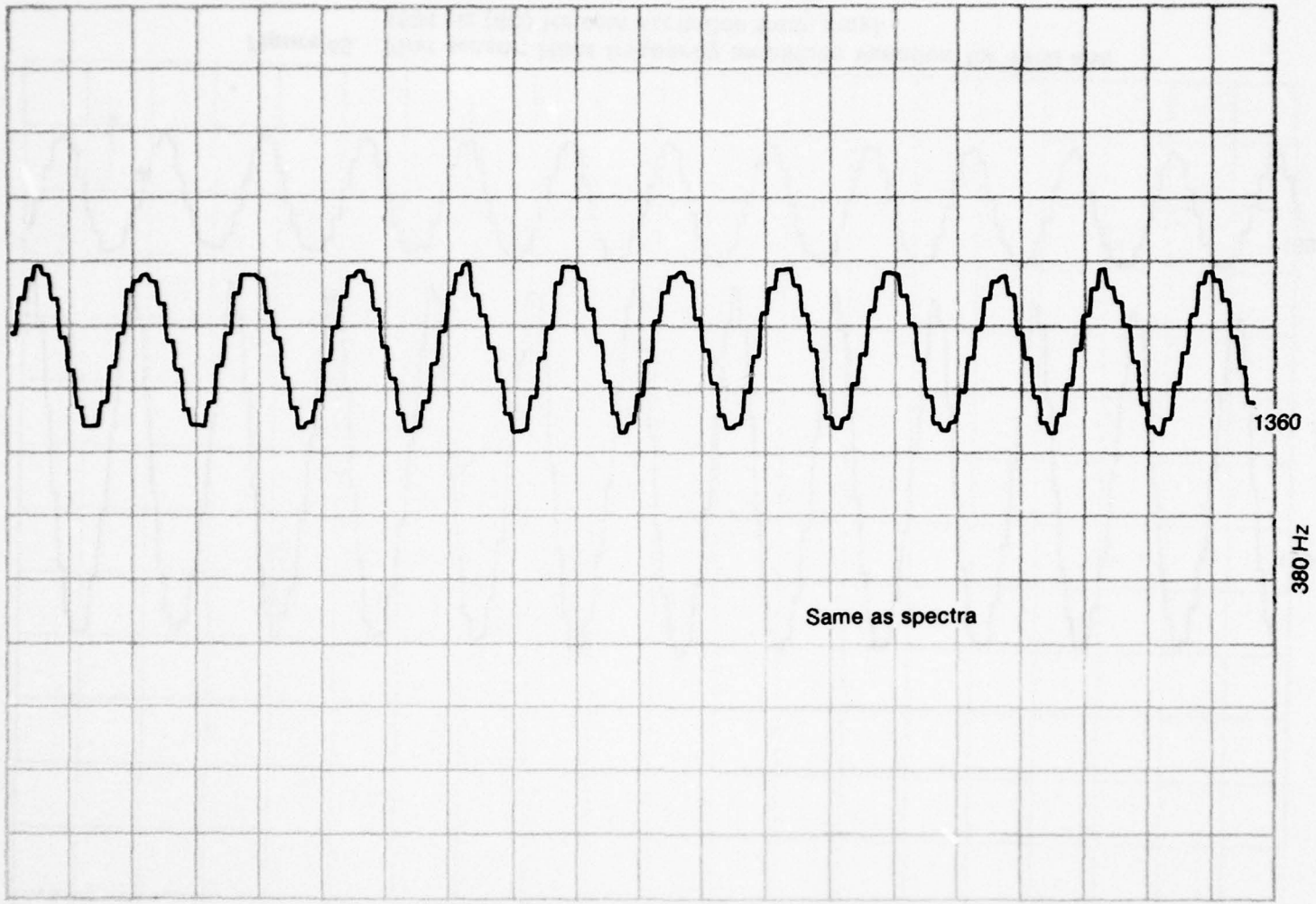

Figure 44. First sensor; Hunt frequency amplitude variation for 1360 Hz (380 Hz spin excitation frequency).

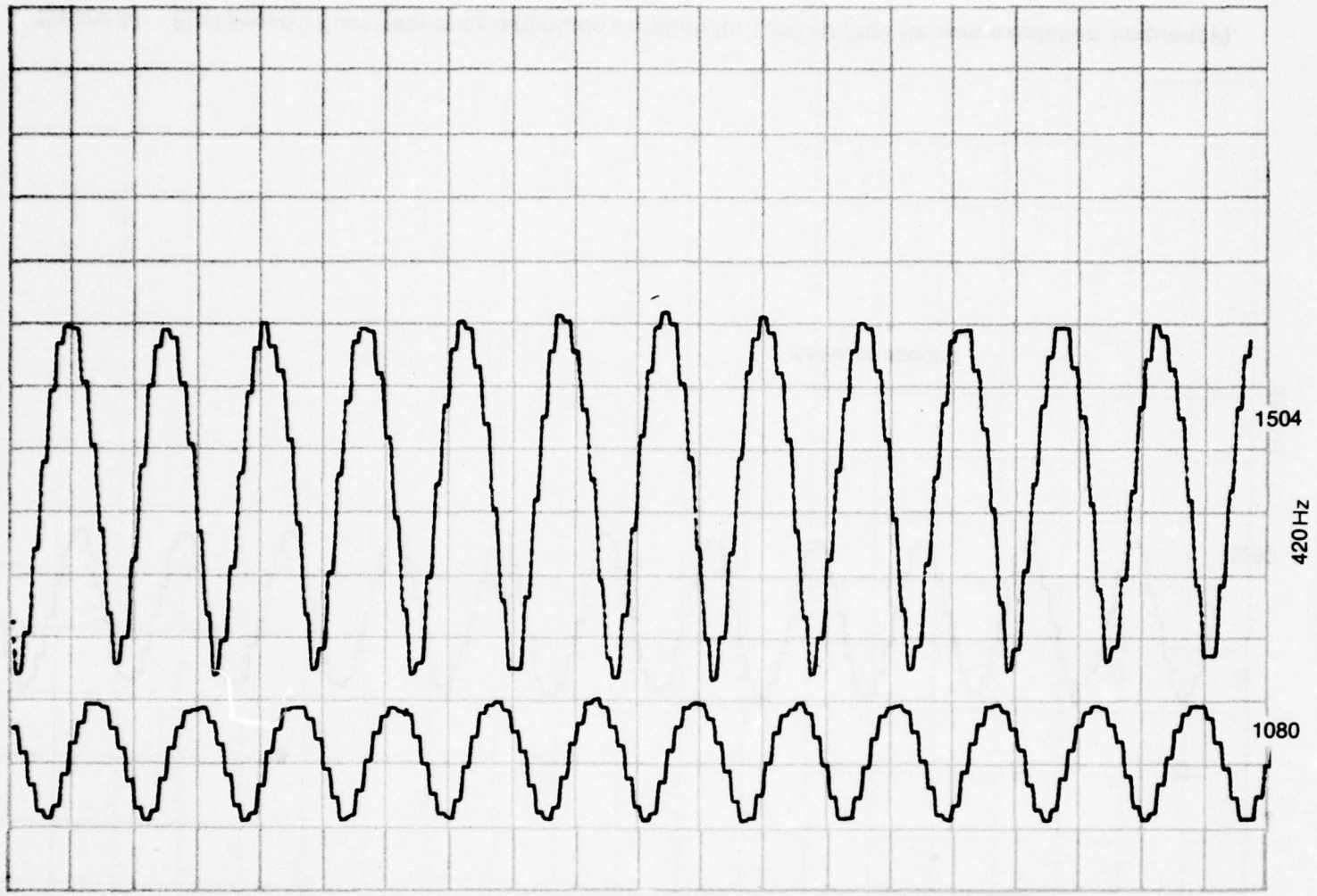

Figure 45. First sensor; Hunt frequency amplitude variation for 1080 and 1504 Hz (420 Hz spin excitation frequency).

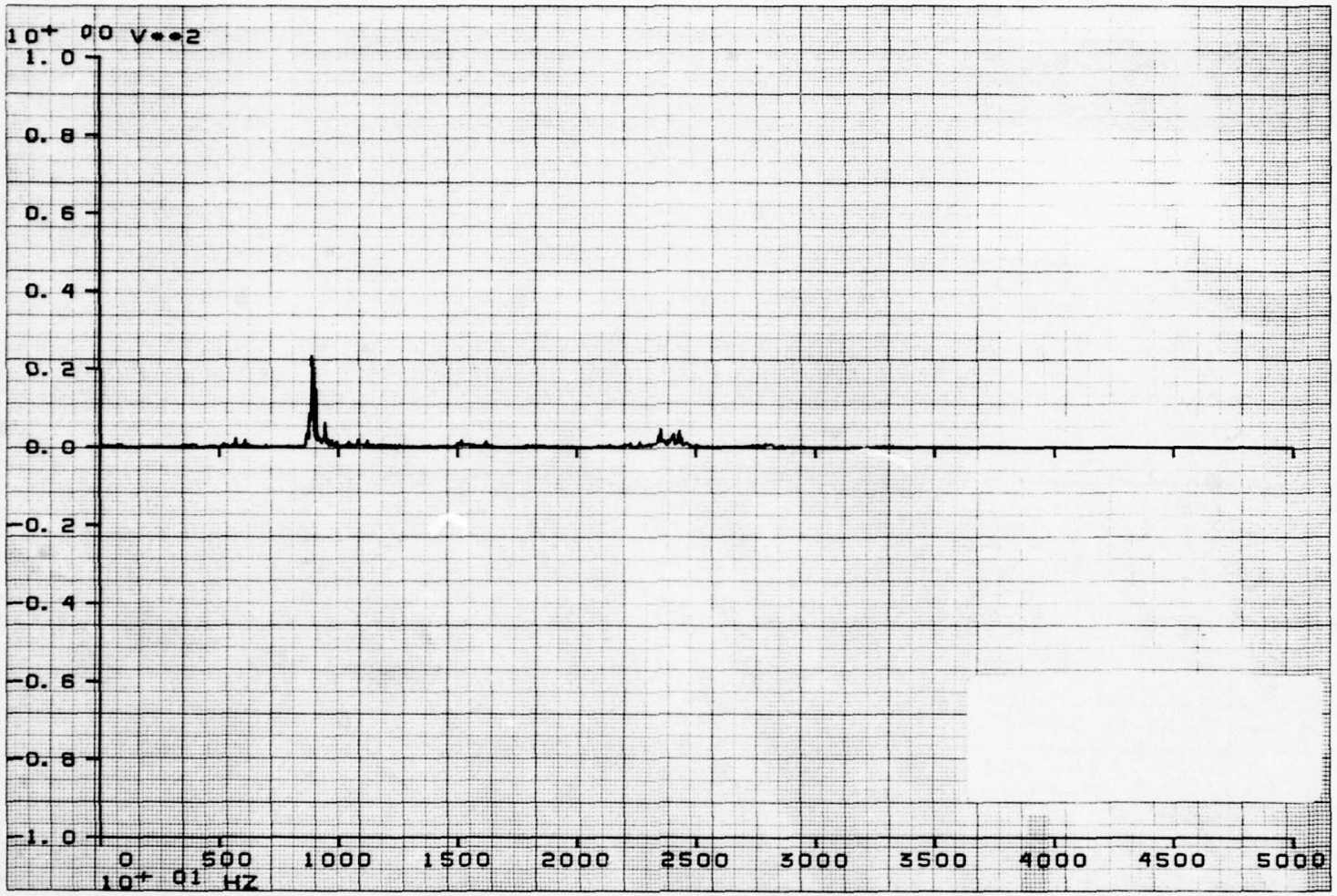

Figure 46. LSI Gyro Serial #405, 2 pole lo-pass filter @ 52 Kc, 26 volt, 1 phase, 400 Hz excitation, scale 52 mg/div

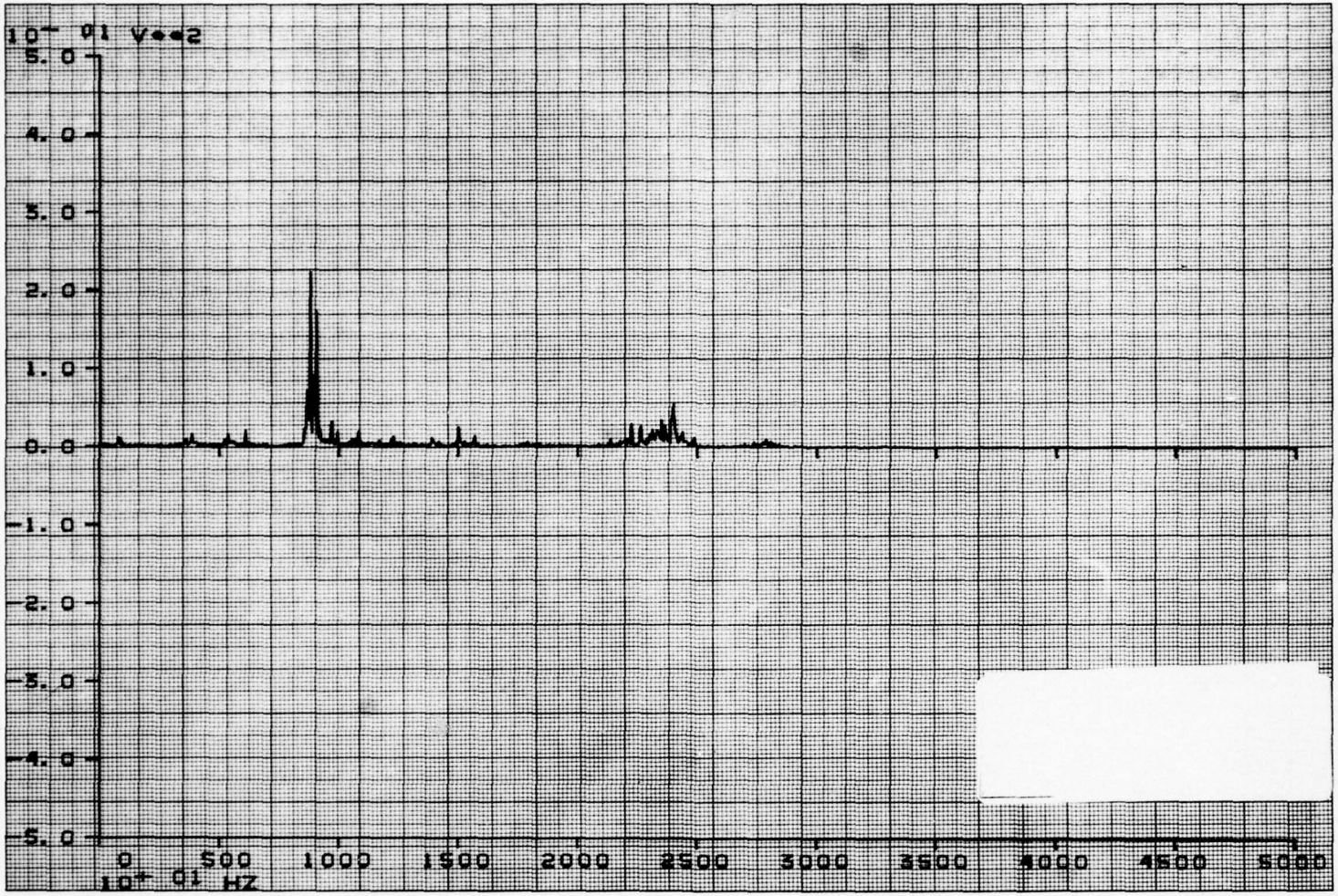

Figure 47. LSI Gyro Serial #405, 2 pole lo-pass filter @ 52 Kc, 26 volt, 1 phase, 400 Hz excitation, scale 37 mg/div

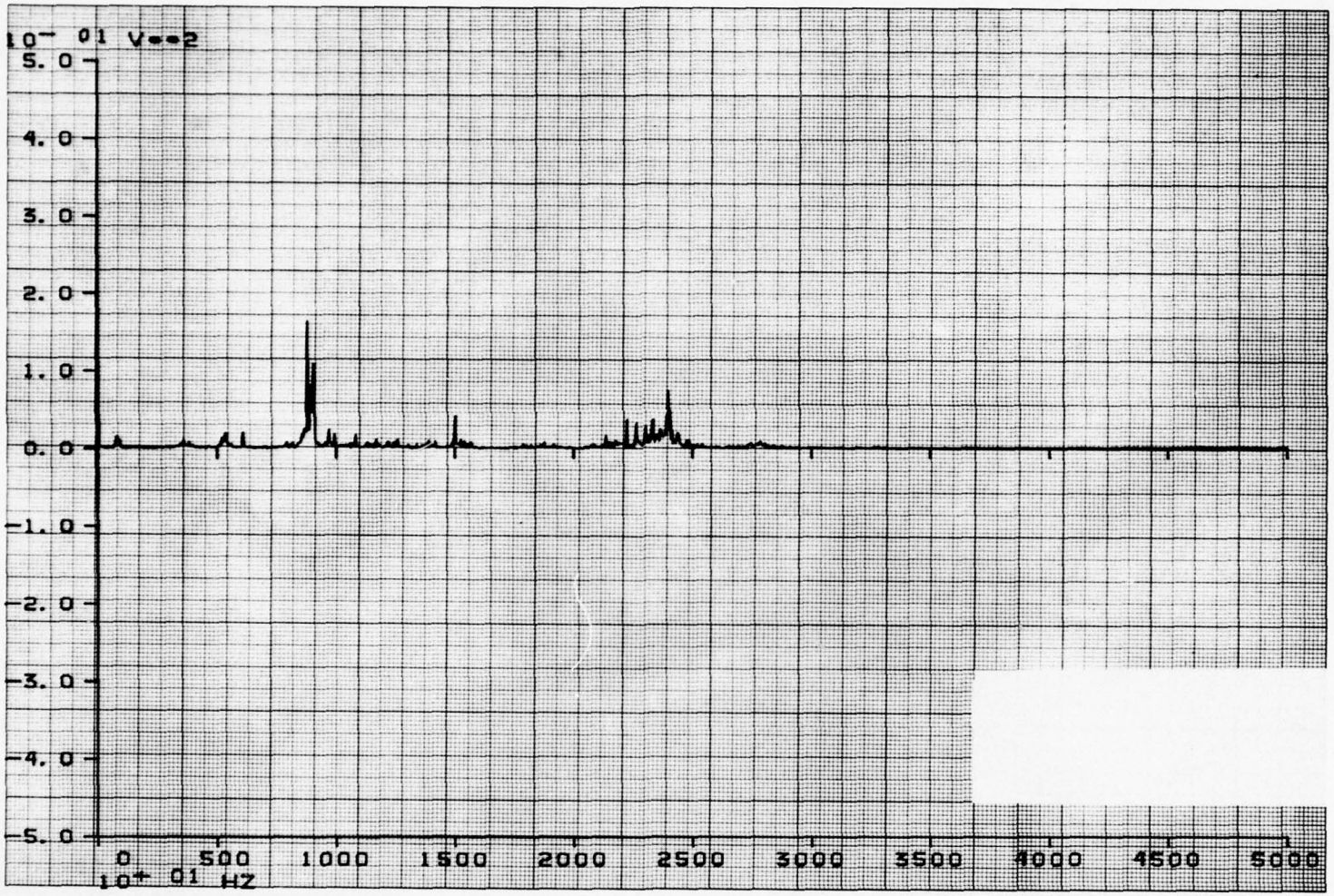

Figure 48. LSI Gyro Serial #405, 2 pole lo-pass filter @ 52 Kc, 26 volt, 1 phase, 400 Hz excitation, scale 37 mg/div

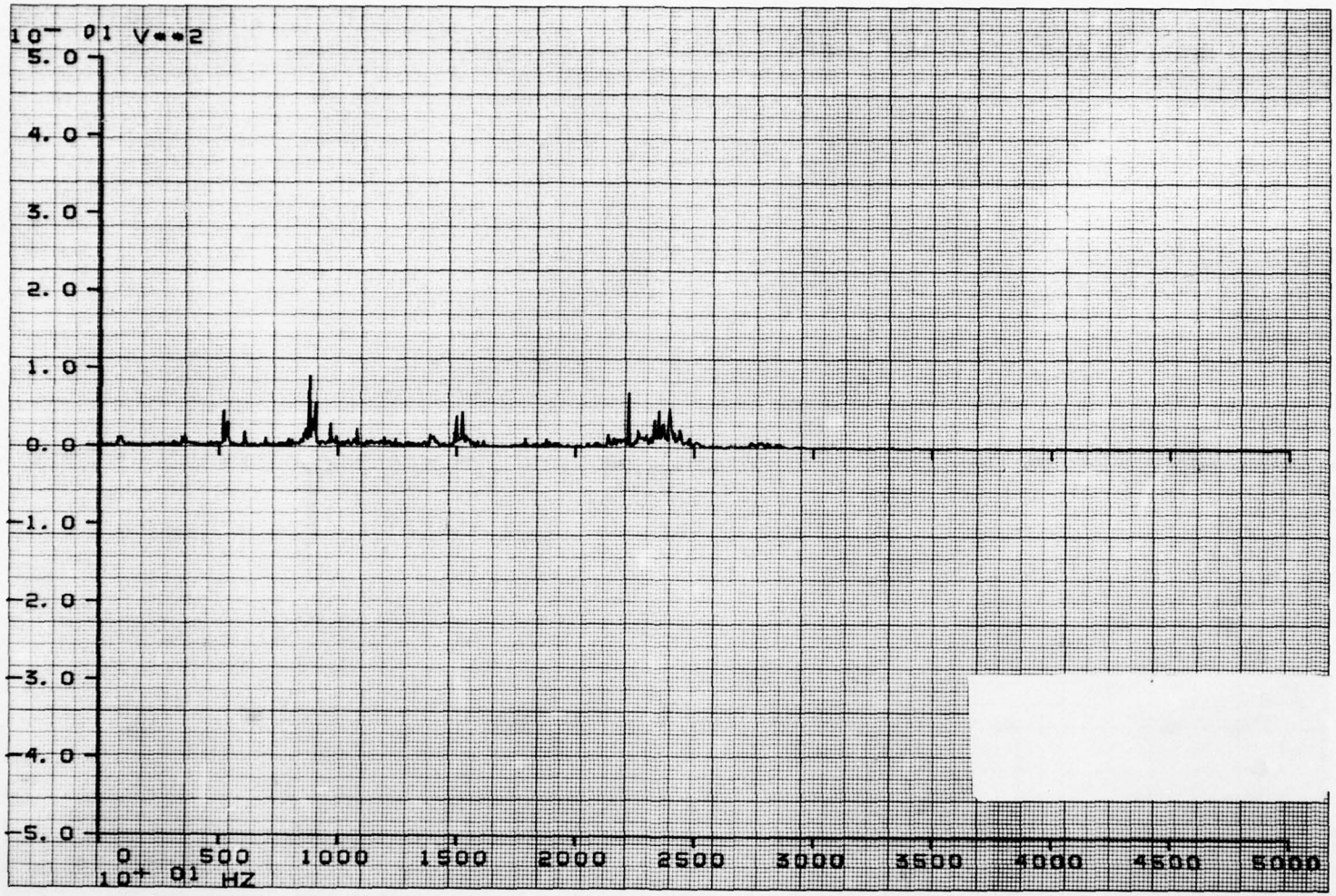

Figure 49. LSI Gyro Serial #405, 2 pole lo-pass filter @ 52 Kc, 26 volt, 1 phase, 400 Hz excitation, scale 37 mg/div

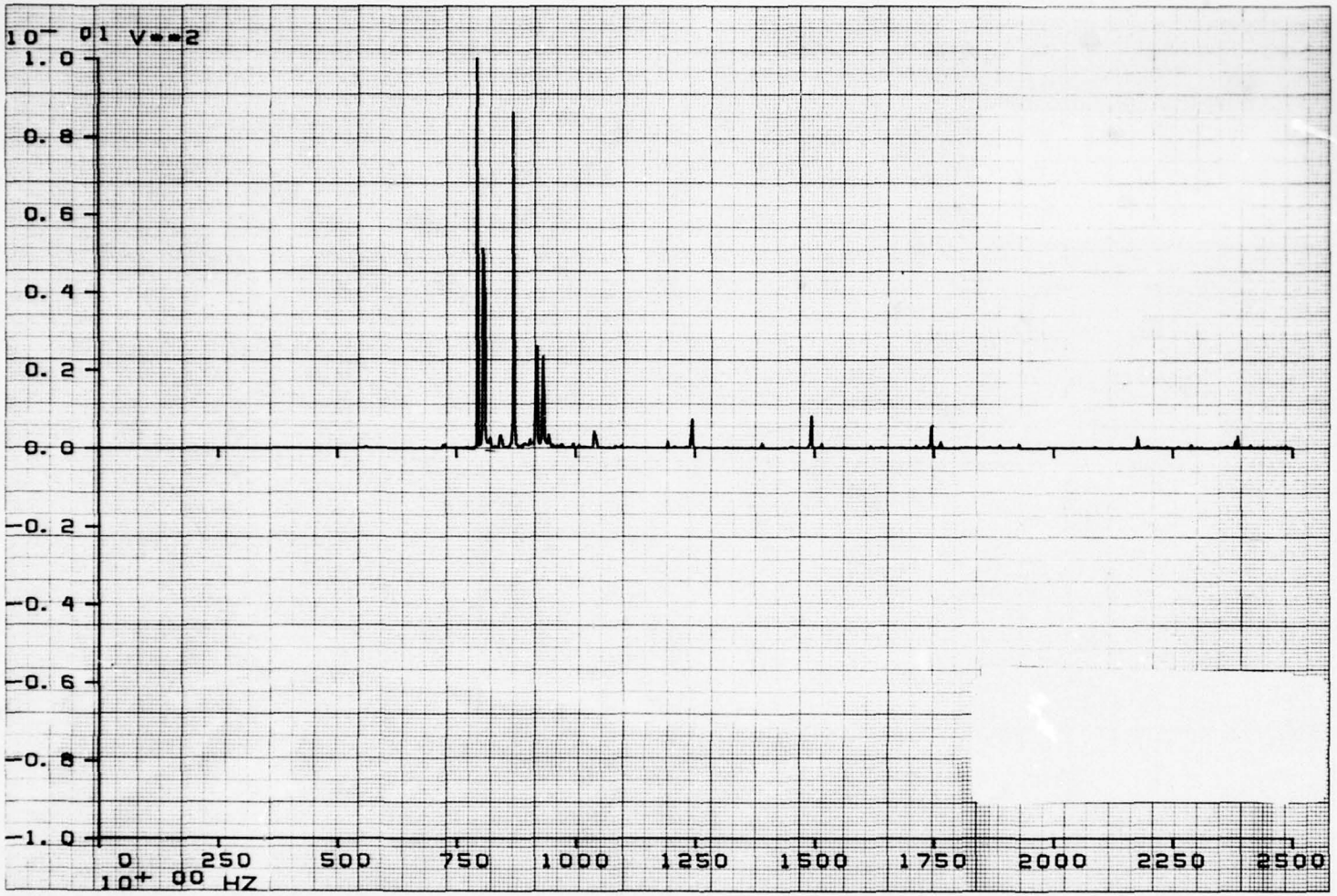

Figure 50. LSI Gyro Serial #405, 2 pole lo-pass filter @ 3 Kc, 26 volt, 1 phase, 400 Hz excitation, scale 15.7 mg/div

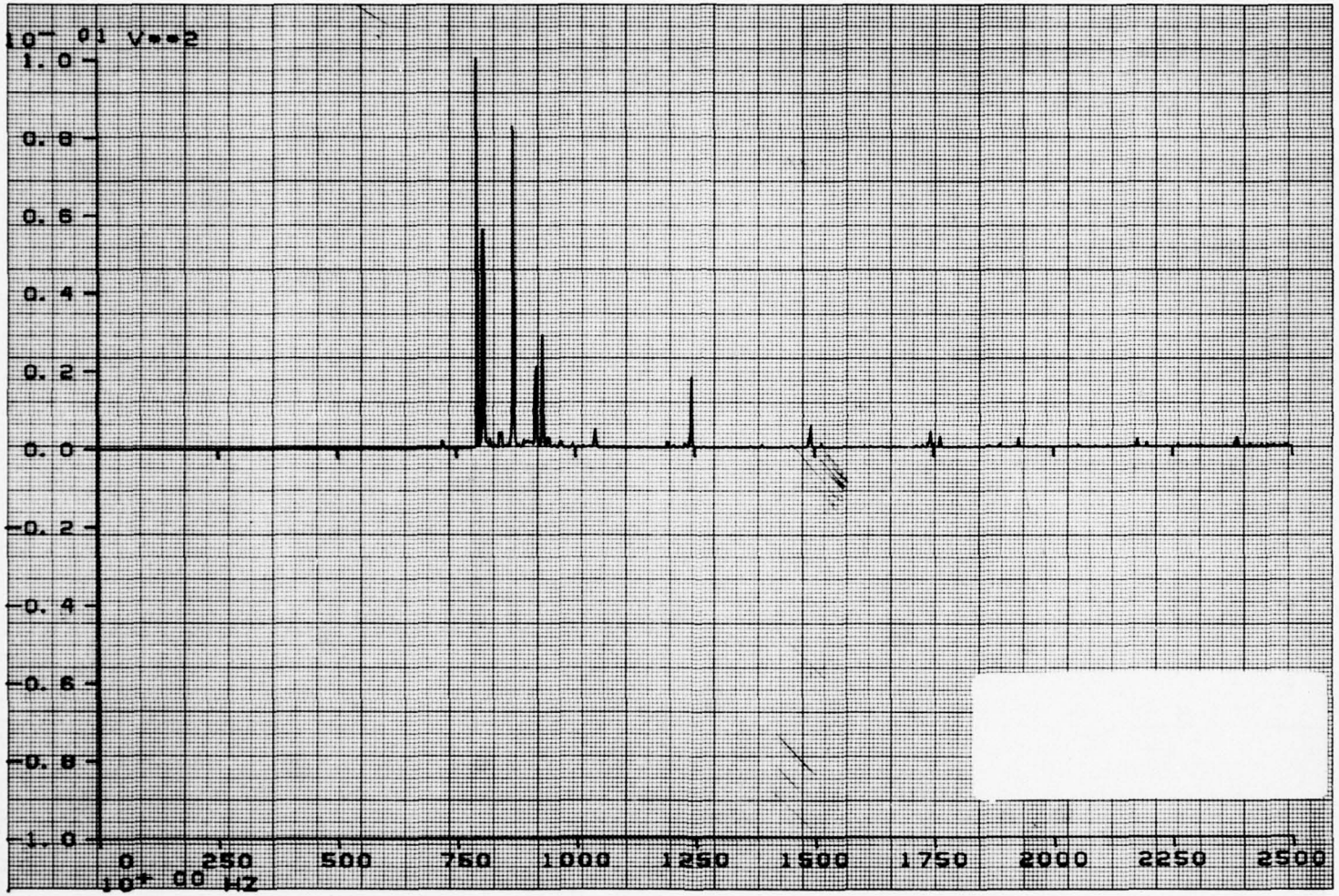

Figure 51. LSI Gyro Serial #405, 2 pole lo-pass filter ® 3 Kc, 26 volt, 1 phase, 400 Hz excitation, scale 15.7 mg/div.

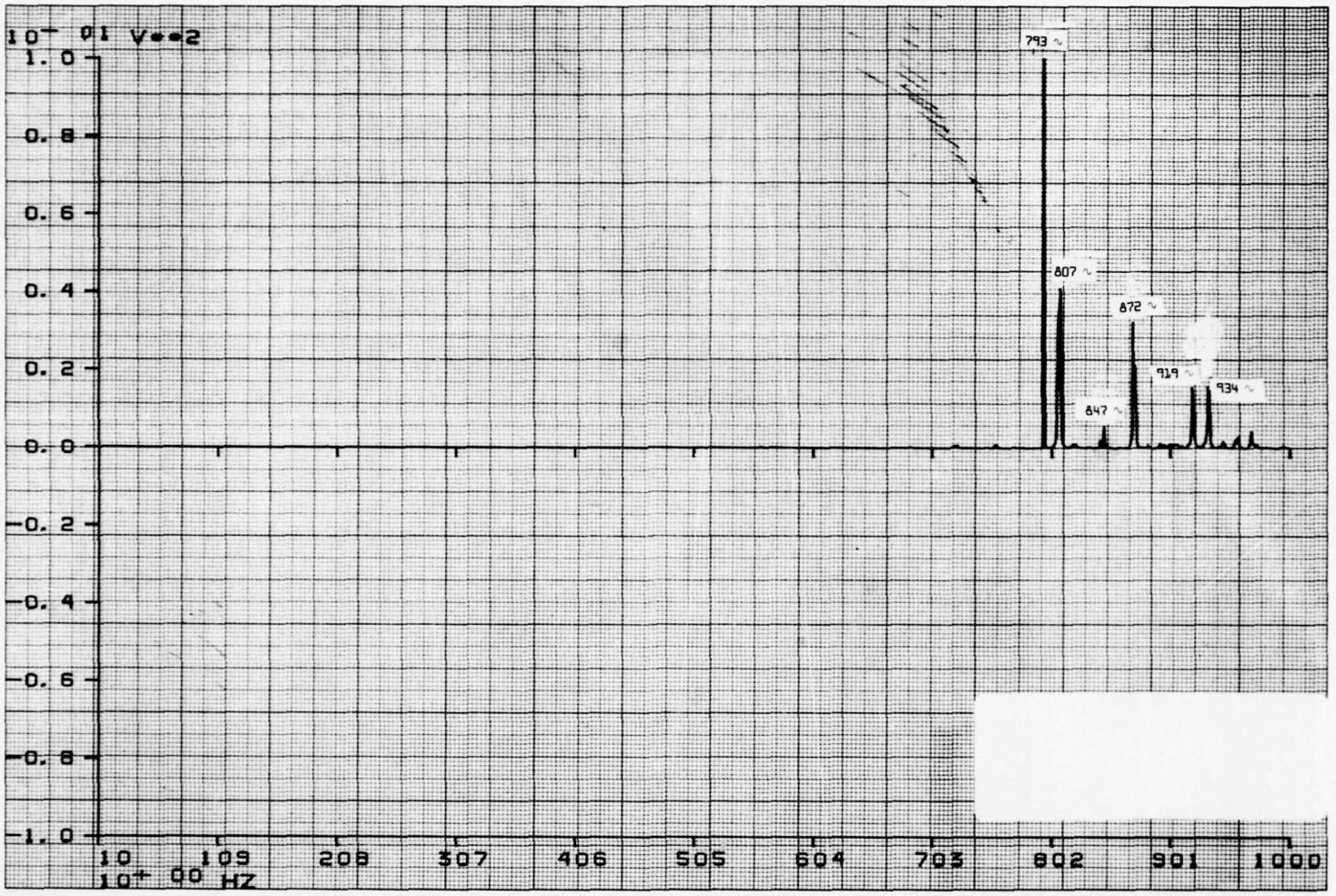

Figure 52. LSI Gyro Serial #405, 2 pole lo-pass filter @ 1 Kc, 26 volt, 1 phase, 400 Hz excitation, scale 15.7 mg/div

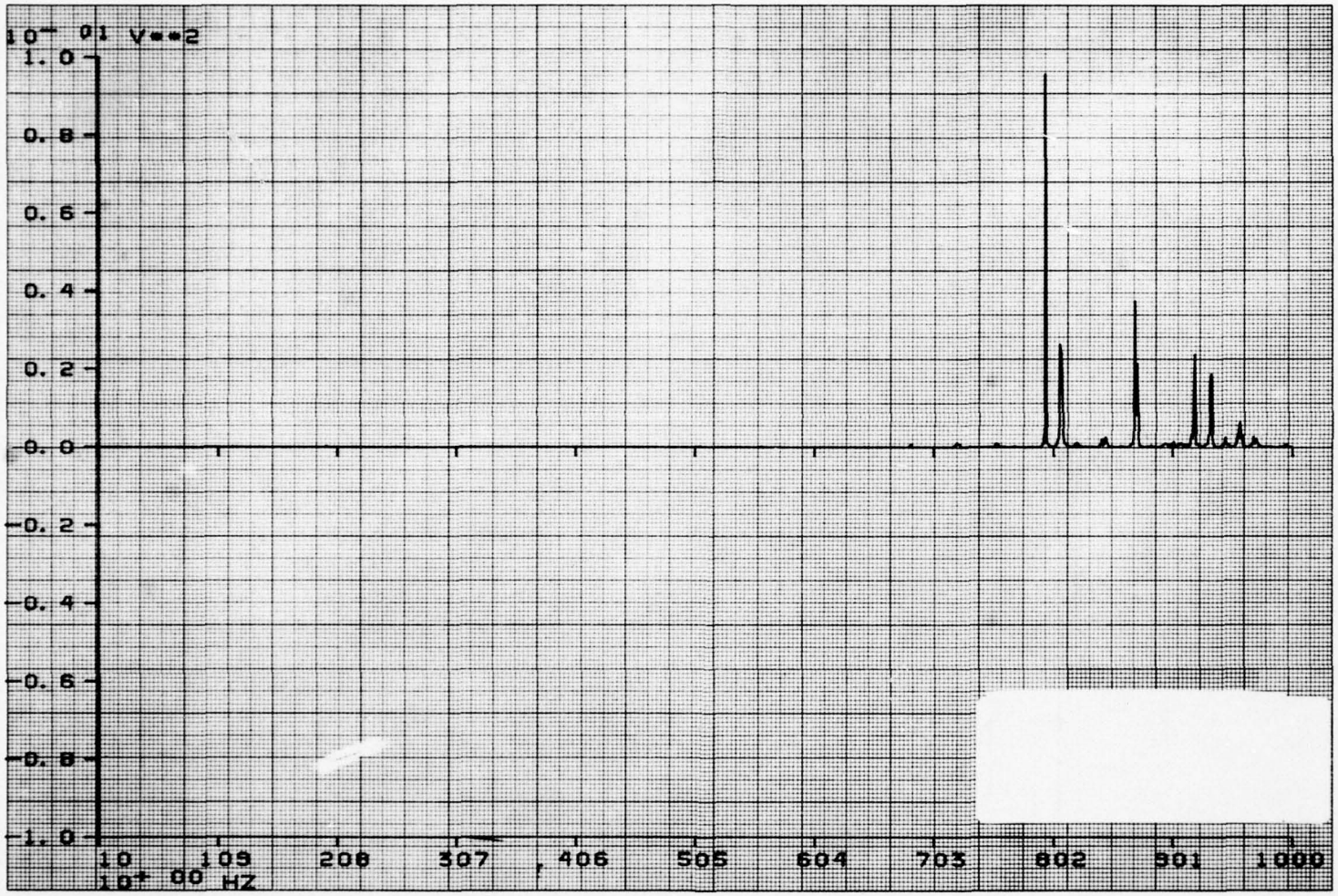

Figure 53. LSI Gyro Serial #405, 2 pole lo-pass filter @ 1 Kc, 26 volt, 1 phase, 400 Hz excitation, scale 15.7 mg/div

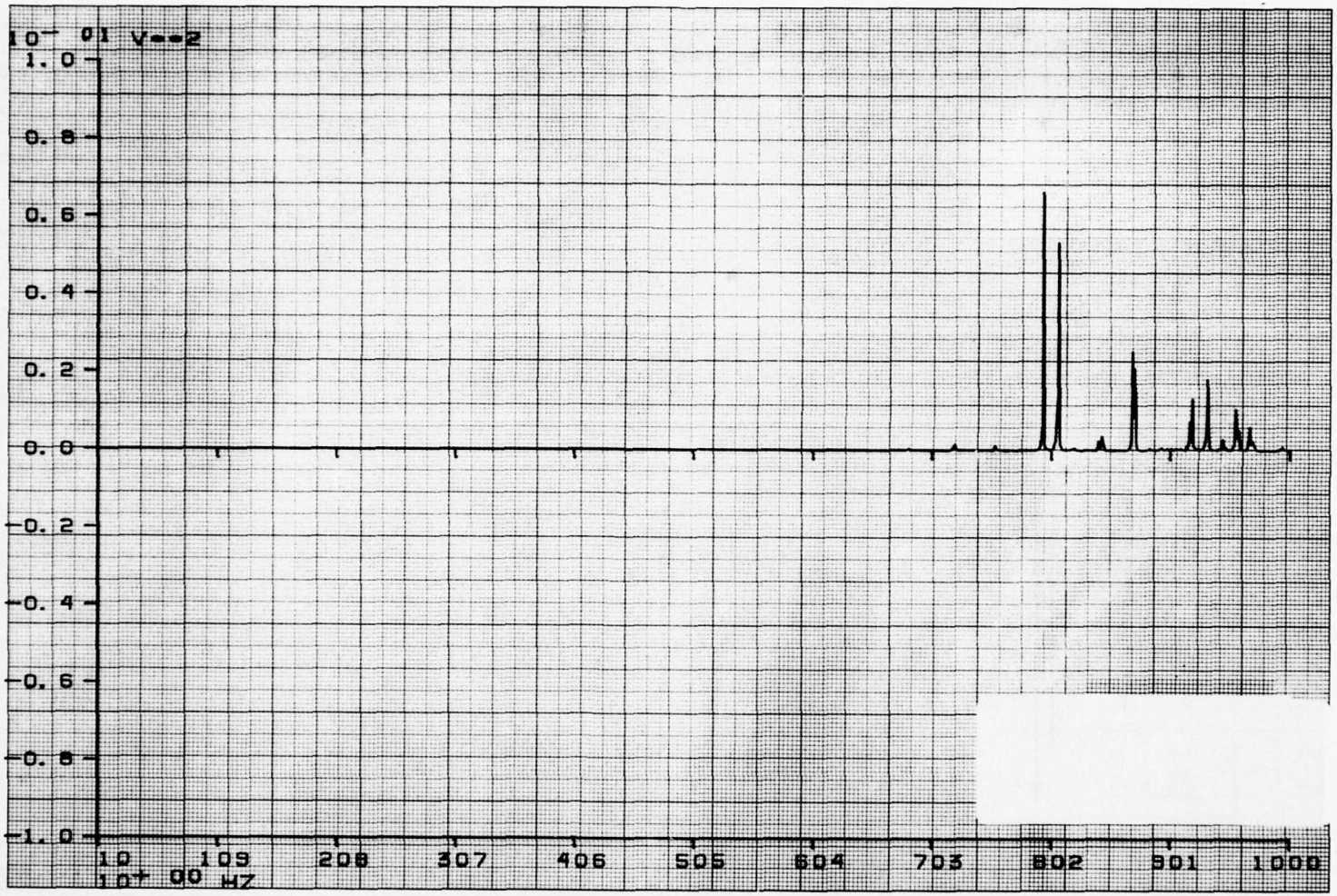

Figure 54. LSI Gyro Serial #405, 2 pole lo-pass filter @ 1 Kc, 26 volt, 1 phase, 400 Hz excitation, scale 15.7 mg/div

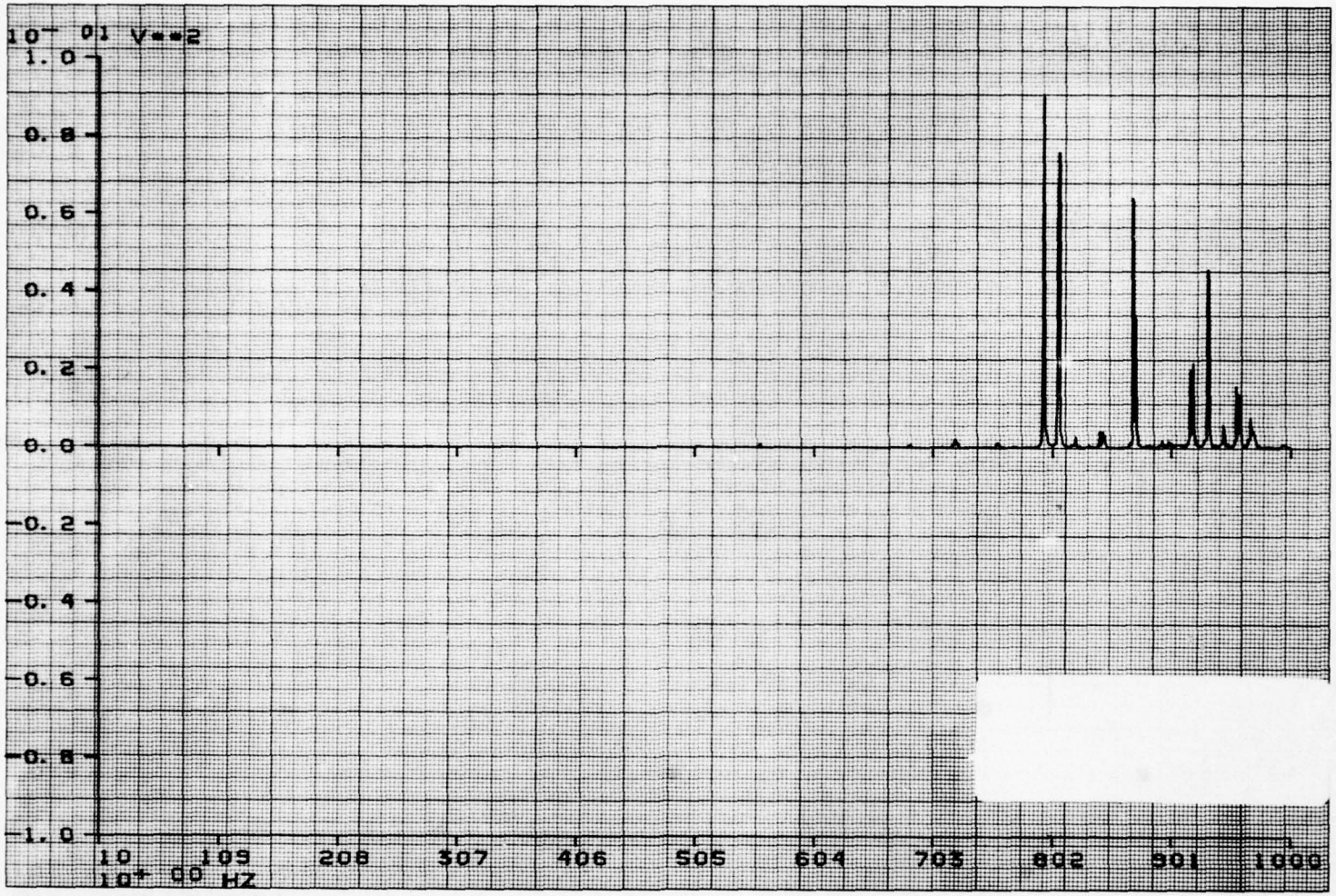

Figure 55. LSI Gyro Serial #405, 2 pole lo-pass filter @ 1 Kc, 26 volt, 1 phase, 400 Hz excitation, scale 15.7 mg/div

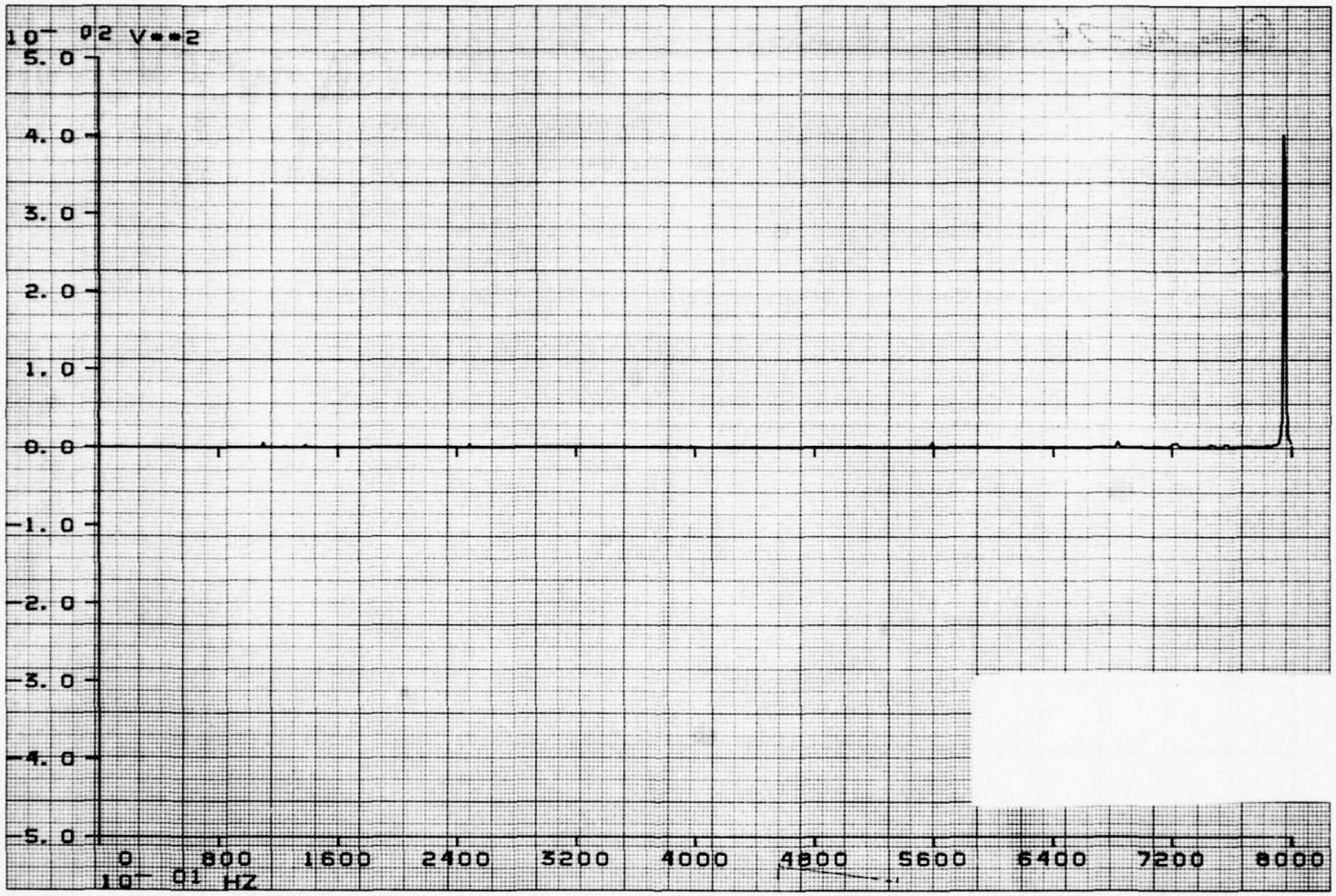

Figure 56. LSI Gyro Serial #405, 2 pole lo-pass filter @ 1 Kc, 26 volt, 1 phase, 400 Hz excitation, scale 11.1 mg/div

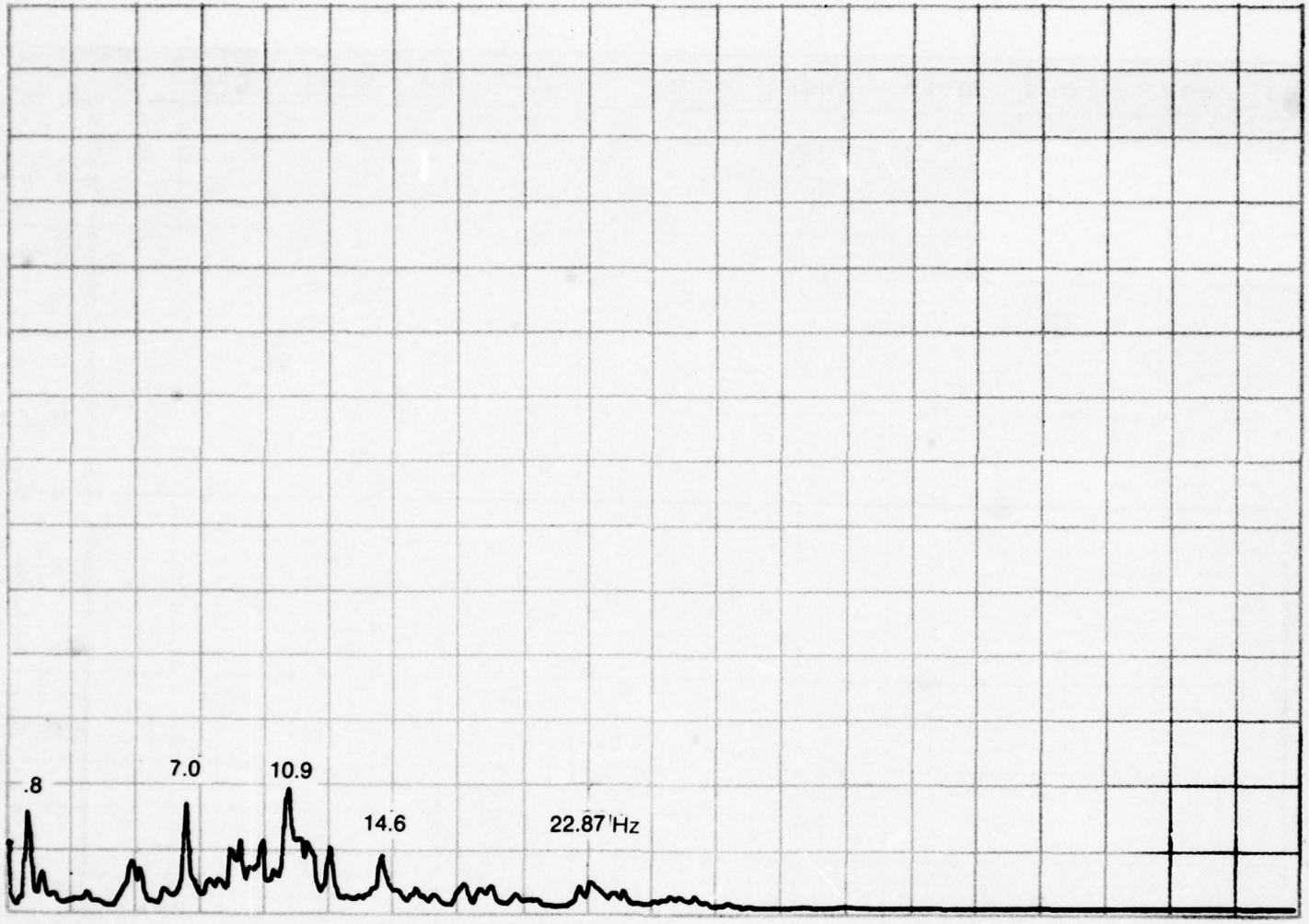

Figure 57. Second sensor; power spectral density 50 KHz.

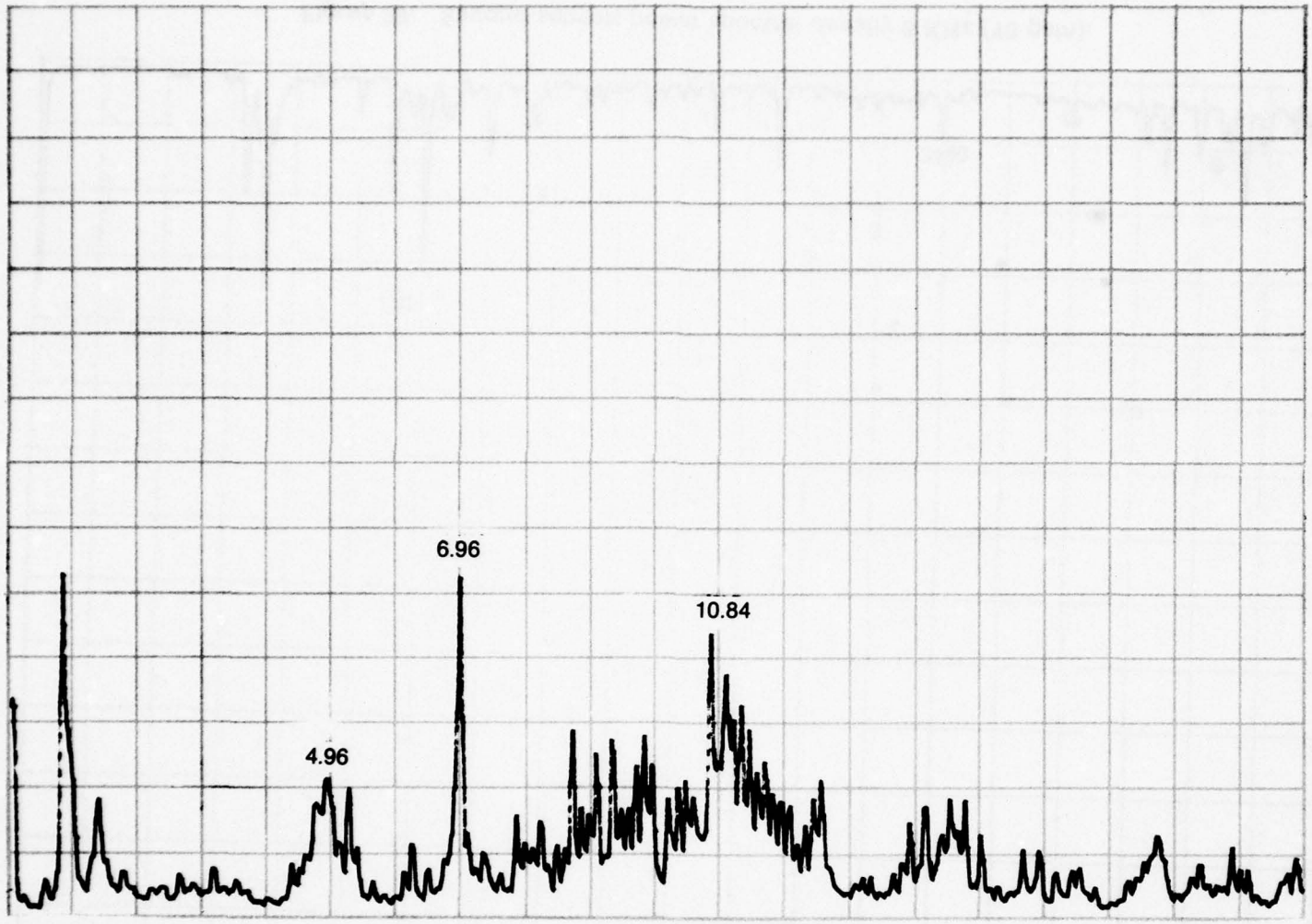

Figure 58. Second sensor; power spectral density 20 KHz.

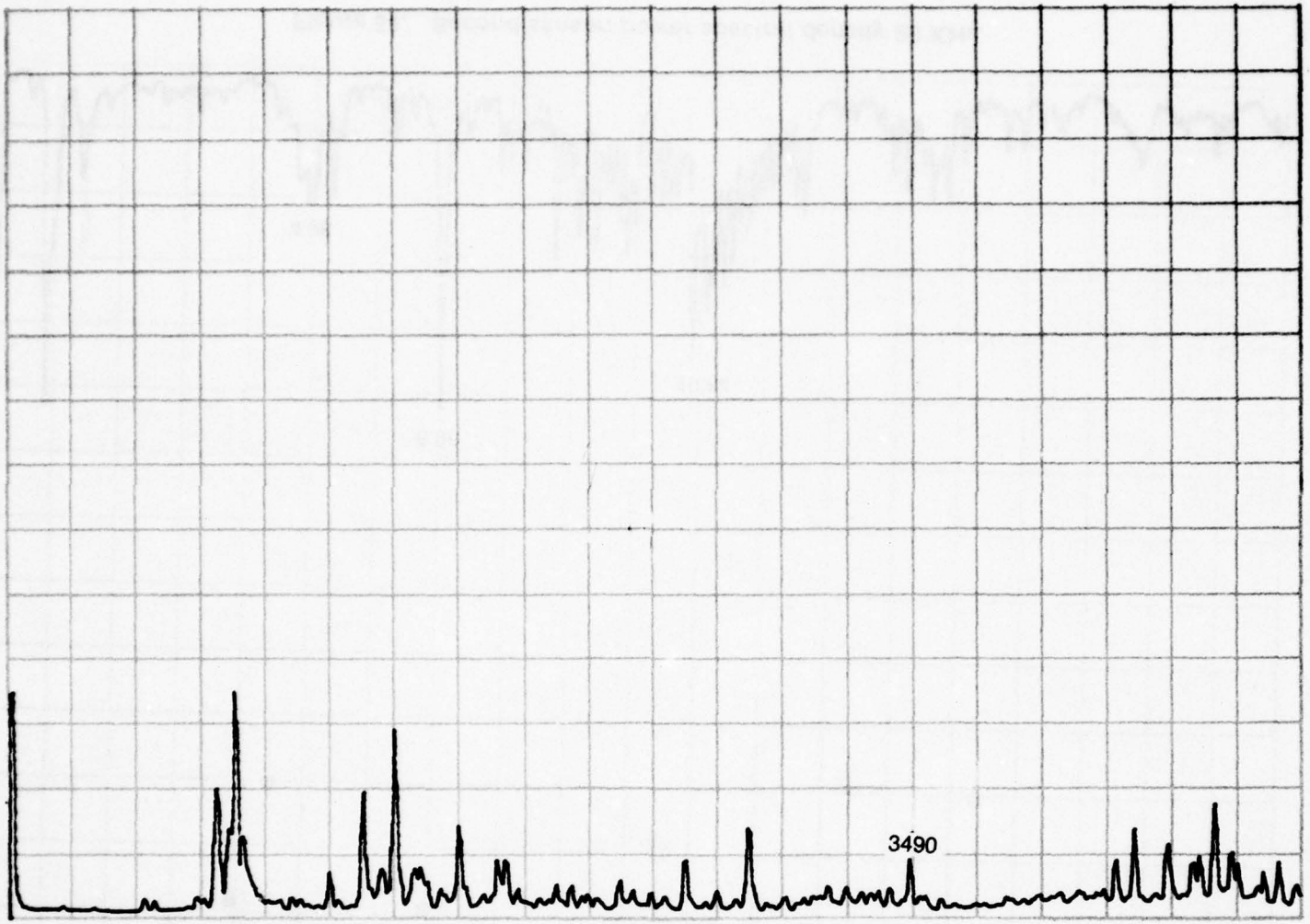

Figure 59. Second sensor; power spectral density 5 KHz (10 gain).

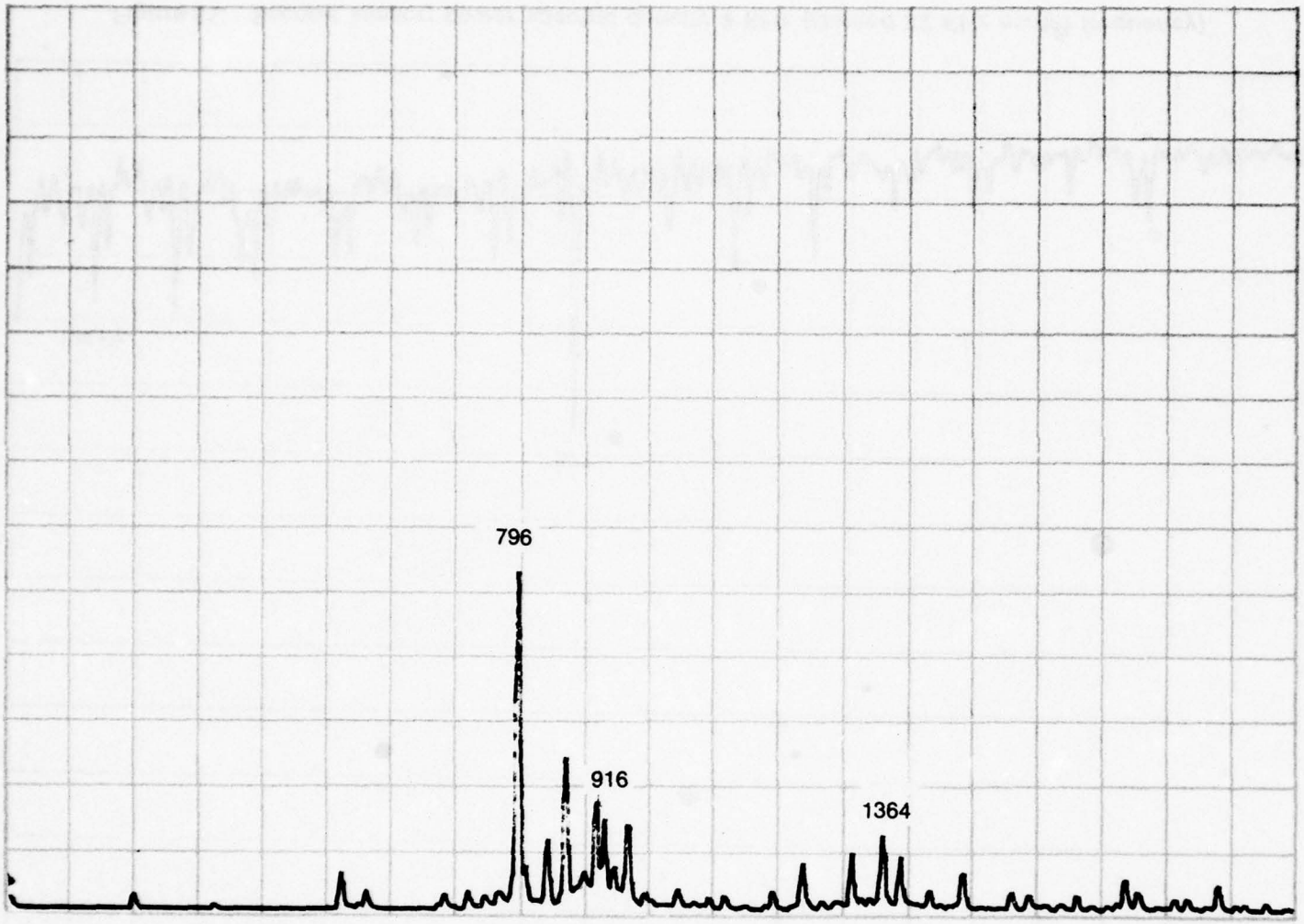

Figure 60. Second sensor; power spectral density 2 KHz (3.2 gain).

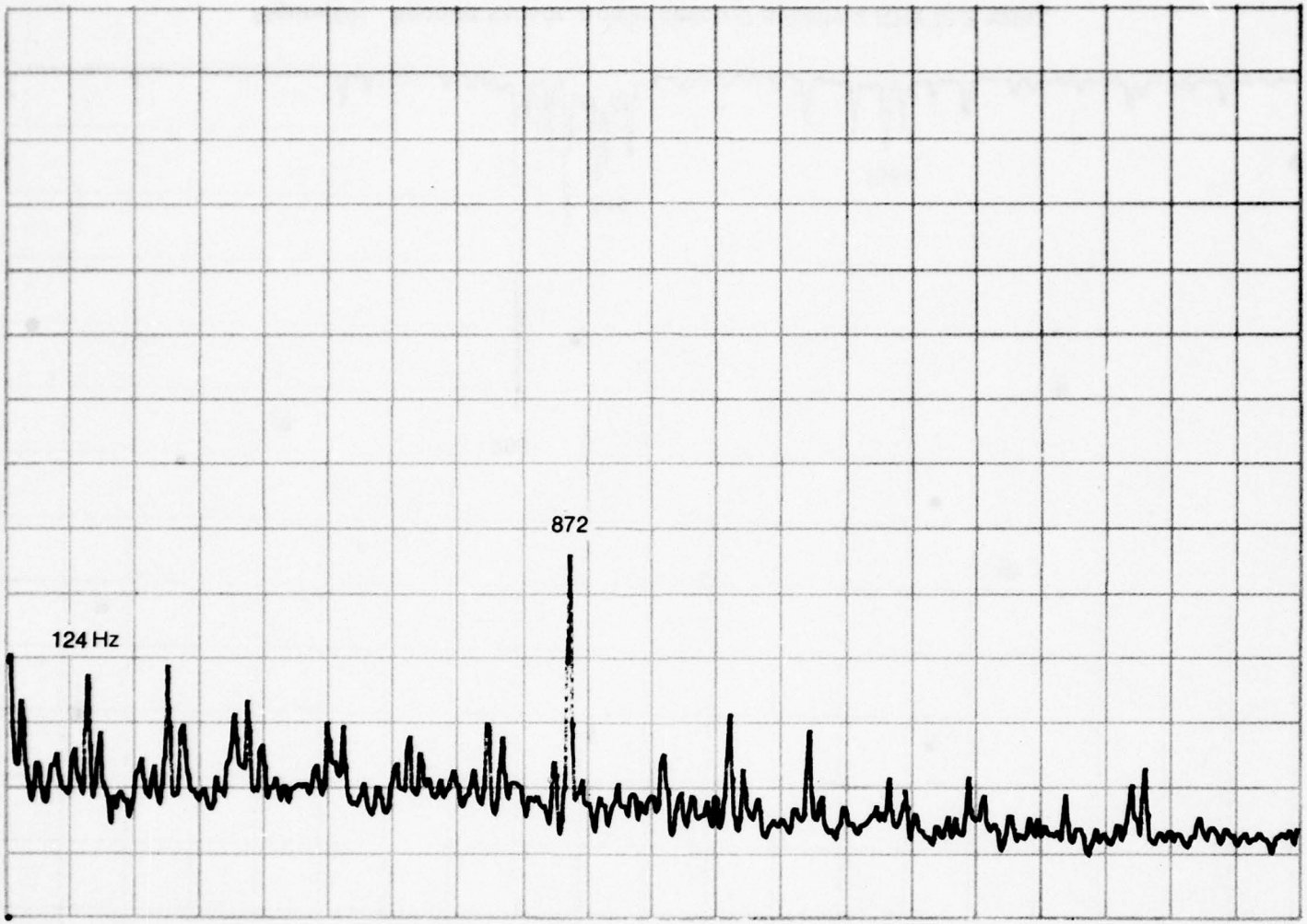

Figure 61. Second sensor; power spectral density 2 KHz (Demod 22 KHz center frequency).

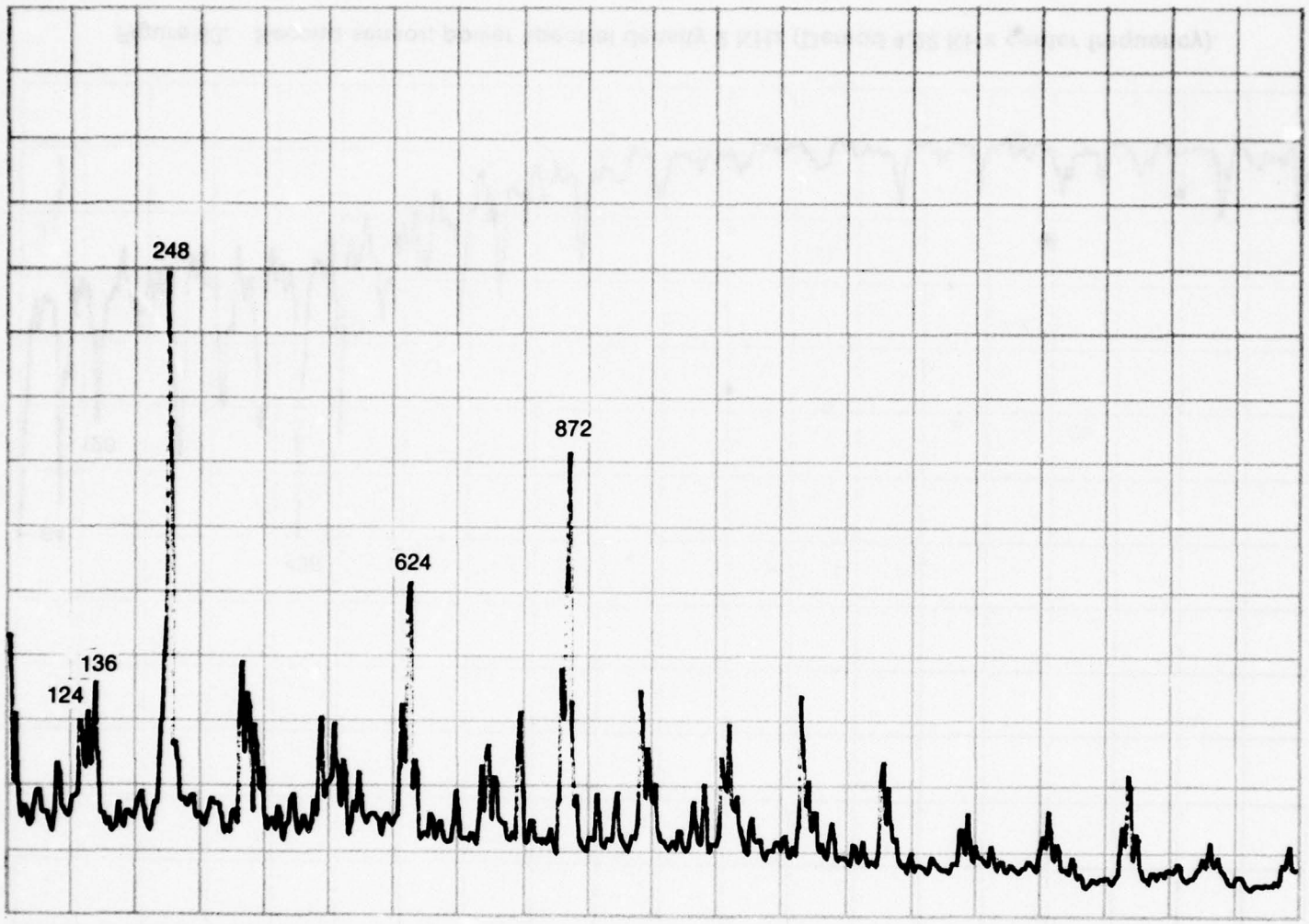

Figure 62. Second sensor; power spectral density 2 KHz (Demod 11.7 KHz center frequency).

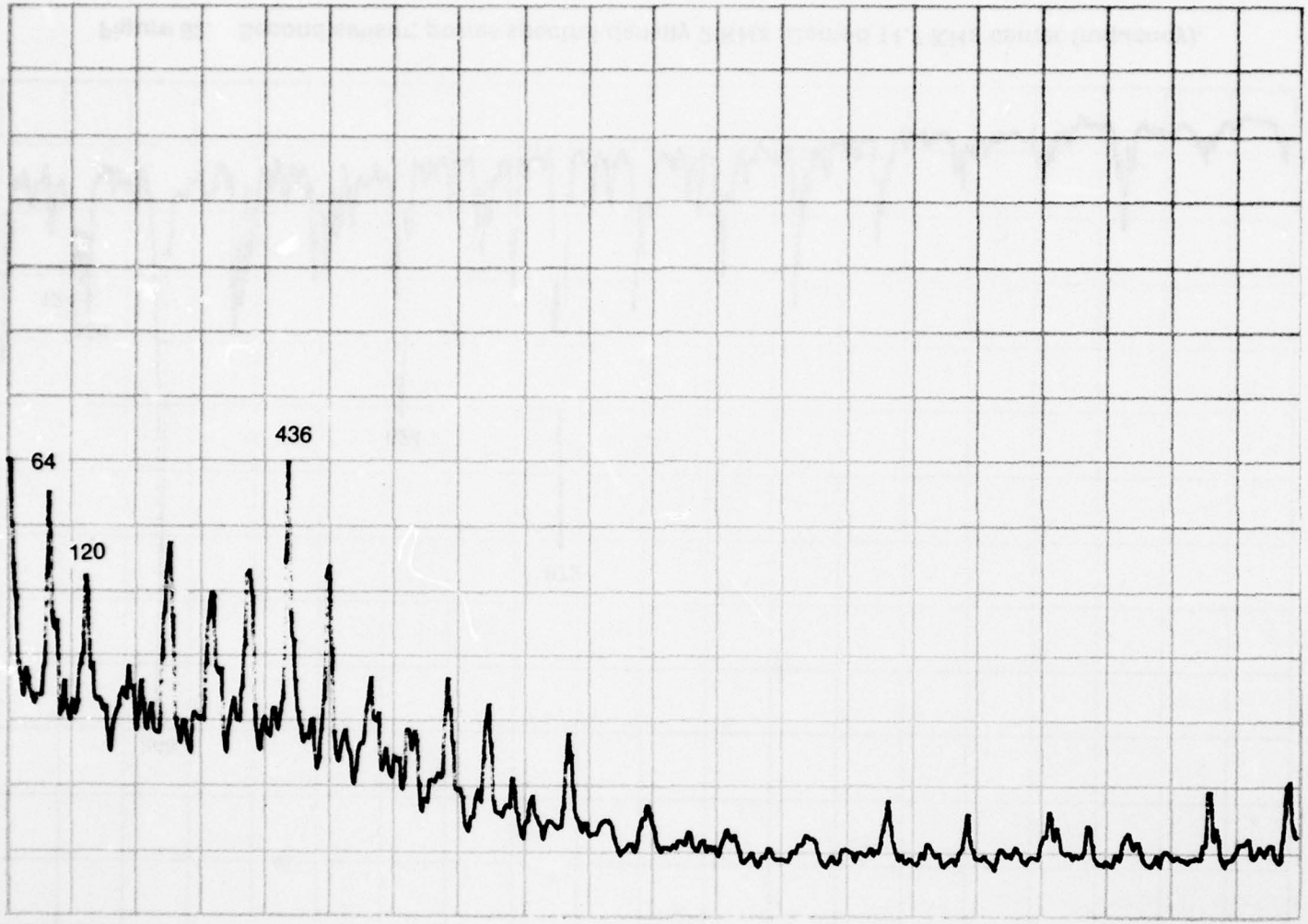

Figure 63. Second sensor; power spectral density 2 KHz (Demod 4.92 KHz center frequency).

constant level of vibration present in the detected signal. The source for this bias is unknown.

The excitation frequency of the wheel was increased to 420 H3 which would increase the rotation rate of the wheel due to the hysteresis synchronous construction. *Figure 64* illustrates no significant change in the 2X excitation frequency nor the discrete that appears at 916 H3 (see *Figure 60*). *Figure 65* indicates that the 916 H3 discrete slips to 830 H3 and the 800 discrete slips to 758 H3 when the excitation frequency is reduced to 380 H3. When the excitation frequency is returned to 400 H3 the 2X excitation discrete returns to 796 H3. *Figure 66* illustrates the time varying nature of the 916 H3 discrete. The amplitude variation appears to be rectified as is the 838 H3 discrete.

Figure 67 is the accelerometer signal from the first trunnion. This data appears greater in magnitude than does the 50 KHz data of *Figure 57*. Again, the peaks in *Figure 68* are distinctly more severe than those of comparable data in *Figure 58*. The peaks of *Figure 68* are more dense and greater in magnitude. *Figure 69* essentially duplicate the peaks in *Figure 59* but the discrete at 3490 Hz is 10.4 times greater in *Figure 69*. *Figure 70* again reflect larger discretes than the comparable data of *Figure 60*.

However, the 22 KH3 center frequency was detected and a strong 872 discrete was present (see *Figure 71 and 72*). Also, in *Figure 71*, a periodic succession of discretes are present throughout the pass band. *Figure 72* show the detected signal at a center frequency of 11 KH3 and there appears to be a duplicate in discrete content from *Figure 71*.

Figure 73 illustrates the change in discrete frequencies as the wheel speed varies. The excitation frequency is varied from 380 H3 to 420 H3.

Figure 74 shows the amplitude variation for the discretes as labeled. The period of each variation appears related but the 850 and 916 H3 discrete show rectification characteristics.

Tables 5 and *6* list the discrete amplitudes in g and the frequency for the Lear Seigler AG7 gyro wheel.

4. CONCLUSIONS

The data illustrated depicts two means of detecting noise sources associated with gyro spin motors. Both techniques enable isolating the amplitude and frequency of the noise sources. However, a larger data base will be required to permit a high degree of confidence in correlating the gyro spin motor power spectral density data to subsequent gyro performance. The

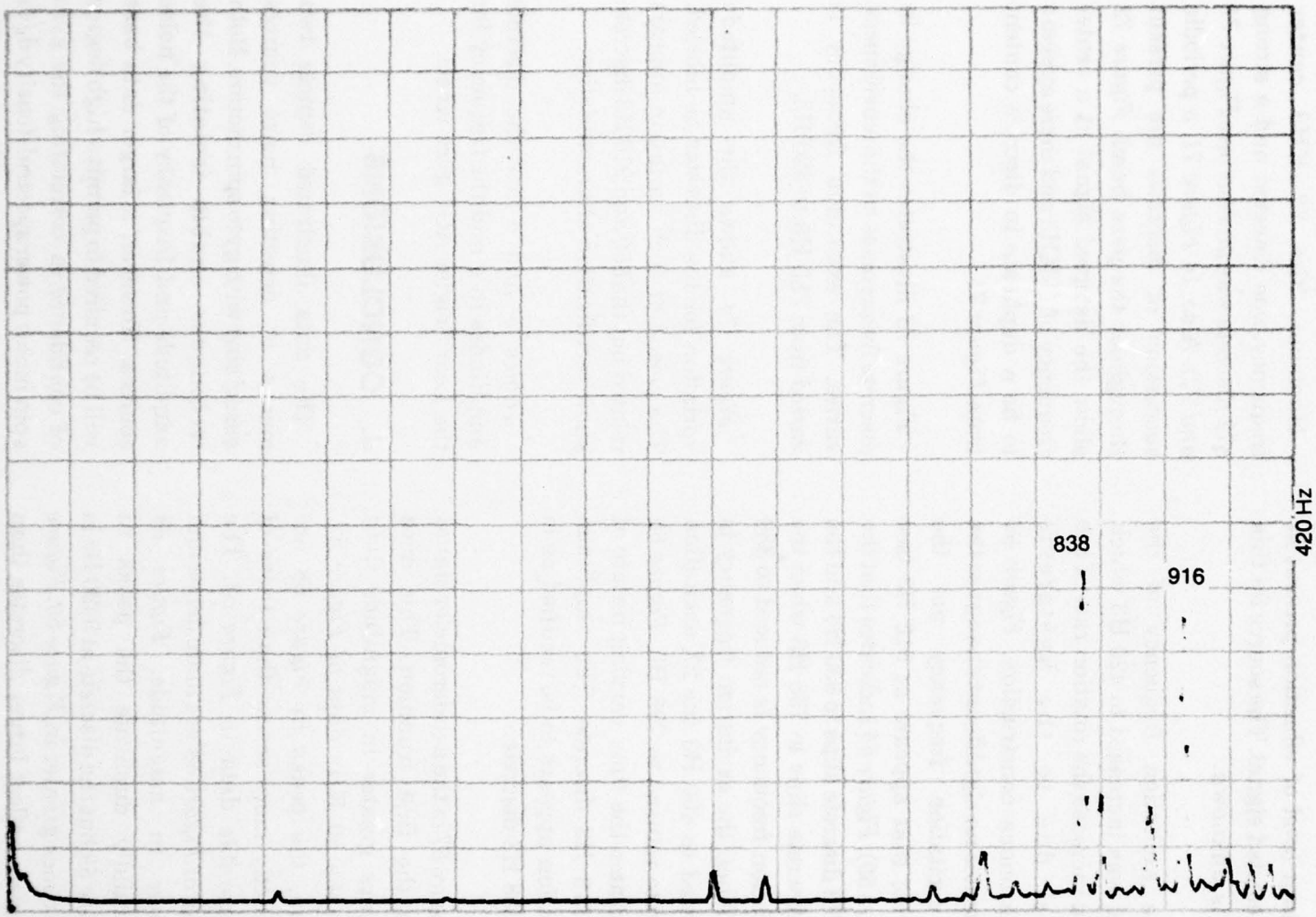

Figure 64. Second sensor; power spectral density 1 KHz (wheel excitation frequency 420 Hz).

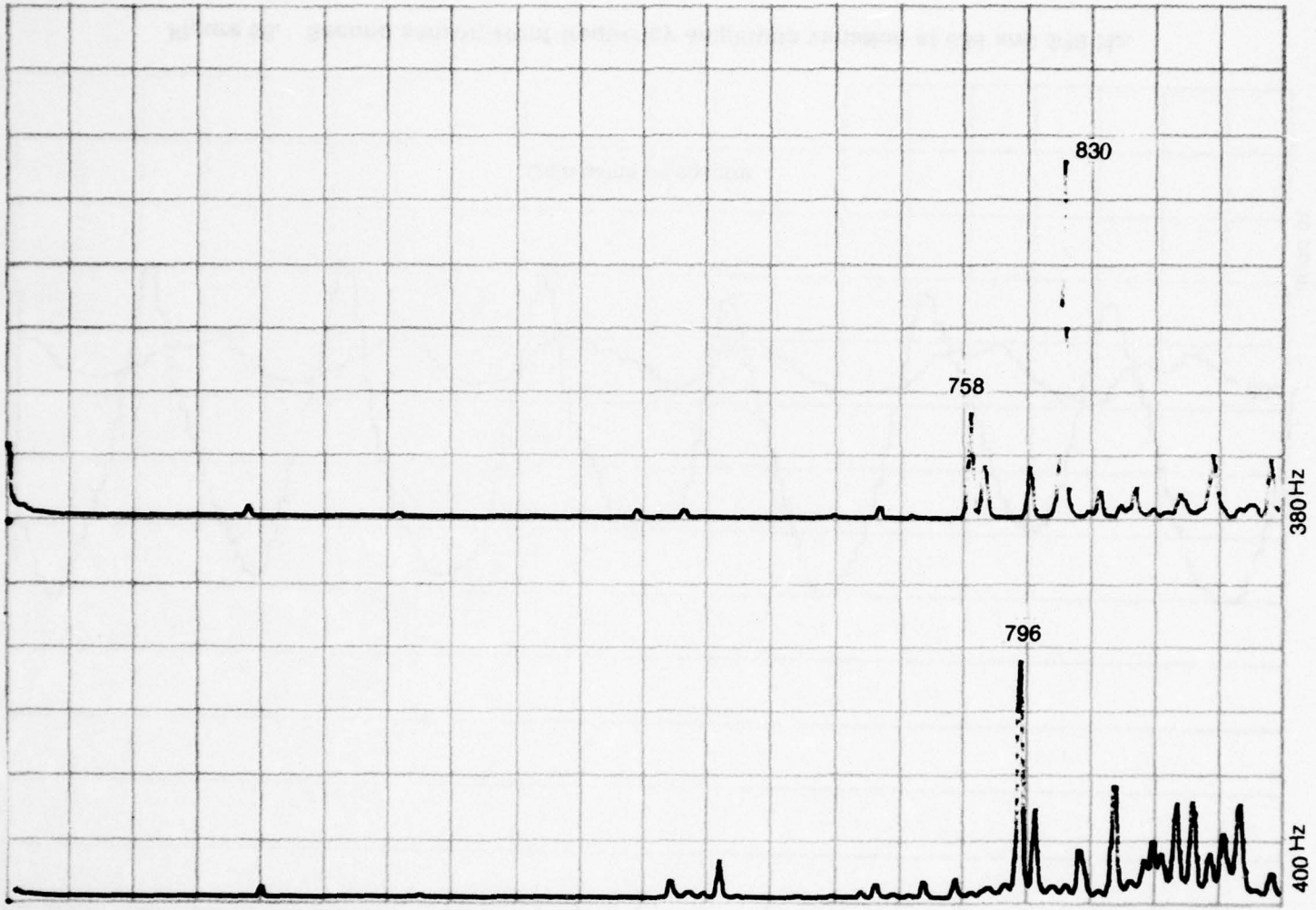

Figure 65. Second sensor; power spectral density 1 KHz (wheel excitation at 380 and 400 Hz).

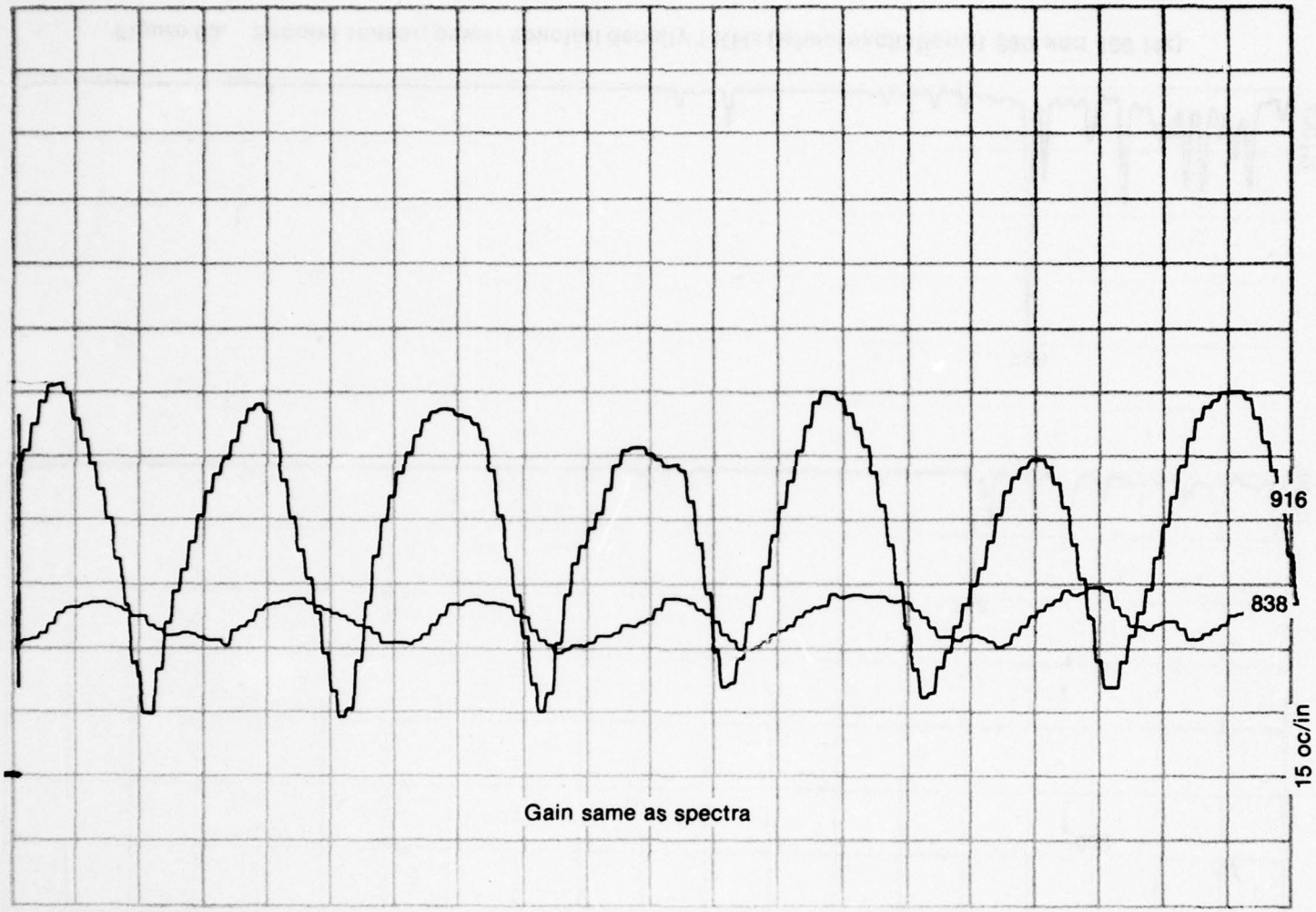

Figure 66. Second sensor; Hunt frequency amplitude variation at 838 and 916 Hz.

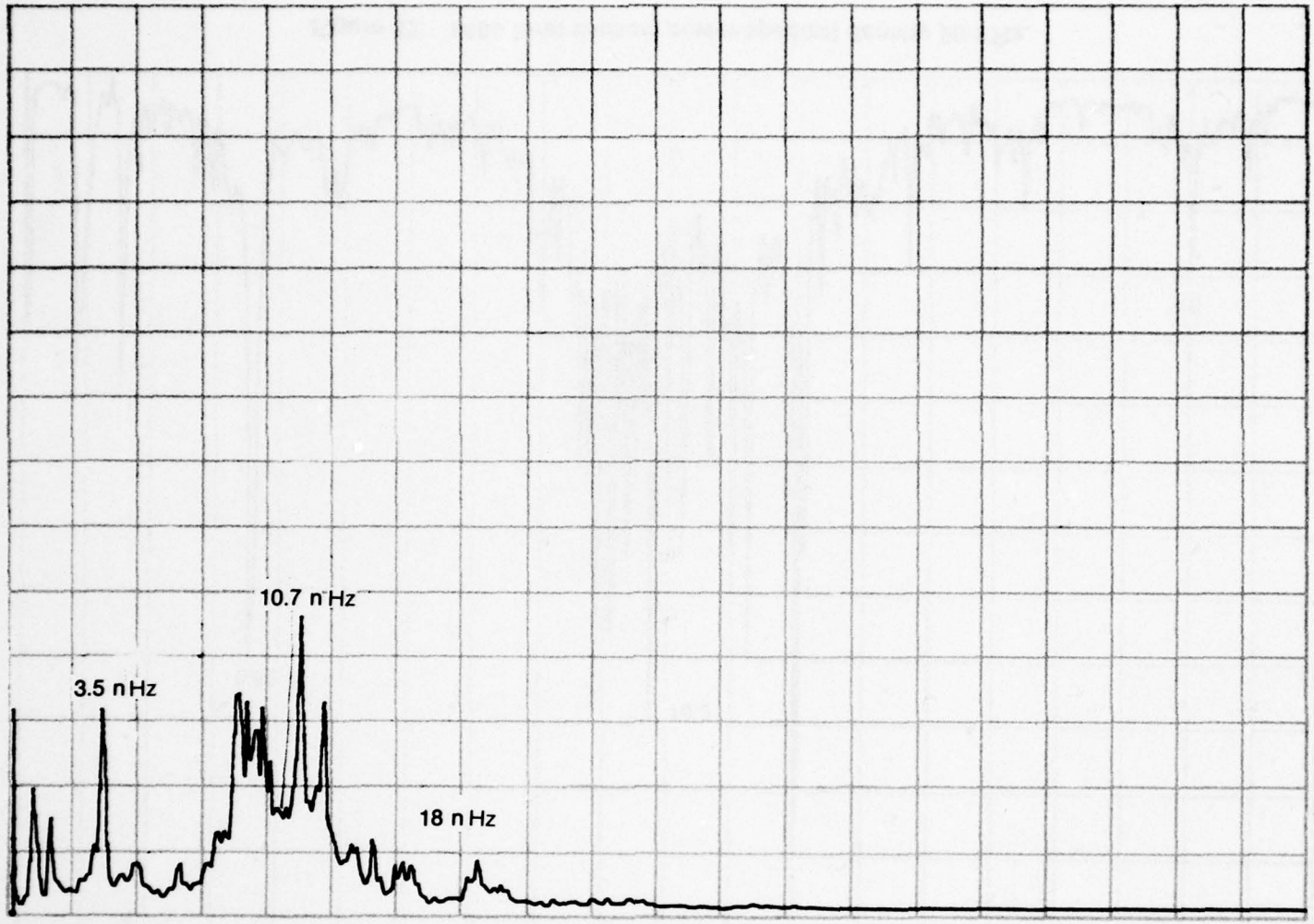

Figure 67. #405 First sensor; power spectral density 50 KHz.

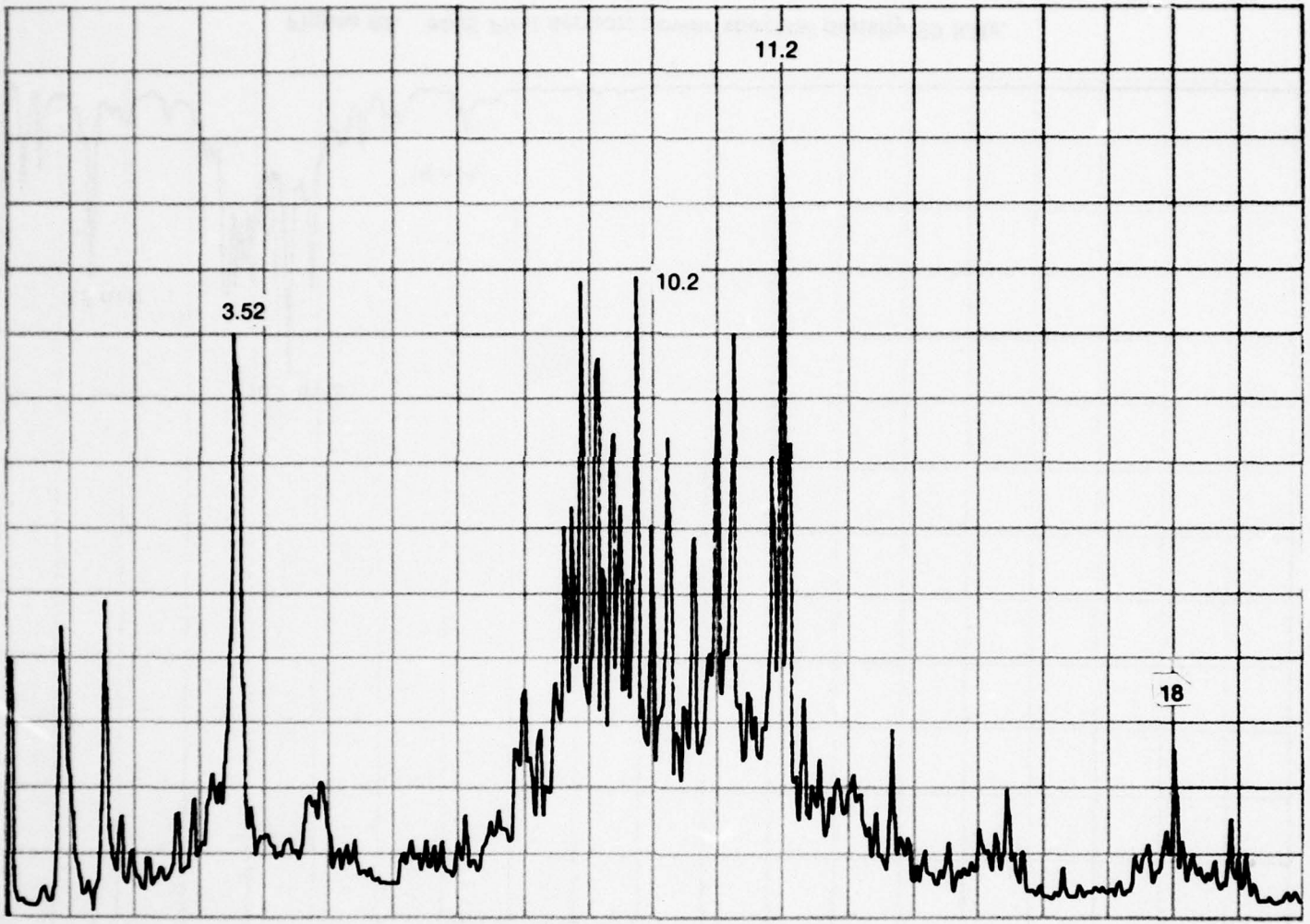

Figure 68. #405 First sensor; power spectral density 20 KHz.

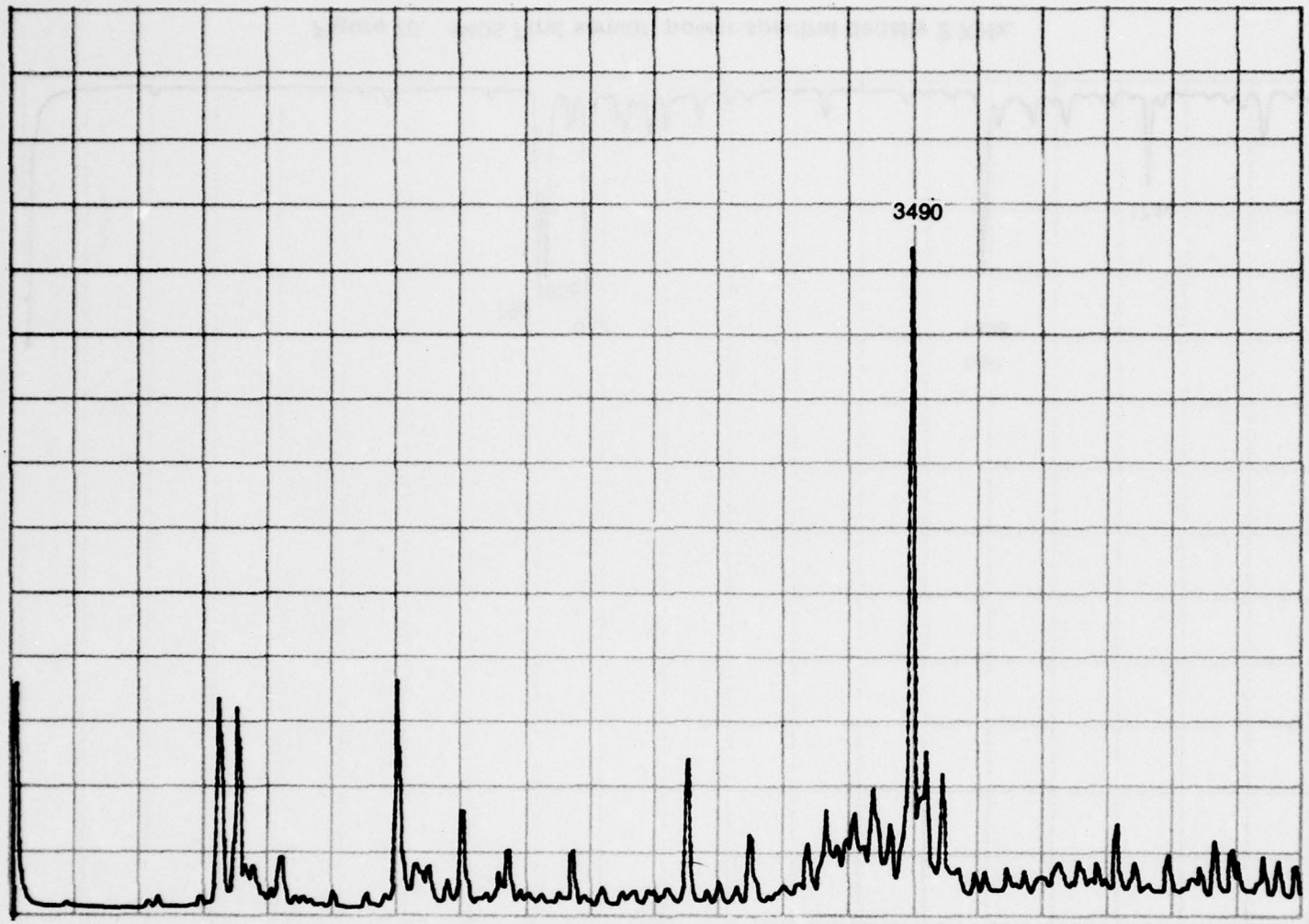

Figure 69. #405 First sensor; power spectral density 5 KHz.

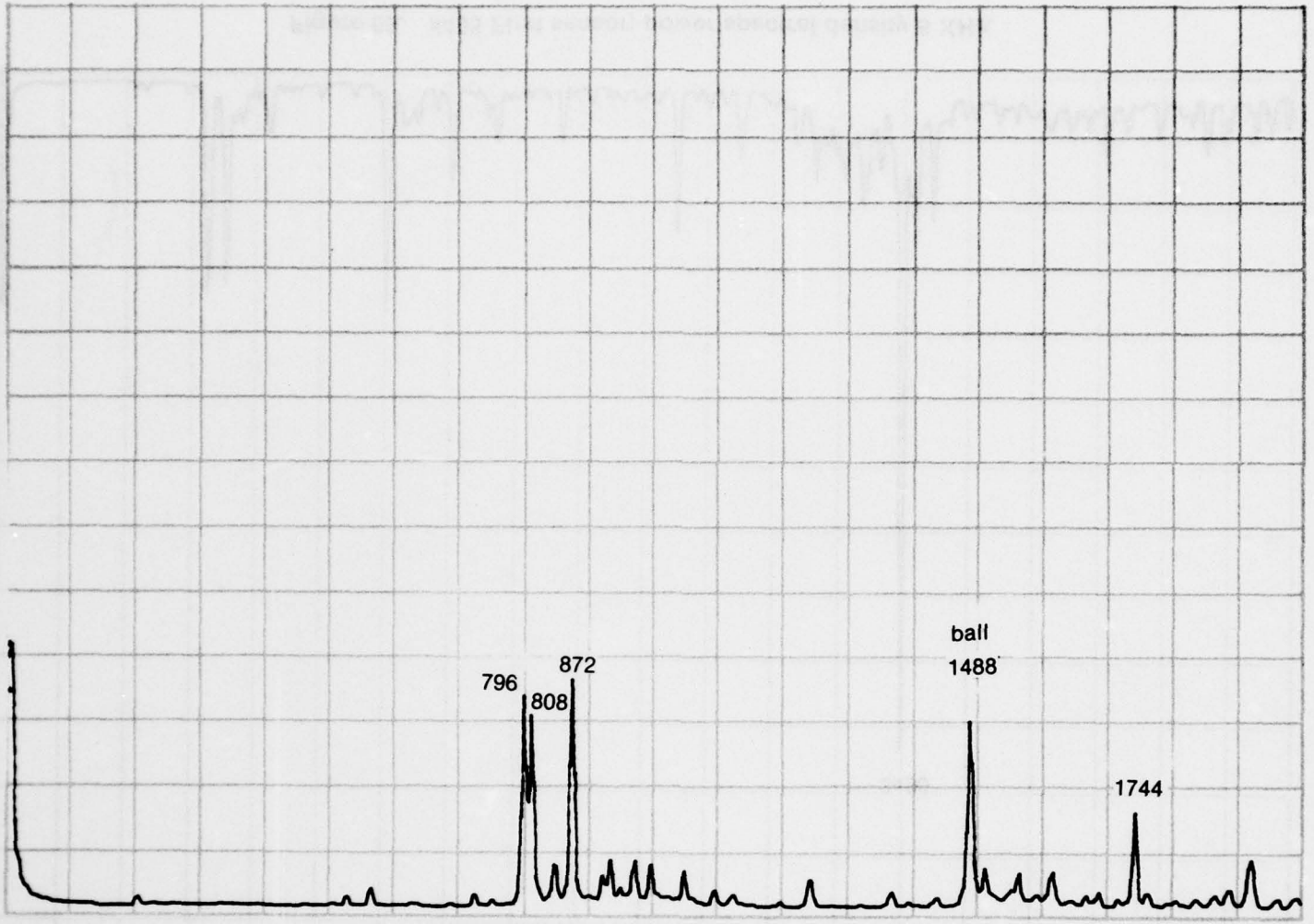

Figure 70. #405 First sensor; power spectral density 2 KHz.

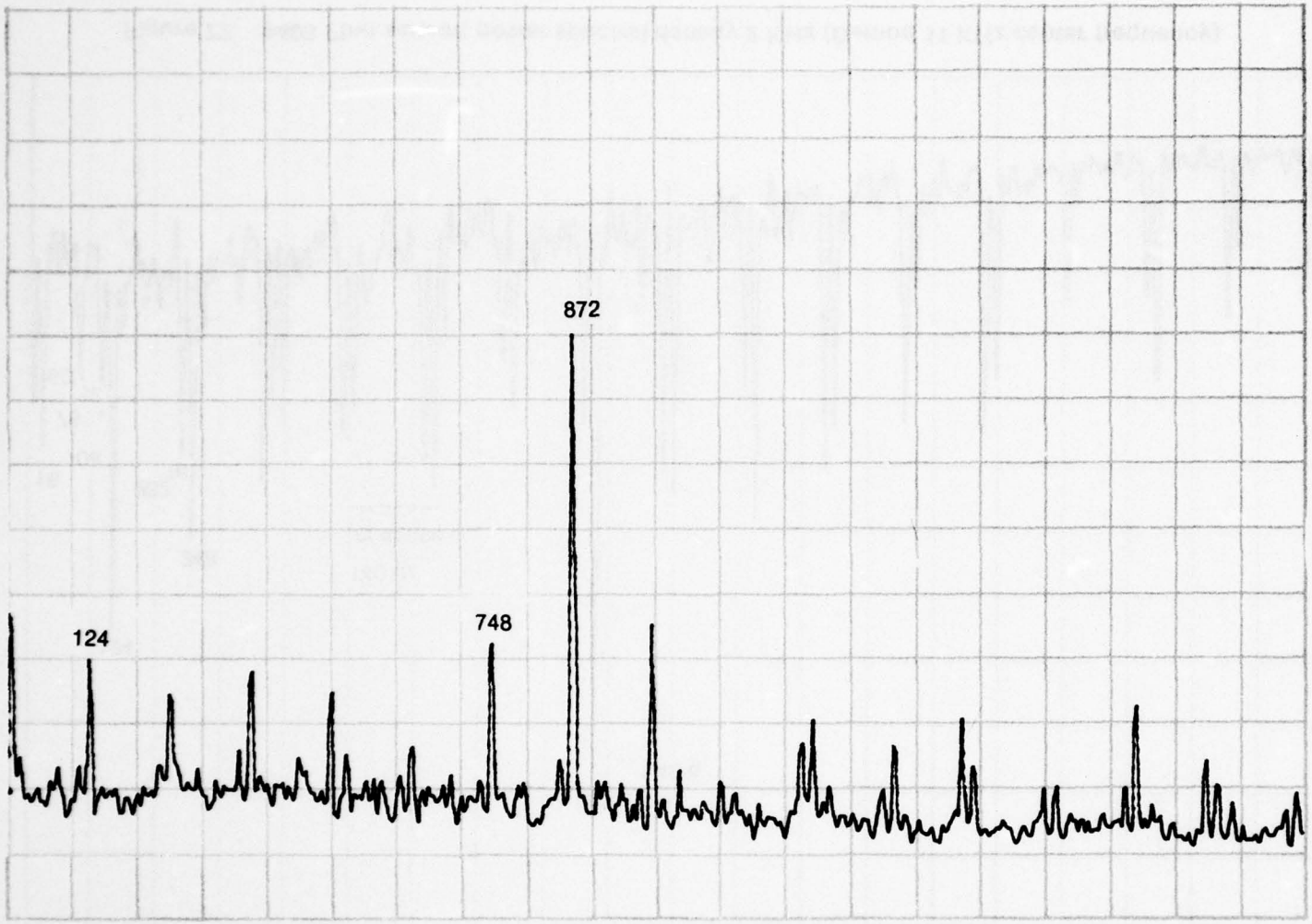

Figure 71. #405 First sensor; power spectral density 2 KHz (Demod 22 KHz center frequency).

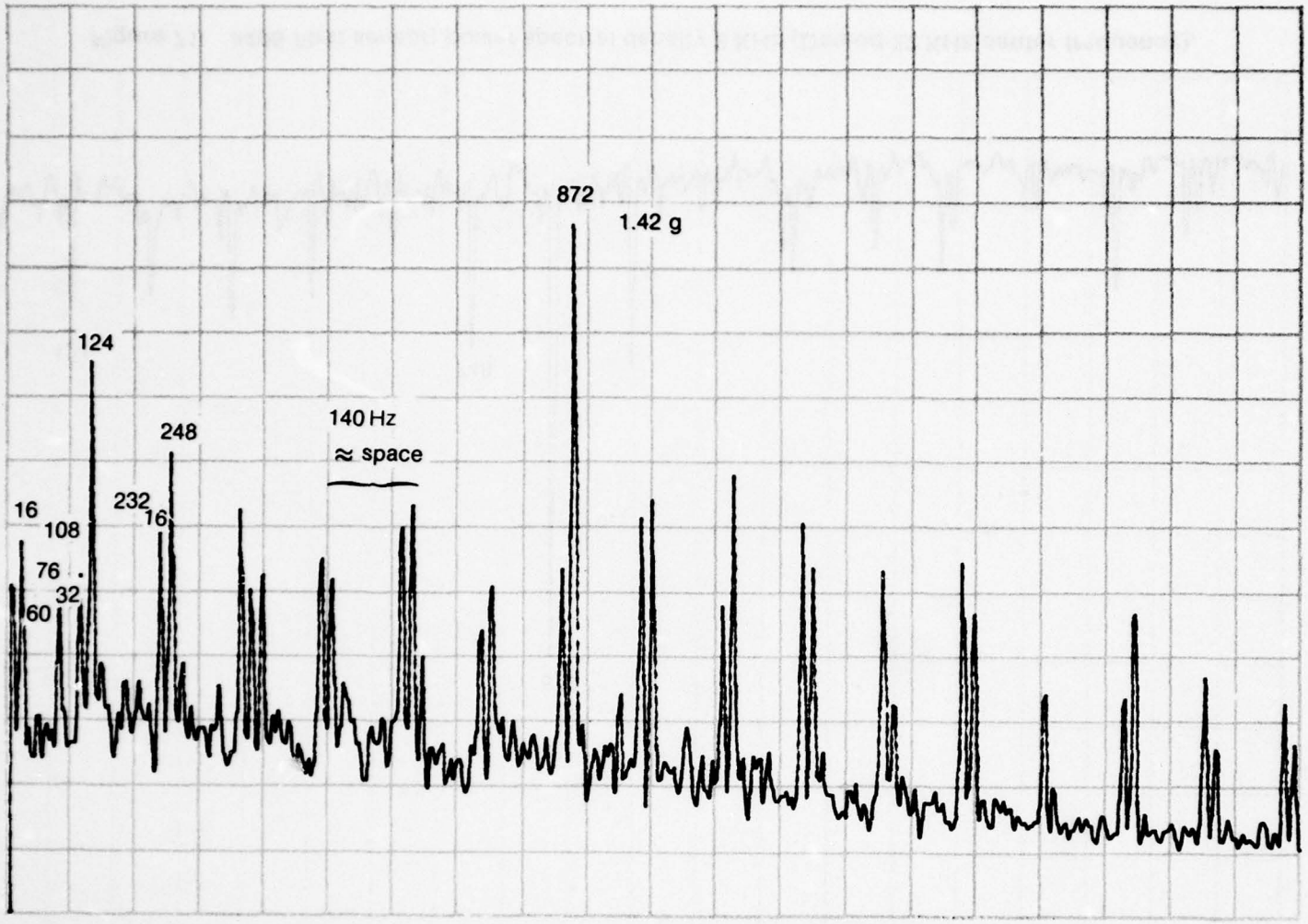

Figure 72. #405 First sensor; power spectral density 2 KHz (Demod 11 KHz center frequency).

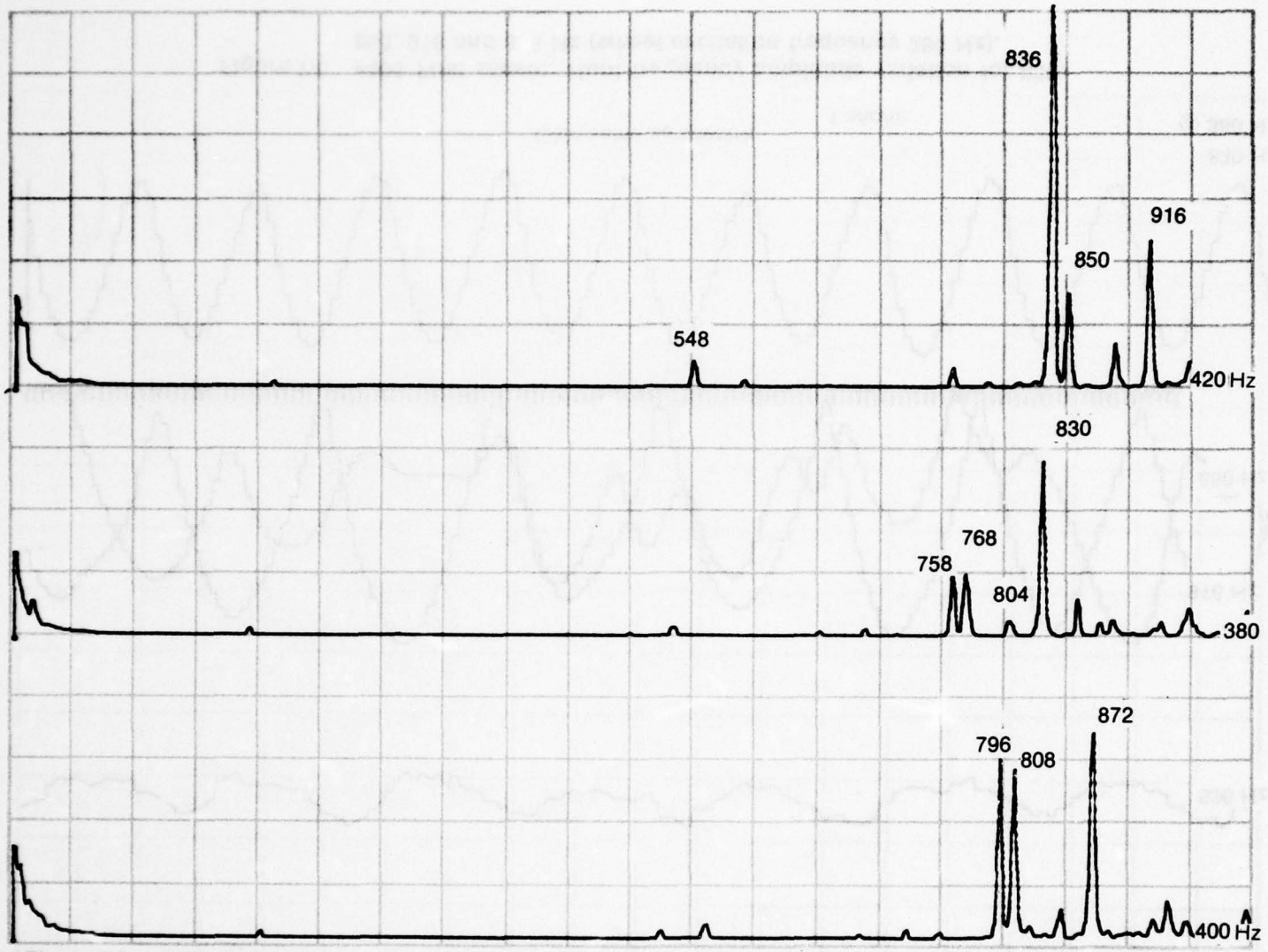

Figure 73. #405 First sensor; power spectral density for wheel excitation frequency 380, 400 and 420 Hz.

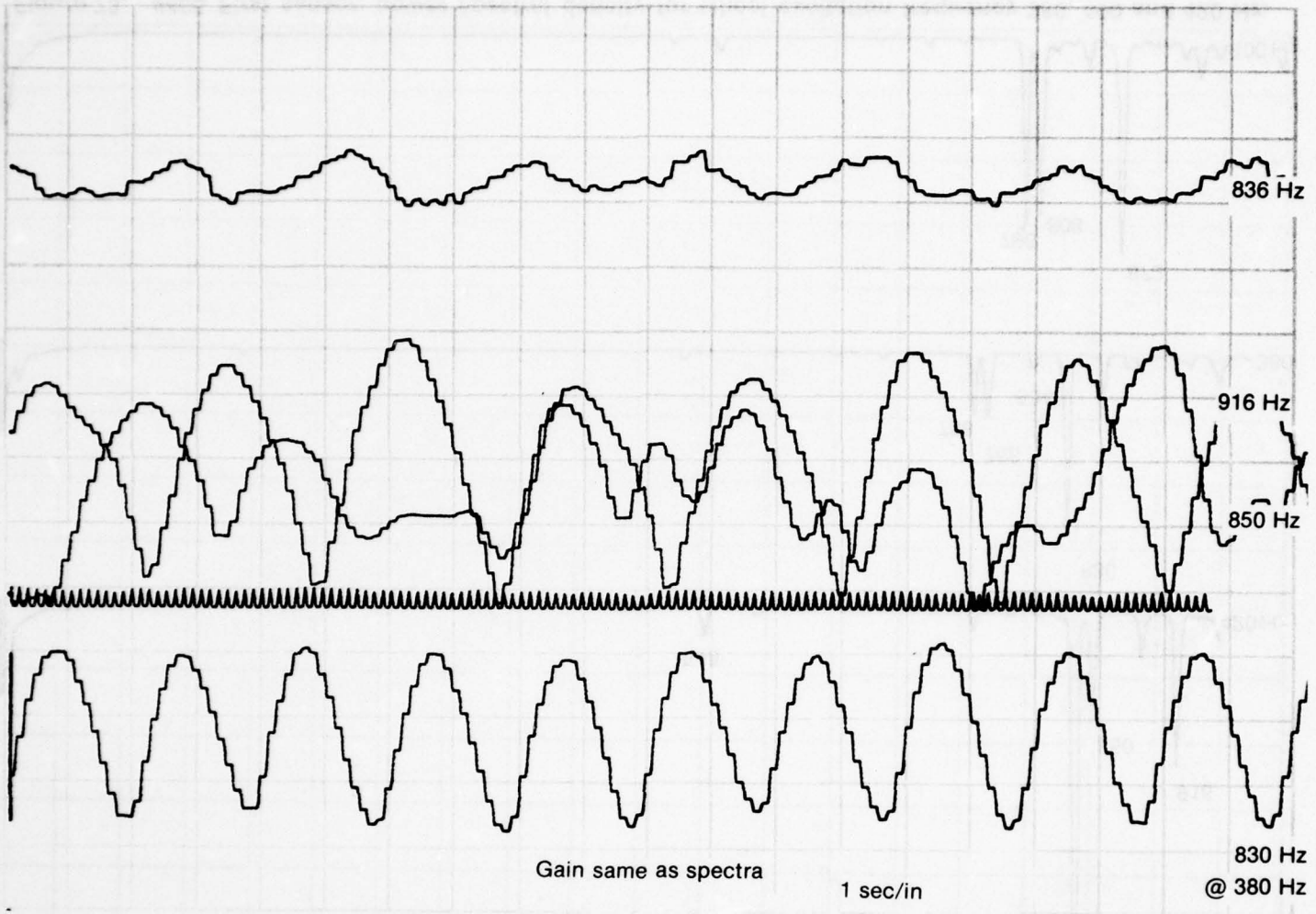

Figure 74. #405 First sensor; Hunt frequency amplitude variation for 830, 850, 916 and 836 Hz (wheel excitation frequency 380 Hz).

TABLE 5. MIRADCOM VIBRATION DATA ON LEAR SEIGLER GYRO WHEEL NUMBER 405	
Discrete HZ	**Vibration mg**
1745	78 mg
1495	109.9 mg
1245	94 mg
1041	62.8 mg
934	204 mg
919	204 mg
872	440 mg
847	78 mg
807	565 mg
793	1382 mg
648	16 mg
560	11.1 mg
248	11.1 mg
109	11.1 mg

TABLE 6. SHAKER RESEARCH VIBRATION DATA ON LEAR SEIGLER GYRO WHEEL NUMBER 405			
Discrete HZ	**First Vibration mg**	**Discrete HZ**	**Second Vibration mg**
1744	683 mg		
1488	1281 mg		
		1364	500 mg
		916	709 mg
			944 mg
			2210 mg
748	176 mg		
		624	678 mg
		436	294 mg
			1330 mg
232	798 mg		
		136	465 mg
			412 mg
		120	218 mg
108	705 mg		
76	625 mg		
		64	273 mg
16	758 mg		

AD-A063 554 ARMY MISSILE RESEARCH AND DEVELOPMENT COMMAND REDSTO--ETC F/G 17/7
SPECTRAL DENSITY ANALYSIS OF GYRO VIBRATIONS.(U)
JUN 78 L J LITTLE

UNCLASSIFIED DRDMI-T-78-59 NL

2 OF 2
AD
063554

END
DATE
FILMED
3 -79
DDC

ability to identify suitable gyro spin motors at an early assembly stage is the ultimate goal associated with this research so that production cost can be minimized. The measurement techniques presented in this report have the potential of being mechanized into a viable quality control tool. The factors associated with the discrete noise signals are generally specific signatures for various sources.

The higher frequency noise is normally attributed to slots of the stator. Design details of the motor are required to resolve this data and can be useful only from experience.

The bearings are a noise source and experience again must be included in resolving problems due to bearings. The bearing retainers normally turn at a rate approximately forty per cent of the inner race rate and multiples.

Frequencies associated with the inner race range from three to five times the inner race rotation rate. Ball contact problems are related to two to three times the outer race rotation rate. Also, the above factors associated with the bearing performance assumes pure rolling motion of the ball but a ten to fifteen percent slip may occur. However, the bearing noise magnitude, in the 10 to 20 KHz range, increases exponentially as the deterioration sets in.

Structural resonances and internal structural stiffness are factors to be considered. Design details are necessary to draw reasonable conclusions from the measured data.

In the main, experience is the most important factor in drawing valid conclusions from the type data collected. Insufficient data is available depicting various known problem and to enable relating specific numbers to gyro performance. Therefore, it would be necessary to collect vibration data on a number of gyros and correlate this data with the pertinent gyro performance. Also, the bad gyro should be disassembled in stages with vibration data being recorded during each stage of the tear down in order to isolate the problem source.

With sufficient development this appears to be a potential quality control and cost effective testing technique for future gyro wheel selection.

DISTRIBUTION

	No. of Copies
Defense Documentation Center Cameron Station Alexandria, Virginia 22314	12
IIT Research Institute ATTN: GACIAC 10 West 35th Street Chicago, Illinois 60616	1
DRSMI-LP, Mr. Voigt	1
DRDMI-T, Dr. Kobler	1
DRDMI-TBD	3
DRDMI-TI (Reference Copy)	1
DRDMI-TI (Record Set)	1
DRDMI-TG, Mr. Little	10

☆U.S. GOVERNMENT PRINTING OFFICE 1978—640-122/291 REGION NO.4